Dissertation

submitted to the

Combined Faculties for the Natural Sciences and for Mathematics

of the Ruperto-Carola University of Heidelberg, Germany

for the degree of

Doctor of Natural Sciences

presented by

Diplom-Geophysicist Daniela Polag

born in Frankfurt am Main, Germany

Oral examination: 28.04. 2009

Kinetic Fractionation of Stable Isotopes in Speleothems -Laboratory and In Situ Experiments-

Referees:

Prof. Dr. Augusto Mangini

Prof. Dr. Margot Isenbeck-Schröter

Abstract

In recent years, stalagmites have become an important archive for paleoclimate. Several studies about stable isotope records in stalagmites show a simultaneous enrichment of $\delta^{18}O$ and $\delta^{13}C$ along individual growth layers, which is associated with kinetic isotope fractionation. However, to deduce paleoclimatic information from calcite which is precipitated under these non-equilibrium-conditions, it is important to improve the understanding of kinetic isotope fractionation in dependence of local conditions like temperature and drip rate. Within this research work, laboratory experiments with synthetic carbonates were carried out under controlled conditions. The $\delta^{18}O$ and $\delta^{13}C$ evolution of the precipitated calcite were studied for different experiment parameters such as the initial composition of the solution, temperature and drip rate. In addition, in situ experiments were carried out in two cave systems in Sauerland (Bunkerhöhle and B7-Höhle). The modern calcite collected at three drip sites was compared with the calcite obtained from the laboratory experiments. All experiments show a distinct isotopic enrichment along the precipitated calcite. Lower drip rates, higher temperatures and higher initial supersaturation with respect to calcite result in a greater total isotopic enrichment and in a lower slope of the linear correlation $\delta^{18}O(\delta^{13}C)$. The latter indicates a larger oxygen isotope buffering from the water reservoir. From a comparison with theoretical models it can be concluded that the conversion reactions between the bicarbonate and the carbon dioxid and the exchange reactions between the oxygen isotopes in the bicarbonate and the water reservoir occur faster than predicted from present publications, particularly in case of higher temperatures ($23°C$). Thus, for higher temperatures other effects might play a role not yet considered in theoretical models.

Zusammenfassung

In den letzten Jahren haben Stalagmiten als paläoklimatische Archive an elementarer Bedeutung gewonnen. Verschiedene Studien zu stabilen Isotopen in Stalagmiten zeigen eine simultane Anreicherung in $\delta^{18}O$ und $\delta^{13}C$ entlang einzelner Wachstumsschichten, welches auf kinetische Isotopenfraktionierung hindeutet. Um paläoklimatische Informationen aus Stalagmiten abzuleiten, welche unter diesen Nicht-Gleichgewichtsbedingungen abgelagert wurden, ist es wichtig, den Einfluß und das Ausmaß kinetischer Isotopenfraktionierung in Verbindung mit lokalen Bedingungen wie Temperatur und Tropfrate abzuschätzen. Im Rahmen dieser Arbeit wurden Laborexperimente mit synthetischen Carbonaten unter kontrollierten Bedingungen durchgeführt. Die Entwicklung von $\delta^{18}O$ and $\delta^{13}C$ im ausgefällten Kalk wurde für verschiedene Experimentparameter wie Lösungszusammensetzung, Temperatur und Tropfrate untersucht. Zusätzlich wurden In-situ Experimente in zwei Höhlensystemen im Sauerland (Bunkerhöhle and B7-Höhle) durchgeführt. Der moderne Kalk, welcher an drei Tropfstellen gesammelt wurde, wurde mit dem Kalk aus den Laborexperimenten verglichen. Alle Experimente weisen eine deutliche isotopische Anreicherungen im Kalk mit zunehmendem Abstand vom Auftropfpunkt auf. Geringere Tropfraten, höhere Temperaturen und eine höhere Übersättigung bzgl. Kalk führen zu einem Anstieg in der absoluten Isotopenanreicherung. Die linear korrelierte Steigung von $\delta^{18}O/\delta^{13}C$ wird hingegen geringer, welches auf eine größere Sauerstoffpufferung durch das Wasserreservoir hindeutet. Ein Vergleich mit theoretischen Modellen zeigt, daß die Umwandlungsreaktion zwischen dem Bicarbonat und dem Kohlendioxid und die Austauschreaktionen zwischen den Sauerstoffisotopen im Bicarbonat und dem Wasserreservoir schneller stattfinden, als es in bisherigen Publikationen angegeben ist, insbesondere für den Bereich höherer Temperaturen ($23°C$). Folglich spielen im Bereich hoher Temperaturen wahrscheinlich noch andere Effekte eine Rolle, die bisher in den theoretischen Modellen noch nicht berücksichtigt wurden.

Contents

1 Introduction **3**

2 Basics **5**

2.1 Stalagmites as paleoclimatic archives 5

2.2 Calcite-carbonate system 6

2.3 Calcite crystallisation 10

2.4 Isotope fractionation 12

2.4.1 Definition and notation 12

2.4.2 Fractionation mechanisms 13

3 Laboratory experiments **15**

3.1 Intention 15

3.2 Summary of previous laboratory experiments 16

3.3 Experimental method 17

3.3.1 Set-up 17

3.3.2 Comparison between cave system and laboratory set-up 19

3.3.3 Research parameters 20

3.3.4 Data analysis 22

3.3.5 Error estimation 24

3.4 Results 27

3.4.1 Calcite crystals 27

3.4.2 Calcite precipitation along the channel 30

3.4.3 $\delta^{13}C$ and $\delta^{18}O$ evolution along the channel 39

3.4.4 Fractionation Factors 47

3.4.5 Comparison with numerical models 50

3.5 Conclusion 54

4 Cave experiments **57**

4.1 General . . . 57

4.2 Bunkerhöhle . . . 58

4.2.1 Location . . . 58

4.2.2 Calcite crystals . . . 59

4.2.3 Calcite precipitation along the channel . . . 61

4.2.4 $\delta^{13}C$ and $\delta^{18}O$ evolution along the channel . . . 61

4.3 B7-Höhle . . . 65

4.3.1 Location . . . 65

4.3.2 Comparison with previous data . . . 66

4.3.3 Calcite crystals . . . 68

4.3.4 Calcite precipitation along the channel . . . 70

4.3.5 $\delta^{13}C$ and $\delta^{18}O$ evolution along the channel . . . 72

4.4 Conclusion . . . 74

5 Summary and outlook **75**

A Data from laboratory experiments **79**

B Data from in situ cave experiments **89**

Chapter 1

Introduction

In recent years, stable isotope records in speleothems (i.e., calcium carbonate deposits found in caves) have become more and more important as proxies of past climate variability (e.g., Spötl and Mangini (2002), Fleitmann et al. (2004), Harmon et al. (2004), Vollweiler et al. (2006) Wang et al. (2008)). Speleothems, which are found in most continental areas provide high resolution records and can be precisely dated by U-series (Scholz and Hoffmann (2008)). The stable isotope signals of carbon ($\delta^{13}C$) and oxygen ($\delta^{18}O$) recorded in stalagmites are the most widely used proxy to reconstruct past climate changes, for example the climate variability in Holocene (Mayewski et al. (2004)). The isotopic composition of the drip water, which feeds the stalagmites, is influenced by several climate dependent processes occuring i) above the cave (e.g., geographical position, amount and type of vegetation, rainfall amount, temperature), ii) in the soil/karst zone (e.g., flow path of the solution, p_{CO_2}, host rock dissolution occuring under open or closed conditions, and, iii) in the cave and on the surface of the speleothems (e.g., drip rate, p_{CO_2}). Inside the cave calcite precipitation results from the difference in p_{CO_2}, leading to a progressive degassing of CO_2 from the drip water, and, hence, to an increase in supersaturation with respect to calcite. The isotopic composition of the precipitated calcite depends on the isotope value of the drip water and on isotope fractionation processes between the different species involved in calcite precipitation. Generally, different fractionation processes must be distinguished. In case of equilibrium isotope fractionation, the relevant fractionation factors only depend on temperature. In case of kinetic isotope fractionation, which is expressed by a simultaneous temporal enrichment of $\delta^{13}C$ and $\delta^{18}O$ in the drip water due to continuous preferential degassing of the lighter isotopes, other parameters such as drip rate and cave p_{CO_2} also influence the isotope values. The isotope enrichment resulting under kinetic conditions can be described by a Rayleigh distillation scenario (Mickler et al. (2006), Scholz et al. (2009)).

Hendy (1971) introduced criteria to identify stalagmite samples influenced by kinetic isotope fractionation. In the so called 'Hendy-Test' the isotopic evolution along individual growth layers is analysed. If enrichment of $\delta^{18}O$ and $\delta^{13}C$ along the growth layer and a positive correlation between both isotopes is observed, this is an indication for calcite precipitation under disequilibrium conditions.

A recent study by Mickler et al. (2006) indicated that most of the investigated stalagmites show evidence for calcite precipitation under kinetic conditions. To interpret the stable isotope signals of such stalagmites in terms of past climate variability, it is necessary to

understand the chemical and physical reactions occuring in the drip water during calcite precipitation.

In recent years, numerical models have been developed describing the evolution of $\delta^{13}C$ and $\delta^{18}O$ in the drip water in dependence of several parameters such as temperature, drip rate, and initial saturation state of the drip water (Mickler et al. (2006), Romanov et al. (2008), Dreybrodt (2008), Scholz et al. (2009), Mühlinghaus et al. (2009)). Most of these models are based on a Rayleigh fractionation process. The model results strongly depend on the rate constants used to describe the chemical reactions and the fractionation factors (equilibrium and kinetic). Important rate constants are i) the exchange time, τ, between the bicarbonate and the CO_2 in the solution, which is the rate limiting step for calcite precipitation (Buhmann and Dreybrodt (1985a), Baker et al. (1998)), and ii) in case of $\delta^{18}O$, the buffering time, b, describing the isotopic exchange reactions between the reservoir of the dissolved inorganic carbon and the water reservoir (Hendy (1971)). Some of these rate constants have not been determined precisely yet.
In addition, the models do not take into account the possible influence of crystal growth mechanisms (Kunz and Stumm (1984), Lebrón and Suárez (1998), Fernandez-Diaz et al. (2006)), which depend on the degree of supersaturation and/or the presence of other ions in the drip water such as organic material or trace elements.

Laboratory experiments are, thus, necessary to quantitatively determine these parameters. Furthermore, they allow to detect processes not yet considered in theoretical models.

Within this work laboratory experiments with synthetic carbonates were performed under controlled conditions to improve the understanding of isotope fractionation of oxygen and carbon stable isotopes in speleothems. Several parameters such as the initial composition of the solution, temperature and drip rate were varied within the experiments.

In addition, in situ experiments with an analogous set-up were carried out in two different cave systems in Sauerland/Germany (Bunkerhöhle and B7-Höhle). The modern calcite collected at three drip sites was analysed and compared with the laboratory experiments.

Chapter 2

Basics

2.1 Stalagmites as paleoclimatic archives

To reconstruct past climate variability, records from several climate sensitive archives are used such as tree rings, ice cores and oceanic sediments. Since the late 1960s, speleothems (calcite depositions in caves) have become more and more important with respect to paleoclimate information. The history of speleothems as paleoclimate archives are for example described in Harmon et al. (2004).
The advantages of speleothems besides their precise dating is their global distribution over about 10% of the planet landmass (Ford and Williams (2007)). Furthermore, the cave environment provides stable conditions with respect to temperature and humidity. The cave temperature represents the mean annual external air temperature with variablility less than $1°C$, and within the most cave systems relative humidity is about 90%.

Paleoclimate proxies most commonly used in association with speleothems are the natural stable isotopes of carbon and oxygen, ^{13}C and ^{18}O [1]. In recent years, numerous isotope records from speleothems taken from caves all over the world were interpreted in terms of climate variability (e.g., Spötl and Mangini (2002) Niggemann et al. (2003), Fleitmann et al. (2004), Frisia et al. (2006), Wang et al. (2008)).
Other speleothem proxies are minor- or trace elements like magnesium, strontium and barium (e.g., Roberts et al. (1999), Fairchild et al. (2000), Johnson et al. (2006)), noble gases within fluid inclusions (Kluge (2008)), $^{13}C -^{18} O$ bonds (Ghosh et al. (2006)), the magnesium isotope ^{26}Mg (Buhl et al. (2007)), and lipid biomarkers based upon bacteria and fungi (Xie et al. (2003)). In this context the minor- and trace elements and the magnesium isotope mainly represent a precipitation signal whereas the noble gases and the $^{13}C -^{18} O$ bonds are correlated to a temperature signal.
For isotopic studies of ^{13}C- and ^{18}O usually stalagmites are preferred over other speleothem samples due to their distinct stratigraphy, often characterised by annual laminations. The growth axis of stalagmites represents a time scale which can be dated for example by U-series (Scholz and Hoffmann (2008)).

[1] ^{18}O and ^{13}C show natural abundances of 0.204% and 1.11%, respectively.

The formation of speleothems is strongly associated with drip water chemistry, drip mechanics (e.g., drip interval) and environmental parameters in the cave (e.g., CO_2 partial pressure). Drip water chemistry is to a large part influenced by processes in the soil and karst zone above the cave (Buhmann and Dreybrodt (1985a)). The processes which control and influence the environmental signals are described in detail in Fairchild et al. (2006). The complexity of speleothem proxies lies in their sometimes ambiguous character. Often stalagmites taken from the same cave show different results in absolute isotope values. The discrepancies may result from local drip water flow path mechanisms or differing drip intervals. These factors have to be considered while interpreting isotope data.

The major problem in paleoclimate interpretation is the transfer from high resolution records to climatic quantities such as absolute temperature and precipitation rate. Theoretic models calculating the isotope evolution during calcite precipitation help to improve general understandings (e.g., Michaelis et al. (1985), Lee and Bethke (1996), Dreybrodt (2008), Scholz et al. (2009), Mühlinghaus et al. (2009)). To test theoretical models and to determine the dependence of several parameters included in speleothem formation, experimental studies simulating stalagmite growth in the laboratory are carried out (e.g., Kim and O'Neil (1997)).

2.2 Calcite-carbonate system

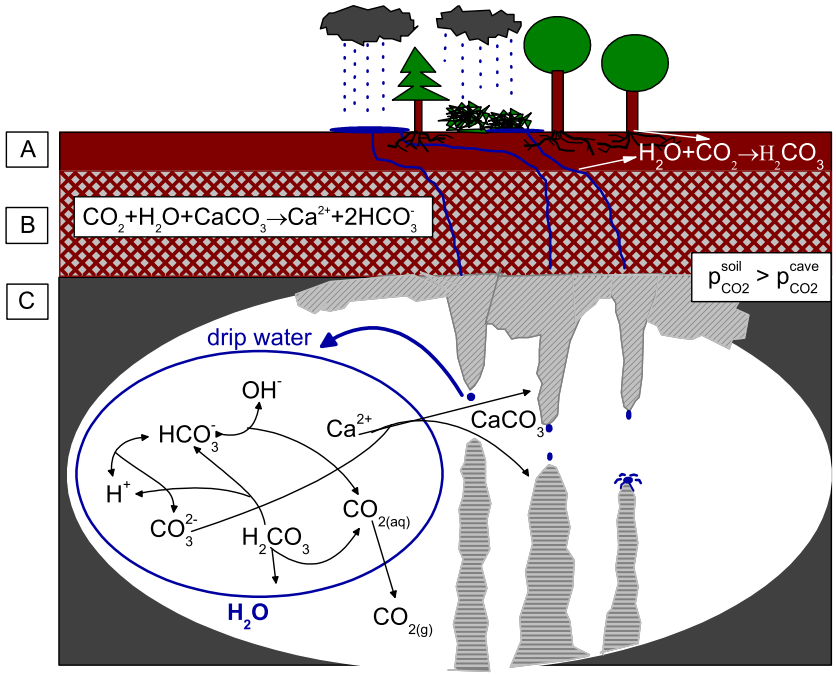

Figure 2.1: *Scheme, basically illustrating the formation of speleothems.*

Calcite precipitation and calcite dissolution are linked to the system $H_2O - CO_2 - CaCO_3$, which is characterised by a complex chemistry including numerous reactions, each with specific equilibrium- and rate constants. Detailed descriptions of this system and related processes can be found in literature (e.g., Holland et al. (1964), Plummer and Busenberg (1982), Salomons and Mook (1986), Matthess et al. (1992), Clark and Fritz (1997)). The fundamental processes of the calcite-carbonate system are presented in Fig. 2.1.

The single physical and geochemical processes i.e., the infiltration of meteoric water into the soil zone, the calcite dissolution in the karst zone and the precipitation of calcite inside the cave environment, can be divided into three steps, also pointed out in Fig. 2.1 by the letters $A - C$.

(A) soil zone: formation of dissolved inorganic carbon (DIC)

Meteoric water infiltrates into the soil zone, in which the CO_2 partial pressure (p_{CO_2}) is 1 to 3 orders above the atmospherical partial pressure ($p^{atm}_{CO_2} \approx 10^{-3.42} \approx 380\ ppm$). The increased p_{CO_2} in the soil zone is caused by root respiration and decomposition of organic matter. Subsequently, the meteoric water equilibrates with the soil p_{CO_2} by dissolving gaseous $CO_{2(g)}$. Carbonic acid is formed due to hydration reaction:

$$CO_{2(g)} + H_2O \rightarrow H_2CO^*_3, \tag{2.1}$$

with $H_2CO^*_3 = CO_{2(aq)} + H_2CO_3$ as a general convention because the concentration of dissolved carbon $[CO_{2(aq)}]$ exceeds the concentration of carbonic acid $[H_2CO_3]$ by a factor of approx. 600 at $25°C$.

Carbonic acid dissociates in two steps:

$$H_2CO^*_3 \rightarrow H^+ + HCO^-_3 \rightarrow 2H^+ + CO^{2-}_3 \tag{2.2}$$

In summary, the total dissolved inorganic carbon content in the water is a composition of the following species: dissolved or aqueous carbon ($CO_{2(aq)}$), carbonic acid (H_2CO_3), bicarbonate (HCO^-_3), and carbonate (CO^{2-}_3). The relative concentration of the individual species is a function of the pH (Fig. 2.2). It is evident that in the pH-range relevant for speleothem drip waters (i.e., 6.5 - 8.9), HCO^-_3 represents the dominant species with a percentage around 95%.

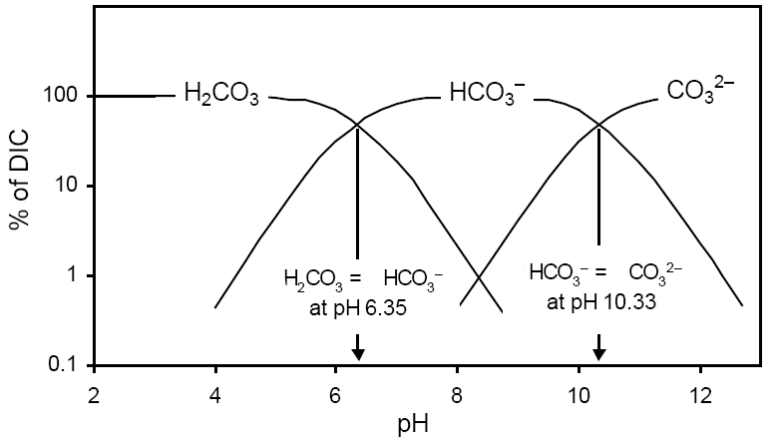

Figure 2.2: *Percentage of carbonate species as a function of pH (from Clark and Fritz (1997)).*

(B) karst zone: dissolution of calcite

If the acidified meteoric water gets in contact with calciferous rocks in the subsoil, calcite is dissolved by different chemical processes depending on the pH-range (Plummer et al. (1978)). In the relevant pH-range the H_2CO_3-dissociation represents the dominant process:

$$CaCO_3 + H_2CO_3^* \rightarrow Ca^{2+} + 2HCO_3^- \tag{2.3}$$

Furthermore, the dissolution process depends on the basic conditions of the system, i.e., if the system is open or closed with respect to CO_2. In an open system the acidified water dissolves $CaCO_3$ in contact with a gas phase of fixed p_{CO_2}. In a closed system the water equilibrates with an available CO_2-reservoir before dissolving $CaCO_3$. Detailed descriptions and calculations can be found in Buhmann and Dreybrodt (1985a) and Buhmann and Dreybrodt (1985b). Dissolution processes in case of turbulent or flowing water films are described in Dreybrodt and Buhmann (1991) and Dreybrodt and Kaufmann (2007). Mixing between open and closed systems can be found in Fohlmeister (2008).

(C) cave environment: precipitation of calcite

When the water finally enters the cave environment, a lot of different chemical processes take place induced by a difference in p_{CO_2} between the cave atmosphere[2] and the solution, which is enriched in CO_2 after percolating through the soil zone.

The major chemical reactions and the net reaction are:

$$Ca^{2+} + CO_3^{2-} \rightarrow CaCO_3 \tag{2.4}$$

$$HCO_3^- \rightarrow CO_3^{2-} + H^+ \tag{2.5}$$

$$H^+ + HCO_3^- \rightarrow H_2CO_3^* \tag{2.6}$$

$$H_2CO_3^* \rightarrow CO_{2(aq)} + H_2O \tag{2.7}$$

$$\overline{Ca^{2+} + 2HCO_3^- \rightarrow CO_{2(g)} + H_2O + CaCO_3} \tag{2.8}$$

To reach equilibrium with the cave p_{CO_2}, the solution has to dissipate the HCO_3^--excess by converting HCO_3^- into CO_2, which is expressed by Eqs. ((2.5)-(2.7)). Subsequently, the CO_2 will degas from the solution due to diffusion processes. The CO_2-degassing can occur continuously, for example in the case of a steadily solution flow along a stalactite or sinter wall. Otherwise, for a dropping down solution the resulting impinge leads to a sudden CO_2-degassing (Dreybrodt (2008)). While due to CO_2-degassing the solution gets closer to CO_2-equilibrium, at the same time the solution departs from $CaCO_3$-equilibrium, expressed by an increase in the saturation index with respect to calcite. The resulting supersaturation causes the formation of calcite from CO_3^{2-}- and Ca^{2+}-ions (Eq. (2.4)), which again is coupled with various chemical reactions. First, the CO_3^{2-}-ions have to be released from the compound of HCO_3^- where they are mainly bound. Hence, the bicarbonate will dissociate (Eq. (2.5)). To fulfill stoichiometry the remaining H^+-ion will combine with another HCO_3^--ion to form $H_2CO_3^*$ (Eq. (2.6)). $H_2CO_3^*$ in turn will dissociate into H_2O and $CO_{2(aq)}$ (Eq. (2.7)). The latter will degas from the solution and the CO_3^{2-}-ion will combine with the Ca^{2+}-ion to form $CaCO_3$ which can precipitate as solid calcite (net reaction Eq. (2.8)).

Other reactions within the solution, which are of great importance for the isotope exchange between the oxygen isotope in the water and the dissolved inorganic carbon content, are the CO_2-hydration and the CO_2-hydroxilation reactions (Eqs. (2.9) and (2.10)). The hydroxilation reaction dominates for $pH > 8$ (Hendy and Wilson (1968)).

hydration:

$$CO_2 + H_2O \rightarrow H_2CO_3^* \rightarrow HCO_3^- + H^+ \tag{2.9}$$

hydroxilation:

$$CO_2 + OH^- \rightarrow HCO_3^- \tag{2.10}$$

Each of the chemical reactions specified in this section is linked to a certain reaction rate (described for example in Dulinski and Rozanski (1990) and Arakaki and Mucci (1995)). The rate limiting step within calcite precipitation kinetics is the combined conversion reaction

[2] $p_{CO_2}^{cave}$ usually ranges between 500 *ppm* and 1500 *ppm*.

$H^+ + HCO_3^- \rightarrow CO_2 + H_2O$ (Eqs. (2.6) and (2.7), Dreybrodt et al. (1997)). The conversion from HCO_3^- into CO_2 and H_2O is generally a slower process than CO_2-degassing from the solution, valid in the case of thin solution films (Buhmann and Dreybrodt (1985a)). However, the conversion rate can potentially get enhanced by special enzymes (carbonic anhydrase), which act as a reaction catalyser. These enzymes, which were also detected in speleothems increase the rate about a factor of 15 (Dreybrodt et al. (1997)).

2.3 Calcite crystallisation

A crystal is defined as a polyhedral, homogeneous solid with specific faces and corners in which the constituent atoms, molecules, or ions are packed in a regularly order extending in all three spatial dimensions. Calcite offers a trigonal crystal system with different habits such as isometric (preferred growth in 3 axes, e.g., cubic), flat/lamellar (preferred growth in 2 axes), and acicular/prismatic/fibrous (preferred growth in 1 axis). A detailed description can for example be found in Onac (1997) and Self and Hill (2003). Furthermore, various structures or fabrics exist for calcite. Typical cave calcite, generally termed as speleothems, include dripstones (stalagmites, stalactites), soda straws, rimstone, flowstones, and crusts or floating rafts within cave pools. The evolution and growth characteristics of cave carbonates are described for example in Kunz and Stumm (1984), Nielsen and Toft (1984), Lebrón and Suárez (1998) or Fernandez-Diaz et al. (2006).

A required criteria for the formation of calcite is the supersaturation of the feeding solution with respect to calcite. To describe equilibrium conditions within solutions the law of mass action is used. For a general reaction $aA + bB \leftrightarrow cC + dD$ the temperature dependent equilibrium constant K is defined as:

$$K = \frac{[C]^c[D]^d}{[A]^a[B]^b} \tag{2.11}$$

In Eq. (2.11) the square brackets specify the activity of the single species or the 'effective concentration', respectively. In contrast to the 'concentration' of a species, the 'activity' describes the correction due to electrostatic shielding effects and complexation of the ions. The correction factor is expressed by the activity coefficient, γ, which can be determined by the Debye-Hückel equation. In case of diluted solutions, and if no other ions are present, γ is equal to one.

To define the saturation state of a species the analytically determined solubility product K is related to the activity product (IAP) of the respective species. The ratio of these two products is defined as saturation state:

$$\Omega = \frac{measured\,activities}{activities\,in\,equilibrium} = \frac{IAP}{K} \tag{2.12}$$

The saturation index SI is defined as the log of Ω:

$$SI = log(\Omega), \tag{2.13}$$

with
$\Omega = 1$ or $SI = 0 \rightarrow$ equilibrium
$\Omega < 0$ or $SI < 0 \rightarrow$ undersaturation
$\Omega > 0$ or $SI > 0 \rightarrow$ supersaturation

The SI with respect to CO_2 can be expressed as:

$$SI_{CO_2} = log(p_{CO_2}[atm]) \tag{2.14}$$

In the case of $CaCO_3$ the SI can be expressed as:

$$SI_{CaCO_3} = log\frac{[Ca^{2+}][HCO_3^-]}{K} \tag{2.15}$$

Hence, the SI_{CaCO_3} depends on the concentration of the species, the temperature and the pH, which correlates with the p_{CO_2}.

The degree of saturation has a significant effect on crystallisation processes. Calcite crystallisation begins stepwise with the formation of a seed crystal or nucleus whereas little is known about the prenucleation state (Gebauer et al. (2008)). Subsequently to the generation of nuclei, crystal growth can occur. Fig. 2.3 (based on Nielsen and Toft (1984)) shows the different saturation regimes in association with crystal growth mechanisms in an activity plot of Ca^{2+} and CO_3^{2-}. The individual zones are separated by straight lines, which represent values of constant growth rates excluding effects like ionic bonds, complexation or transport-controlled growth. In the undersaturated zone solely dissolution processes can take place, while crystal growth is not possible. Subsequent to the transition area between the undersaturated zone and the supersaturated zone, the metastable phase indicates a zone, in which existing crystals may grow further, sometimes denoted as 'crystal growth'. With increasing supersaturation heterogeneous nucleation may occur, where crystal growth is accompanied by nucleation at existing surfaces or substrates, which act as crystallisation seeds. If a certain degree of supersaturation is reached, homogeneous crystallisation is possible. In this case nucleation occurs without an accretion seed. From laboratory experiments conducted by Kunz and Stumm (1984) homogeneous nucleation begins at least at a 10-times supersaturation.

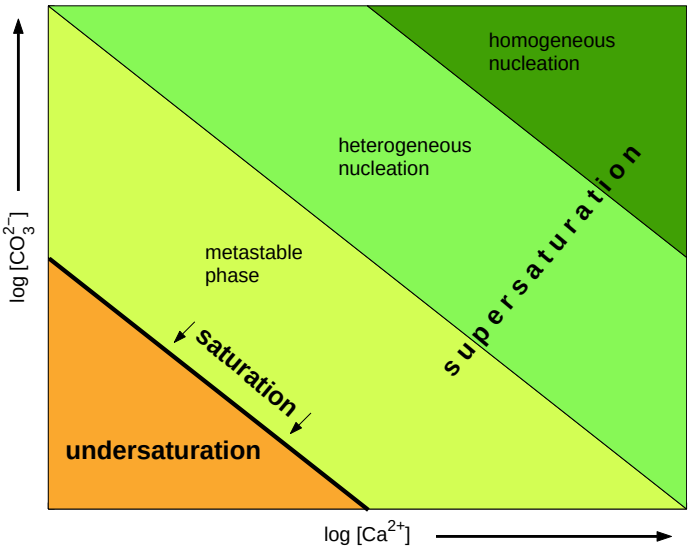

Figure 2.3: *Crystal growth in dependence of the saturation state (modified after Nielsen and Toft (1984)).*

2.4 Isotope fractionation

2.4.1 Definition and notation

Isotope fractionation is defined as an isotopic exchange between different species or phases in a reaction. The stable isotopes ^{13}C and ^{18}O are usually expressed by the δ-notation. $\delta^{13}C$ and $\delta^{18}O$ indicate the ratio of the number of rare isotopes and abundant isotopes in a sample relative to the ratio of a classified standard:

$$\delta^{13}C = \left[\frac{(^{13}C/^{12}C)_{sample}}{(^{13}C/^{12}C)_{standard}} - 1\right] \cdot 1000‰, \text{ with } (^{13}C/^{12}C)_{standard} = 0.011237 \text{ (VPDB)}^3$$

$$\delta^{18}O = \left[\frac{(^{18}O/^{16}O)_{sample}}{(^{18}O/^{16}O)_{standard}} - 1\right] \cdot 1000‰, \text{ with } (^{18}O/^{16}O)_{standard} = 2.005 \cdot 10^{-3} \text{ (VSMOW)}^4$$

The $\delta^{18}O$-value of the precipitated calcite depends on both the oxygen isotopic composition of the cave seepage water, which mainly reflects the isotopic composition of the rainwater, and the temperature dependent fractionation mechanisms between the calcite and the water as dominant source for oxygen in the solution (Ford and Williams (2007)).

The $\delta^{13}C$-value of the precipitated calcite depends on the isotopic composition of the dissolved inorganic carbon in the drip water, which is a combination of several effects (Ford and Williams (2007)). Factors which contribute to the carbon isotopic content in the drip water are the atmospheric CO_2, the biogenic CO_2 (vegetation above the cave), the dissolved carbonate of the host rock (mainly ancient marine carbonate rocks, Salomons and Mook

[3] Vienna Pee Dee Belemnite
[4] Vienna Standard Mean Ocean Water

(1986)), the ratio of open to closed limestone dissolution system (Buhmann and Dreybrodt (1985a), Buhmann and Dreybrodt (1985b)), and the degassing rate of CO_2. Due to the high number of carbon sources, the interpretation of flucuations in $\delta^{13}C$-records are more ambiguous. Hence, in paleoclimate studies $\delta^{18}O$ is preferentially taken as proxy (Fairchild et al. (2006)).

2.4.2 Fractionation mechanisms

Isotope fractionation between two chemical phases is based on the different physical characteristics of lighter and heavier isotopes (in detail see Mook (2000)).
During calcite precipitation isotope fractionation occurs not only between the drip water and the solid calcite, but also between the drip water and the gaseous CO_2. Generally, the fractionation between two species or phases A and B is expressed by the dimensionless fractionation factor, α, which ideally depends only on temperature:

$$\alpha_{A-B} = \frac{R_B}{R_A}, \tag{2.16}$$

with $R = \frac{N_i}{N} = \frac{number\ of\ rare\ isotope}{number\ of\ abundant\ isotope}$

Because α is close to 1, an enrichment factor, ϵ, is defined indicating the isotopic enrichment between two phases:

$$\epsilon = 1000 \cdot (\alpha - 1) \approx 1000 \cdot ln(\alpha) \tag{2.17}$$

Values of α and ϵ depend on the particular fractionation mechanism, i.e., if the fractionation occurs under equilibrium- or kinetic conditions. In case of equilibrium fractionation the reactants and products within a chemical reaction have adequate time for isotope exchange. If a reactant or product is rapidly added/removed to/from a reaction system, non-equilibrium or kinetic fractionation occurs. Kinetic fractionation occurs for example in case of fast calcite precipitation (Turner (1982)), fast CO_2-degassing (Hendy (1971)), or if evaporation is present (Wiedner et al. (2008)). Fast CO_2-degassing can be described via a special kinetic model, the so called Rayleigh fractionation[5] (e.g., Mook (2000)): If dN_i molecules of the rare isotope and dN molecules of the abundant isotope with the ratio $\frac{dN_i}{dN}$ will be removed from a phase with the molecule ratio $\frac{N_i}{N}$, then fractionation can be expressed by:

$$\frac{dN_i}{dN} = \alpha \cdot \frac{N_i}{N} \tag{2.18}$$

After substitution and integration with the initial values R_0 and N_0, Eq. (2.18) yields:

$$\frac{R}{R_0} = \left(\frac{N}{N_0}\right)^{(\alpha-1)} \tag{2.19}$$

[5]Rayleigh originally derived a formula to calculate the products of distillation for a mixture of liquids with different boiling points. In this context Rayleigh fractionation is sometimes denoted as Rayleigh distillation but both expressions are related to the same process.

The term $(\frac{N}{N_0})$ in Eq. (2.19) describes the remaining fraction, f, of the reactant, because $\frac{N_i}{N} << 1$, and therefore $N \approx N + N_i$, which leads to:

$$R = R_0 \cdot f^{(\alpha-1)} \tag{2.20}$$

Eq. (2.20) demonstrates that the isotope ratio, R, in a diminishing reservoir of the reactant is a function of the initial isotope ratio, R_0, the remaining fraction of the reservoir, f, and the equilibrium fractionation factor, α. In general, α represents a combination of the participating species $\alpha_{product-reactant}$.
Converting the isotope ratios into δ-values, considering $\delta << 1$ yields:

$$ln\left(\frac{\delta + 1000}{\delta_0 + 1000}\right) = (\alpha - 1) \cdot ln(f) = \frac{\epsilon}{1000} \cdot ln(f) \approx (\delta - \delta_0)/1000 \tag{2.21}$$

Generally, in paleoclimate interpretation equilibrium isotope fractionation is preferred because the fractionation factors only depend on temperature. To test stalagmite samples on equilibrium conditions, the drip water of active growing stalagmites is compared to modern calcite precipitation. Furthermore, in certain cases it is possible to compare isotope records of neighbouring speleothems but this is not necessarily univocal due to different epikarstic flow routes and storage of the drip water. A better test is the so called Hendy-test (Hendy and Wilson (1968)), carried out along individual growth layers of a stalagmite. A progressive enrichment of $\delta^{13}C$ and $\delta^{18}O$ along a single layer and/or a positive correlation of both isotopes indicate fractionation under kinetic conditions.

Chapter 3

Laboratory experiments

3.1 Intention

Calcite precipitation in caves is influenced by several parameters such as temperature, drip rate, solution composition, and p_{CO_2}. Low temperatures, high drip rates and low supersaturation of the solution with respect to calcite preferentially lead to equilibrium isotope fractionation between the calcite and the corresponding drip water. In this case the fractionation factor, α, only depends on temperature and could theoretically and experimentally be determined for the different species involved in the calcite precipitation process. However, for the most natural cave systems this is only valid to some extent. More often evidence exist for kinetic fracitionation between calcite and drip water indicated by the enrichment of both $\delta^{13}C$ and $\delta^{18}O$ along a single growth layer and by a positive correlation between these isotopes along a growth layer, respectively (Hendy (1971)). In this case interpretation of the isotope data in terms of climate change is much more complicated because kinetic isotope fractionation not only depends on temperature, but also on various parameters, which can be temperature-dependent themselves.

By now several model calculations have been carried out to describe the evolution of the $\delta^{13}C$- and $\delta^{18}O$-value of the bicarbonate in the solution (e.g., Mickler et al. (2006), Romanov et al. (2008), Dreybrodt (2008), Scholz et al. (2009), Mühlinghaus et al. (2009)). All model calculations depend on the different chemical reaction rates included in the calcite precipitation mechanism such as calcite precipitation rate, HCO_3^--CO_2-conversion rate, or the CO_2-hydration and CO_2-hydroxilation rates. The latter are important in the case of modelling the evolution of $\delta^{18}O$, which is much more complicated than $\delta^{13}C$ because of the influence of the water reservoir, which buffers the oxygen isotope composition.

Laboratory experiments help to investigate and quantify the effects induced by kinetic isotope fractionation under varying parameters such as temperature, drip rate, or solution composition. In addition, the experiments provide information about the general aspects of calcite precipitation and crystallisation characteristics under varying parameters.

3.2 Summary of previous laboratory experiments

Up to now several laboratory experiments with synthetic carbonate were carried out under varying aspects (e.g. Fantidis and Ehhalt (1970), Kim and O'Neil (1997), Huang and Fairchild (2001), Fernandez-Diaz et al. (2006), Wiedner et al. (2008)).
Kim and O'Neil (1997) studied the effect of different initial concentrations of calcium- and bicarbonate-ions on the oxygen isotope composition by bubbling N_2 through a saturated $CaCO_3$-solution. This promotes supersaturation, and, hence calcite precipitation by removal of CO_2. They conclude that the oxygen isotope fractionation factor strongly depends on the initial concentration of the calcium- and bicarbonate-ions and present a new oxygen isotope equilibrium fractionation factor resulting from 'appropriate conditions of precipitation'.
Huang and Fairchild (2001) simulated stalagmite conditions by pumping initial $CaCl_2$- and $NaHCO_3$-solutions through a tube, where the solutions are mixed. Afterwards the solution drips out of a natural or glass straw (analoguous to a stalactite) onto a natural stalagmite or a precoated convex glass plate. The intention of their experiments was the determination of the temperature dependent partitioning coefficients for Sr^{2+} and Mg^{2+}.
Fernandez-Diaz et al. (2006) investigated the influence of divalent cations on the calcite crystal morphology using a column of porous silica hydrogel, in which calcite precipitated during a period of one year.

The laboratory experiments accomplished in this study are based on the set-up of Fantidis and Ehhalt (1970), who used 1.5 m long semicircular glass channels with a diameter of 15 mm, which were slightly inclined. On the channels a steadily flowing bicarbonate solution with an adjustable flow speed led to the precipitation of calcite by degassing of CO_2. This set-up, which is described in detail in the PhD-thesis of Fantidis (1969) mimics the flow of the solution along a stalagmite. In contrast to the drip experiments of Huang and Fairchild (2001) the channels provide a time axis. Thus the isotopic evolution of the precipitated calcite can be investigated with the main focus on the kinetic isotope fractionation. In general, their experimental set-up has some deficiencies: (i) The experiment was conducted in the laboratory under free air with maximum humidities of only 40%, which facilitates the possibility of evaporation. (ii) The initial solutions were produced by dissolving 30 g of calcite in 60 l of distilled water under supply of gaseous CO_2. Prior calcite precipitation can, thus, not be ruled out. Furthermore, the composition of the solution, which finally dripped on the top of the channel was not determined for all species for example the amount of dissolved Ca^{2+}.
In recent years, Wiedner (2004), Gewies (2003) and März (2006) modified and improved the set-up of Fantidis and Ehhalt (1970) and carried out laboratory experiments to investigate the fractionation processes of the stable isotopes $\delta^{13}C$ and $\delta^{18}O$ within synthetic carbonates. Wiedner (2004) studied the fractionation processes in stagnant water (beaker experiments) as well as in experiments using a flowing solution (channel experiments) under varying parameters such as temperature, solution composition, beaker volume and solution flow velocity. In contrast to the experiments of Fantidis and Ehhalt (1970), the experiment was now located in a gas distributor placed inside a refrigerator to control temperature and atmosphere. Furthermore, the initial solution for calcite precipitation was created from two separate solutions, which were mixed within a mixing cell before reaching the channel.

Gewies (2003) mainly tested and improved the technical parameters of the experiment set-up. Finally, März (2006) investigated the influence of magnesium on the fractionation process and determined the temperature dependent magnesium distribution factor with the same experiment set-up. The determined factor agreed quite well with the published value range confirming the experimental set-up.

3.3 Experimental method

3.3.1 Set-up

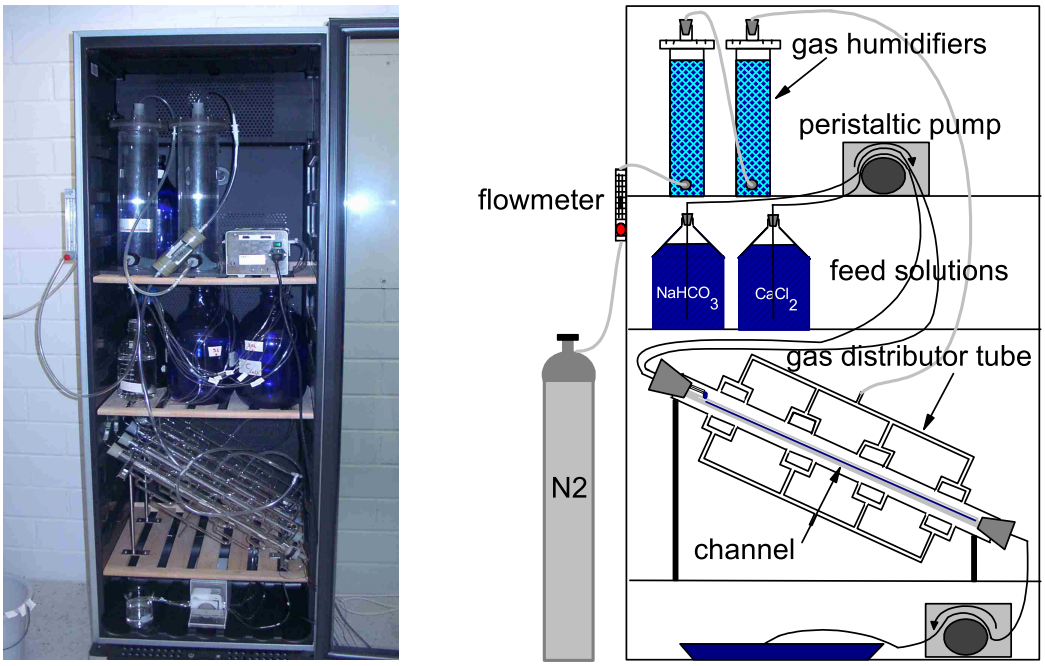

Figure 3.1: *Picture (left) and sketch (right) of the experiment set-up used to precipitate synthetic carbonates under controlled conditions in the laboratory.*

Fig. 3.1 shows the laboratory experiment set-up first implemented by Wiedner (2004) and Gewies (2003) which later was subsequently modified by März (2006) and also within this work.
The experiment itself is conducted in a refrigerator to provide stable temperature conditions. The feed solutions were prepared likewise to the method of Huang and Fairchild (2001). Inside two separate glass vessels the pure anorganic salts of $NaHCO_3^-$ and $CaCl_2$ were

dissolved in Milli-Q®-water before equilibrating the solution with atmospheric p_{CO_2}[1] by bubbling humidified air into the vessels. The mix of the two solutions is chemically expressed by the reaction:

$$CaCl_{2\,(aq)} + 2NaHCO_{3\,(aq)} \rightarrow Ca^{2+}_{(aq)} + 2HCO^{-}_{3\,(aq)} + 2Na^{+}_{(aq)} + 2Cl^{-}_{(aq)} \tag{3.1}$$

If the resulting solution is supersaturated with respect to calcite, which depends on the concentrations of the inorganic salts, temperature and the p_{CO_2}, calcite will precipitate by the reaction:

$$Ca^{2+}_{(aq)} + 2HCO^{-}_{3\,(aq)} + 2Na^{+}_{(aq)} + 2Cl^{-}_{(aq)} \rightarrow CaCO_3 + H_2O + CO_2 + 2Na^{+}_{(aq)} + 2Cl^{-}_{(aq)} \tag{3.2}$$

In this context dissolved ions of halite ($NaCl$) are negligible because they will afloat with the rest of the solution. Supersaturation with respect to calcite does not necessarily result in calcite precipitation within a certain time range, because the rate of the equilibrium reaction depends not only on the degree of supersaturation but also on the specific surface over which the solution is flowing. For example a coarse surface would promote heterogeneous calcite crystallisation whereas on a smooth surface the accumulation of crystal seeds is unlikely.
In the experiments a binder-free glass microfibre from Whatman® with a thickness of 260 μm and a basis weight of 530 g/m^2 was used as a substrate for calcite precipitation. The glass fibre was cut into stripes with a length of 50 cm and a width between 0.4 cm and 0.6 cm before it was put into a u-shaped glass channel (Fig. 3.2) and wetted with Milli-Q®-water.

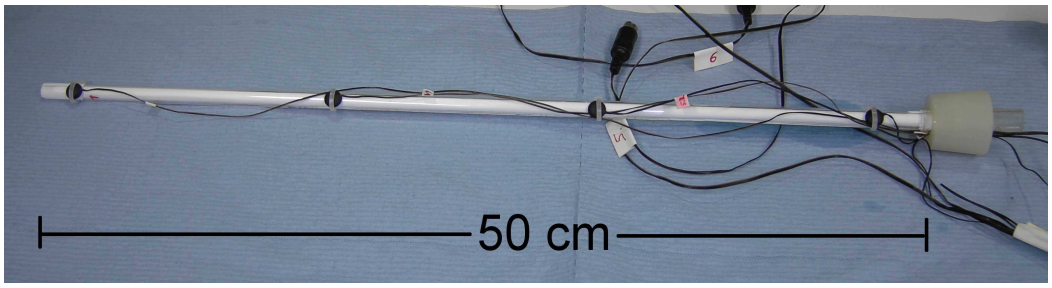

Figure 3.2: *Picture of the u-shaped glass channel with the glass fibre stripe inside. Four temperature sensors attached at the undersurface of the glass channel were used for spatial and temporal temperature control during the experiment.*

After starting the experiment the feed solutions were pumped into the channel system via a peristaltic pump through Tygon®-LFL tubes. Subsequently, the mix solution dripped out of stainless steel drop capillaries and aggregate as single drops to the initial solution before dripping into the channel and flowing along the glass fibre stripe. It is important that the mixing of the solutions takes place directly before dripping into the channel to prevent prior calcite precipitation inside the tubes or capillaries. The mixing reaction is supposed to proceed fast enough to provide full mixing (pers. comm. Andrea Seehuber).
The 32°-sloped channel is located inside a gas distributor, which is flushed with nitrogen (nitrogen N40 from AirLiquide) with a rate of approx. 80 ml/min through 8 openings to

[1] The term 'atmospheric' refers to the laboratory atmosphere with $p^{lab}_{CO_2} \approx 480\ ppm$

provide a constant air flow over the solution. To avoid evaporation effects, the nitrogen gas was humified in advance by bubbling the gas via frits through two plexiglas®-colums filled with pure water. After the humidifier colums the nitrogen is assumed to be saturated with water to provide humid conditions within the channel system.
To assure a permanent gas flow and to avoid back-diffusion and exchange effects between the gas and the solution, at the end of the channel the solution is pumped down together with the enriched gas.
To increase the amount of data, a device was constructed holding 4 channels systems in total. Thus, 4 experiments could be carried out simultaneously.

3.3.2 Comparison between cave system and laboratory set-up

Fig. 3.3 shows a comparison of a natural cave system and the laboratory system. Both systems offer similar basic conditions for calcite precipitation. They offer a gradient in p_{CO_2} and the sloped channel represents the analogue to the stalagmite where the solution flows along the side forming the single growth layers. Single mechanisms, however, are different for both systems.
1) While for the cave drip water supersaturation with respect to calcite mainly results from the sudden loss of CO_2 during the impinge of the drop on the stalagmite tip, the laboratory experiments do not include this process due to the small distance between the drip capillaries and the glass fibre stripe causing the drops rather to slide onto the filter instead of falling.
2) However the initial solution within the experiment is already supersaturated with respect to calcite comparable to the values of the drip water after impinging. In addition, the solution is far from CO_2-equilibrium in the experiments when reaching the channel system due to the nitrogen atmophere. For cave drip water it is not really clear to which degree the equilibrium with the cave p_{CO_2} is reached after the impinging. Dreybrodt (2008) for example states that after the impinging the drip has equilibrated with the cave p_{CO_2}, but quantitative measurements are lacking.

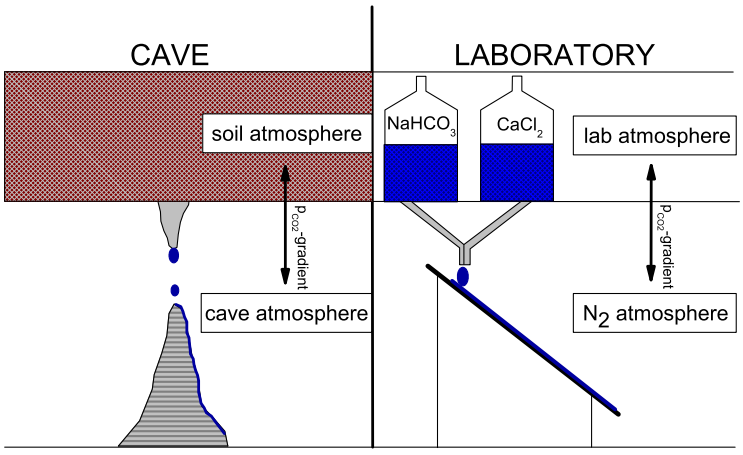

Figure 3.3: *Comparison between the cave system (left) and the laboratory set-up (right).*

3.3.3 Research parameters

The basic conditions of the experiments with synthetic carbonate in the laboratory were adjusted such as in a natural cave environment. Nevertheless some limitations have to be made to keep the experiment conditions practicable. Potential effects resulting from the technical set-up must be avoided. In addition, the number of parameters was limited to focus on the effects caused by the change of selective parameters.
The main parameters varied within the laboratory experiments were temperature, drip rate, and initial concentration of $Ca^{2+}-$ and HCO_3^--ions. Additionally, in some experiments different channel materials and substrates were used to study the influence of different surfaces on the calcite precipitation. Furthermore, experiments with humid and dry laboratory atmosphere instead of N_2 were carried out to test if CO_2-degassing or calcite precipitation is the dominant factor driving calcite precipitation within the channel experiments. A summary of the parameters used for the single experiments is given in Appendix A. Tab. 3.1 lists parameter ranges of the laboratory experiments together with observed parameter ranges from the monitoring-caves included in the DAPHNE research project (Bunkerhöhle and Grotta di Ernesto).

	laboratory	monitoring caves
temperature-range $[°C]$	$10-23$	$5.4-11.8$
drip rate-range $[s]$	$12-60$	$0.5-200$
pH-range	$8.16-8.62$	$7.7-8.3$
SI_{CaCO_3}-range	$0.68-1.08$	$0.37-0.73$

Table 3.1: *Parameter ranges used in the laboratory experiments and observed for the monitoring caves of the DAPHNE research project (Bunkerhöhle in Sauerland/Germany and Grotta di Ernesto in northern Italy).*

Temperatur

Most experiments were carried out at a temperature of $10°C$ equal to the average temperature of Bunkerhöhle. Lower temperatures would lead to less calcite precipitation because the solubility of Ca^{2+} increases with decreasing temperature. Thus, some laboratory experiments were run at $23°C$ comparable to temperatures of tropical cave systems to investigate the influence of temperature on the evolution of the isotope composition.

Drip rate and flow velocity

The drip rate used for the experiments is adjusted via the pump rate, and is technically limited by the diameter of the tube, which allows a maximum drip interval of 60 s. The drip rate was varied by a factor of ~ 5 within different experiments but the important criterion with respect to degassing and precipitation is the residence time of the solution on the channel. This is expressed by the flow velocity.
Assuming that the solution flow along the glass fibre stripe is constant, the theoretical flow velocity $v_{solution}$ can be calculated by:

$$v_{solution} = \frac{v_p}{d \cdot b} \tag{3.3}$$

$v_{solution}$ depends on the pump rate v_p as well as on the width b and thickness d of the solution film. The width of the solution film is theoretically identical with the width of the glass fibre stripe, which in most experiments was equal to 0.6 cm. The film-thickness of the solution was previously determined by Gewies (2003). He carried out a test experiment where he weighed the total amount of solution on the channel after stopping the solution flow (pump rate: 0.6 ml/min), taking into account the geometry of the glass fibre stripe. He determined the film-thickness for various inclinations of the channel and obtained values of 0.4 ± 0.02 mm for 30°.
Here in this work the solution flow velocity was again experimentally determined for two different pump rates (0.12 ml/min and 0.02 ml/min). To visualise the solution flow along the glass fibre, the filter stripe was completely saturated with an indicator solution. Subsequently, a saline solution was pumped onto the channel resulting in a stepwise red coloration of the glass fibre until the whole stripe was soaked with the red color.
Fig. 3.4 shows the flow velocity in cm/s versus the location on the glass fibre stripe in cm. The plot implicates that the flow velocity is not constant along the glass fibre stripe. When a single drop gets in contact with the wetted filter stripe, it spreads out with a relatively high velocity, subsequently decelerating, and reaching a more or less constant velocity after $5 - 7$ cm flow distance.

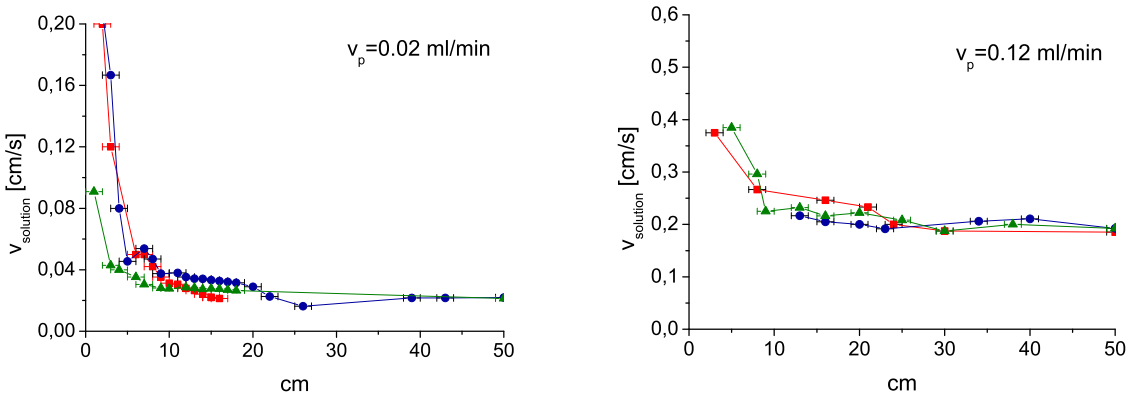

Figure 3.4: *Experimental determination of the flow velocity for two different pump rates (three tests in each case).*

Comparing the theoretical value for the solution flow velocity (Eq. 3.3) with the average of the experimentally determined values and omitting the values for the first 7 centimeters, it turns out that the theoretical value is half the amount of the experimental value. This is related to the fact that for the calculation of the theoretical value the whole width of the glass fibre stripe was used. In the experiment, however, it was observed that after a few centimeters the drop branches out covering half of the filter width whereas the wetting of the remaining filter area occurs batch-wise with the successive arrival of the next drops. If one calculates the theoretical flow velocity with $d = 0.04$ cm and $b = b/2$ the observed experimental value agrees with the theoretical value within 7%. The values for $v_{solution}$ in Appendix A refer to the experimentally determined velocities and linear interpolation in the case of other pump rates. It is likely that also the film thickness d slightly varies for

different flow velocities, but this effect should be negligible. In natural systems usually a film thickness between 0.005 *cm* and 0.01 *cm* is observed (Dreybrodt (1988), Dulinski and Rozanski (1990)).

Saturation Index of calcite

Previous to the experiments theoretical calculations were carried out using PHREEQC, a widely-used program for geochemical calculations (Appelo and Postma (2005)). Input parameters are the concentration of the initial salts of $NaHCO_3^-$ and $CaCl_2$, temperature and the $p_{CO_2}^{lab}$, which is used for the equilibration of the feed solutions. In the outputfile of PHREEQC the concentration of the single species and ions are listed together with the pH-value and the SI_{CaCO_3}. The pH-value here serves as a control parameter to test if the initial solutions are preparated correctly.
The relativly high SI_{CaCO_3}-range within the experiments (see Tab. 3.1), which represents the upper range of natural speleothem drip waters, is necessary to provide a reasonable experiment time of $30 - 40$ days at maximum, in which enough calcite is precipitated for a later analysis.

Channel materials

Usually a glass channel was used as a basis for the glass fibre stripe but other materials were also tested such as teflon®, plexiglas and metal. The solution flowing along the glass fibre stripe also has a lateral boundary with the surrounding channel, and, thus its surface properties have an influence on the flow characteristics of the solution. Substances with a high degree of surface energy have better wetting properties than substances with a lower surface energy such as teflon®. Waterdrops on a glass surface have a contact angle of 0° whereas in the case of teflon®, which is superhydrophobic, the contact angle is 119°. Using a layer of teflon® between the glass channel and the glass fibre stripe leads to different results with respect to the isotopic development, which is described in März (2006).
However, the degree of wetting has no effect on the rate of calcite crystallisation because this mainly depends on possible crystallisation seeds. Only at a SI_{CaCO_3}-value of at least 1, homogeneous crystallisation is possible. This, however, does not mean automatically that the generated microcrystals also do precipitate on a dipped flat surface like the glass channel. Without any kind of substrate the solution film along the glass channel frays out after 25 *cm* independent of the drip rate. Furthermore, the water retains at the bottom of the channel. Thus, the glass fibre stripe as a substrate does not only provide a crystallisation seed but also guarantees a more or less constant film thickness.

3.3.4 Data analysis

Subsequent to the experiments, samples were prepared for analysis of the isotope composition, the cation content and in case of the solution samples the pH-values and carbonate hardness. The analysis of the solution samples is necessary to test if the concentration of the different cation and anion components match the parameters set prior to the experiments. The knowledge of these parameters allows to set up a mass balance. To determine the amount of bicarbonate dissolved in the solution a carbonate hardness test was carried out indicating the degree of 'deutsche Härte' (dH), which can be converted by a factor of

21.7919 to the concentration of HCO_3^- in mg/l. In Tab. 3.2 all samples taken for every single experiment are listed together with their measured parameters.

sample	measured parameters
feed solution $NaHCO_3$	pH, carbonate hardness, $\delta^{13}C$, $\delta^{18}O$
feed solution $CaCl_2$	pH, cations
mixed solution before entering channel system	pH, carbonate hardness, $\delta^{13}C$, $\delta^{18}O$, cations
mixed solution after leaving channel system	pH, carbonate hardness, $\delta^{13}C$, $\delta^{18}O$, cations
glass fibre stripe section	$\delta^{13}C$, $\delta^{18}O$, cations

Table 3.2: *Listing and description of experiment samples and measured parameters. The following sample nomenclature was applied: x = number of experiment (1-7); y = part experiment (A-D); n = number of glass fibre stripe section (1-50)*

The solution samples for the isotope measurement were stored in glass vessels, preferably free of air bubbles. The glass fibre stripe was cut into sections of equidistant length (~ 1 cm). These single sections (50 in total) were weighed and randomly examined under optical microscope or SEM (scatter electron microscope). 15 to 20 sections of each glass fibre stripe were sent to the University of Bremen where the calcite was extracted from the stripe and then analysed for $\delta^{13}C$ and $\delta^{18}O$ with a Finnigan MAT 251-mass spectrometer. The smallest analysable amount of calcite corresponds to 0.05 mg/cm^2. 5 to 15 other sections of the same glass fibre stripe were analysed with regard to their cation content (Ca^{2+}, Mg^{2+}, Ba^{2+}, Sr^{2+}, Na^+, K^+) by ICP-OES (inductively coupled plasma optical emission spectrometry). All measured values related to the filter segments are generally integrated values over the length of the filter segment (1 cm). Tab. 3.3 gives an overview of the analysis parameters and the respective methods together with the required sample amounts and measurement errors.

analysis parameter	analysis method	required amount	error
pH	pH-meter	-	0.03
$[HCO_3^-]$	titration (carbonate hardness)	$5\,ml$	$8\,mg/l$
$[Ca^{2+}]_{solution}$	ICP-OES (Heidelberg)	$6\,ml$	4%
$[Ca^{2+}]_{CaCO_3}$	ICP-OES (Heidelberg)	$6\,ml$	4%
$\delta^{13}C_{solution}$	Finnigan DELTAplus XL mass spectrometer (Innsbruck)	$3\,ml$	0.1‰
$\delta^{18}O_{solution}$	Finnigan DELTAplus XL mass spectrometer (Innsbruck)	$3\,ml$	0.08‰
$\delta^{13}C_{CaCO_3}$	Finnigan MAT 251-mass spectrometer (Bremen)	$0.05\,mg/cm^2$	0.05‰
$\delta^{18}O_{CaCO_3}$	Finnigan MAT 251-mass spectrometer (Bremen)	$0.05\,mg/cm^2$	0.07‰

Table 3.3: *Overview of investigated parameters and the corresponding analysis methods. Also given are the required sample amount and the measurement error.*

The values can be used for a backward calculation with PHREEQC. This means that the actual SI_{CaCO_3} can be calculated using the ion concentration and pH of the intitially mixed solution[2] together with the temperature.

[2]The term 'inititally mixed solution' refers to the mixed solution before entering the channel system.

3.3.5 Error estimation

In the laboratory experiments various different parameters are involved, and all are associated with minor or major uncertainties. Possible sources of error within the experiments are qualitatively and quantitavely described in the following.

Temperature

For temperature control 4 T-sensors were installed equidistantly along the bottom of the glass channel. It turned out that the temperature is neither constant along the channel nor temporally constant. The temperature in the refrigerator is subject to fluctuations in time due to the regular cooling cycles occuring with a frequency of approx. 20 min. This leads to variations of maximum $\pm 0.3°C$ around the average temperature value. Because the mean value of these fluctuations is constant, it should have no effect on the experiment results. A stronger temperature effect results from the spatial fluctuations along the channel which range from $0.1°C$ to $0.8°C$. Here the values fluctuate independently of the position except for the temperature at the bottom of the glass channel, which in general possesses higher values probably due to the position close to the door of the refrigerator. The door does not perfectly seal, which is expressed by the fact that the channel systems which are located more inwardly or closer to the back wall show less lateral temperature variability. For $\delta^{18}O$ a temperature increase of $1°C$ would lead to a depletion of $-0.23‰$ under equilibrium conditions. Since the lateral temperature variations along the channel show no consistent trend, the isotope values can not be corrected. However, this has to be kept in mind while interpreting the data.

Drip rate

The drip rate or pump rate, respectively, was controlled in regular intervals during the experiments. Deviations from the adjusted pump rate were observed in the range of 5%, which have no significant effects on the results.

Ion concentration

The initial solutions were prepared with the theoretical specification of concentrations, which were afterwards controlled by ICP-OES and a carbonate hardness test. The concentrations of HCO_3^- and Ca^{2+} agreed with the intended values in the range of 5% in most cases. Single larger variations could result from erroneous mixture ratios of the feed solutions, which would also effect the initial SI_{CaCO_3}. For example a $3:2$ mixture ratio would lead to a SI_{CaCO_3}-variation of 0.1. Measurement of the ion-concentration subsequent to the experiment allows a relatively exact determination of the solution composition. Thus, the SI_{CaCO_3} can be calculated by PHREEQC. The most uncertain factor in the calculation of the SI_{CaCO_3} is the pH, which has an error of 0.03 at maximum whereas variations in the pH result in $1:1$ variations in the SI_{CaCO_3}.

The inorganic salts which were used to prepare the solutions have a high degree of purity. A cation analysis of the mixed solutions (Fig. 3.5) show that in average sodium and calcium represent the largest percentage. All other cations like magnesium, strontium etc. are below 0.05% except for potassium with 0.2%. The high amount of potassium is probably a consequence of the pH-measurement because the pH-sensor is kept in a KCl-solution, which may not be thouroughly removed before measuring the pH of the feed solutions.

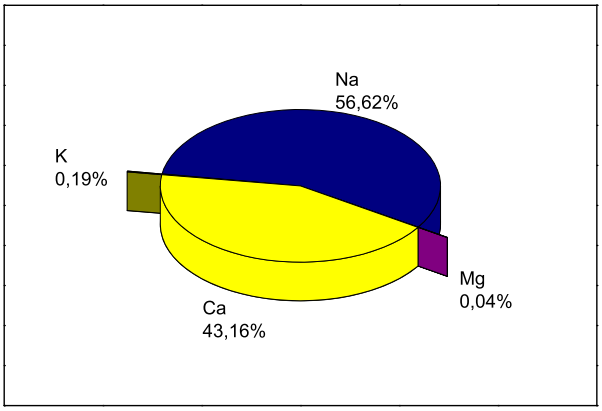

Figure 3.5: *Average cation content of the initial solution used calcite precipititation.*

Additionally, a cation analysis was carried out for two filter blanks ($0.5x1\ cm$) yielding 3.6 μg of barium and 2.5 μg of potassium in average which are not relevant for the experiment results. In contrast, the two filter blanks also yielded 2.2 μg and 8.9 μg of calcium, respectively. For filter samples where only a minor amount of calcite has precipitated (i.e., in the range of the detection limit) the filter itself can contribute to the total measured amount of calcite with 50% at maximum. Because this is only the case for few samples there will be no effect on the isotope evolution along the channel.
Another source of error is the sample preparation. Small air bubbles in the solution isotope samples lead to isotope exchange between the solution and the small air volume within the vessel resulting in an isotopic enrichment of up to 2‰. A test was carried out to simulate the sampling in the cave where the sample vessels often are placed openly underneath a drip stone, sometimes for a time interval of one month. In case of the laboratory experiments a sample vessel with approx. 8 ml of solution was put inside the experiment atmosphere for 11 days in total. Afterwards it was analysed for $\delta^{13}C$ and compared to a solution sample measured immediately after sampling. The sample kept under laboratory atmosphere was enriched by 4‰ in comparison to the directly measured sample implying that CO_2-degassing still continues if the solution is not kept under air free conditions.

Glass fibre stripe

The advantages of the glass fibre stripe are its easy handling because it can easily be removed from the channel and cut into single sample segments. Furthermore, the fibrous structure of the glass fibre surface supports the heterogeneous crystallisation. Without such substrate calcite would not be deposited and the crystals forming within the solution would presumably afloat.
There are also some critical points with regard to the glass fibre as an adequate substrate. An undefined factor regarding the filter is its surface area. The determination of the surface area is important for example when calculating the precipitation mechanisms including a term V/A with V = volume of the solution and A = surface area. With its special fabric consisting of fine hairs and equally distributed dents, observable by scanning electron mi-

croscopy its influence on heterogeneous crystallisation is unclear.
Furthermore, it is not clear how the flow characteristics of the solution are modified by this kind of material because the glass fibre stripe represents a two-dimensional flow through a porous medium. Exchange processes between the solution volume within the filter and the solution film at the surface of the filter are possible.
To determine the absorbency of the filter, single filter segments were weighed, then soaked with water and subsequently weighed again. In total the filter can absorb a solution volume of 0.067 ml/cm^2, which means that the completely soaked filter stripe used for the laboratory experiments has an additional mass of 2 mg. It is likely that after the filter stripe is completely soaked it can be treated as a quasi-solid surface, where no significant exchange takes place between the water 'inside' the filter and the solution flowing along the surface and subsurface of the filter.

Other possible sources of error

Despite of the use of stainless steel capillaries it is possible that the solutions, based on pure Milli-Q®-water, dissolve ions from the drip capillaries. For some experiments this leads to brown iron oxide precipitation, partly coating the glass fibre stripe.
Another potential source of error is associated with the gas distributor. The nitrogen is saturated with water, but when the temperature increases the gas will supersaturate, leading to condense water, which distributes on the surface of the gas distributor. This condensed water might block the transport of fresh gas or even drip onto the glass fibre stripe. Furthermore, the 8 openings of the gas distributor are located directly above the channel probably leading to a locally increased degassing.
In case of very low drip rates and if the humidity in the system falls below a certain value, evaporation might play a significant role. General effects caused by evaporation are tested by carrying out one experiment without gas supply.

3.4 Results

3.4.1 Calcite crystals

To get an overview of the precipitated calcite crystals, in a first step the single filter segments were studied via an optical stereo microscopy (magnification: $60x$). It was observed that translucent crystals in the size range of some tenth of microns precipitate preferentially at the edges of the filter as well as at small bulges of the filter surface and subsurface. Asperities also promote calcite precipitation due to small crinkles or cracks in the filter surface. Another observed characteristic is the correlation between the initial SI_{CaCO_3} of the solution and the size of the precipitated calcite crystals. For a higher degree of supersaturation crystals are usually of a smaller size. Furthermore, a change of crystal size along the channel could be detected. In the upper part of the glass fibre stripe lots of small, round crystals dominate. In the lower sections, less, but bigger crystals are observed. This characteristic is explainable by the decrease of the SI_{CaCO_3} along the channel during precipitation. A high degree of supersaturation leads preferentially to the creation of numerous small crystals due to primary nucleation whereas in case of a low SI_{CaCO_3} crystal growth dominates over nucleation resulting in few but larger crystals (pers. comm. Margot Isenbeck-Schröter).

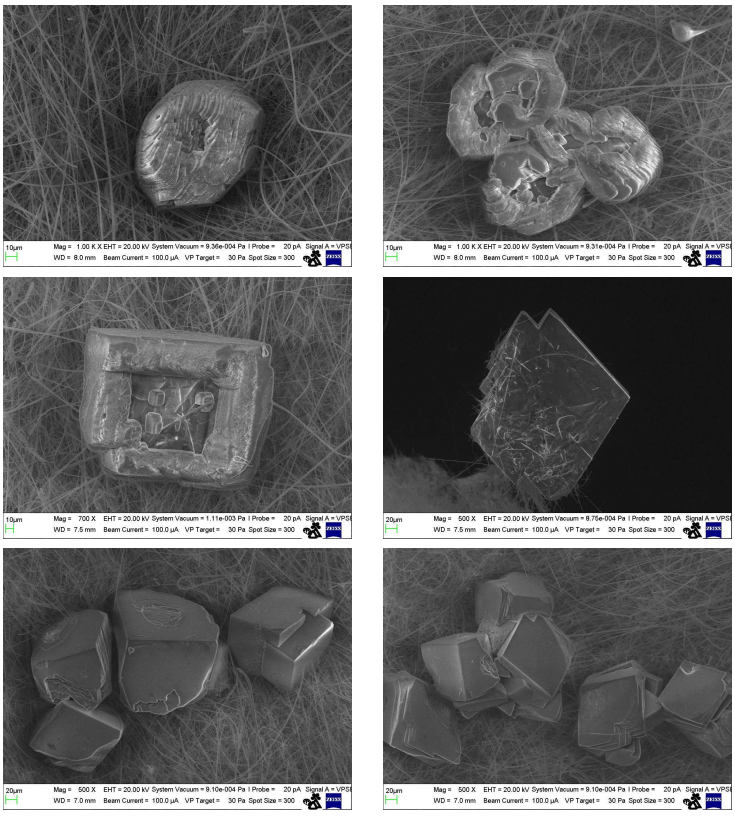

Figure 3.6: *SEM-pictures of the calcite precipitated on the glass fiber stripe in laboratory experiment 1: top: experiment 1A (section 43); middle: experiment 1C (left: section 18, right: section 48), bottom: experiment 1D (section 8).*

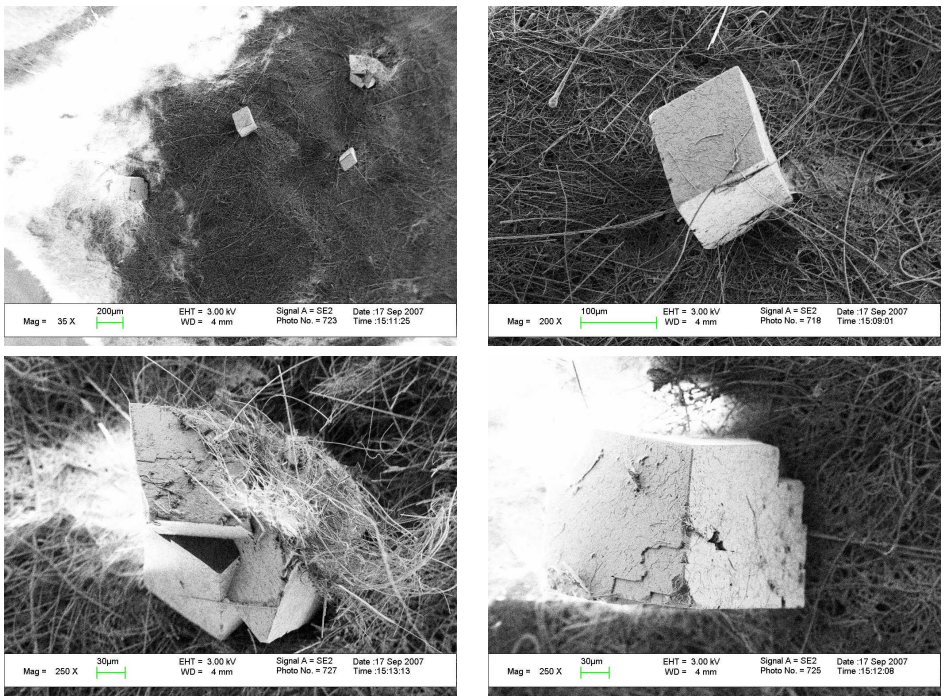

Figure 3.7: *SEM-pictures of the calcite precipitated on the glass fibre stripe in laboratory experiment 4B (section 5).*

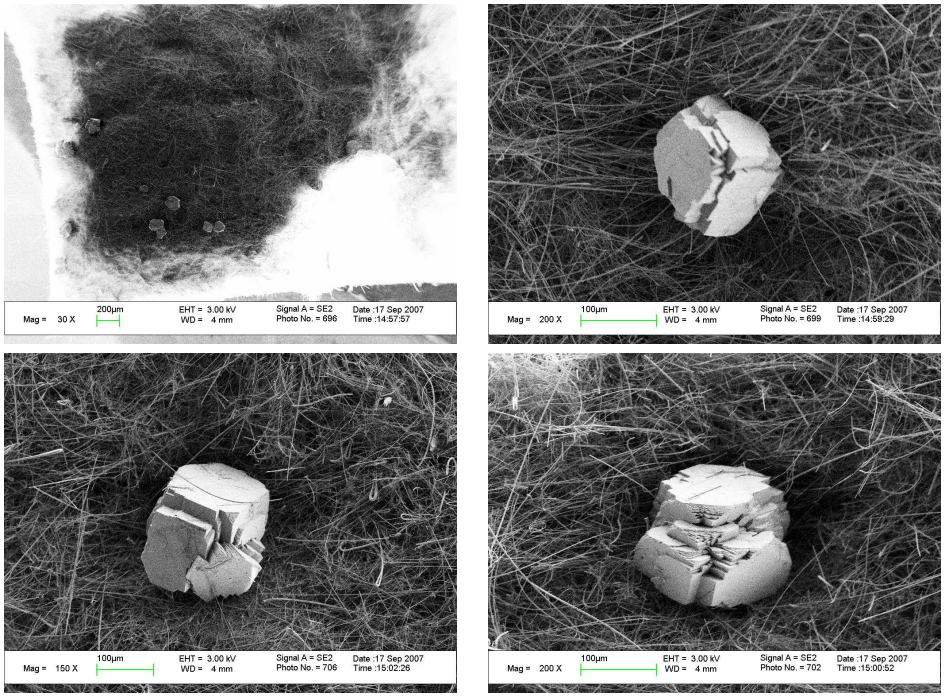

Figure 3.8: *SEM-pictures of the calcite precipitated on the glass fibre stripe in laboratory experiment 4B (section 47).*

In a second step SEM (SEM=scanning electrone microscope)-pictures were taken for selected samples which are displayed in Figs. 3.6, 3.7, 3.8. This allows to study the crystal character of the calcite with respect to mass density, crystal size, and crystal structure in detail. With respect to laboratory experiments $1A$, $1C$, $1D$, and $4B$ in total 7 glass fibre stripe sections (0.6×1 cm) were studied by Silvia Frisia in Trento (exp. 1) and in the Chemical Institute, Heidelberg (exp. 4).

All examined samples are characterised by a low mass density predominantly exhibiting single isolated crystals with edge lengths between 100 μm and 150 μm. The crystals can be described as equant or isometric rhombohedra, sometimes with flat surfaces (e.g., segment 5 in exp. $4B$, Fig. 3.7). In the same experiment but in a lower section crystals mostly exhibit defects like steps and kinks (segment 47, fig. 3.8) where calcite growth preferentially takes place (Kunz and Stumm (1984)). Furthermore, some examples for crystal aggregation wherein crystals are partly nested and twinned (e.g. fig. 3.7 bottom left) where found. In experiment $1A$ some single calcite crystals even exhibit spherical shapes with radii below 30 μm (fig. 3.6 top) potentially suggesting replacement by vaterite (pers. comm. Silvia Frisia), a polymorphic hexagonal modification of $CaCO_3$, which is rarely found in nature due to its instability (Kralj et al. (1990)). In the laboratory vaterite typically evolves from highly saturated solutions although little information exists about the exact conditions of vaterite formation. The initial saturation index of the solution of exp. $1A$ was calculated as $SI_{CaCO_3} > 1$, thus representing the solution with the highest degree of supersaturation in comparison to the other experiments investigated on SEM-picures and for which no spherical crystal shapes could be detected. Furthermore, exp. $1A$ was carried out with a very low drip rate providing additional time for CO_2-degassing resulting in a further increase of the initial SI_{CaCO_3} while the solution flows along the channel. All these facts would promote formation of vaterite. If the calcite crystals of experiments $1A$ indeed are partly replaced by vaterite, which could only be confirmed by IR spectroscopy and X-ray diffraction, then the experiment parameters of $1A$ would be an indication under which conditions vaterite is produced. However, with respect to isotope studies there is little information in the literature indicating a significant difference in the isotope fractionation factors for calcite and vaterite. Large differences are assumed to be rather unlikely (Grasby (2003)).

3.4.2 Calcite precipitation along the channel

The mass distribution of calcite was studied for a number of filter segments by ICP-OES and weighing. Furthermore, the total amount of precipitated calcite can be determined by integrating the single mass values over the whole length of the filter. The methods described in chapter 3 were applied on the single experiments whereas an uncertainty in the mass determination has to be taken into account. The main error is related to the removement of the glass fibre stripe from the glass channel. Because calcite also precipitates on the subsurface of the filter, an undetermined amount of calcite crystals got stuck on the glass fibre stripe, consequently not contributing to the total mass value. In this respect the determined calcite mass per filter segment is always underestimated to a different extent of up to approx. 10%.

In the following the influence of different experiment parameters on calcite precipitation along the channel are studied by comparing two experiments, which only differ in one single parameter (Tab. 3.4).
Generally, it appears that the single data points are subject to fluctuations probably caused by small inhomogenities on the filter leading to locally varying crystal growth mechanisms, and, hence, to different precipitation rates. However, for all experiments a general trend of mass development along the channel can be observed.
The amount of calcite precipitated on the glass fibre stripe per day ranges from 0.1 mg to 0.7 mg for the different experiments. These measured values agree well with the range observed for the Bunkerhöhle where modern calcite was sampled on watchglasses at 3 drip sites. The growth rate, a specification typically used for stalagmites to describe the annual growth, unfortunately can not be calculated for the calcite precipitated in the laboratory experiments because the sparse crystal coverage on the glass fibre stripe precludes the usage of the mineralogical calcite density of 2.7 g/cm^3 which is required for growth rate determination.

	experiments compared to each other	differing parameter
(A)	$4A$-$4B$	surface area
(B)	$6A$-$7A$	channel atmosphere (p_{CO_2})
(C)	$4B$-$6C$	temperature
(D)	$6B$-$6D$	$SI_{CaCO_3}$of initial solution

Table 3.4: *Overview of the respective experiments compared to each other and the differing parameters. The related quantities of these parameters are specified in the single plots of fig. 3.9-3.14. All parameters not depicted in the plot are constant for both displayed experiments.*

(A) Filter surface area

Fig. 3.9 shows the calcite mass distribution for exp. $4A$ and $4B$, which differ in filter surface area. The surface area of exp. $4B$ exceeds that of exp. $4A$ for a factor of 1.5 whereas the total precipitated mass of exp. $4B$ differs by a factor of 3 in comparison to exp. $4A$ (Fig. 3.9). The difference in calcite precipitation is related to the solution flow speed, which depends amongst other things on the available surface area (Eq. (3.3) in chapter 3). A longer residence time of the solution on the channel, leads to a larger amount of calcite precipitation.
Interestingly in the upper part of the glass fibre stripe at a distance of up to 12 *cm* the amount of precipitated calcite seems to be almost similar for both experiments. This can be related to the drip mechanics or flow characteristics of the single drops in connection with the characteristics of the glass fibre stripe. When the drop gets in contact with the filter, the rate of spread shows no significant dependency on the filter area. Subsequently, when the drop thins out and further mixing reactions with successive drops occur, the geometry of the filter seems to dominate leading to a difference in flow velocity, and, hence, to different precipitation rates.

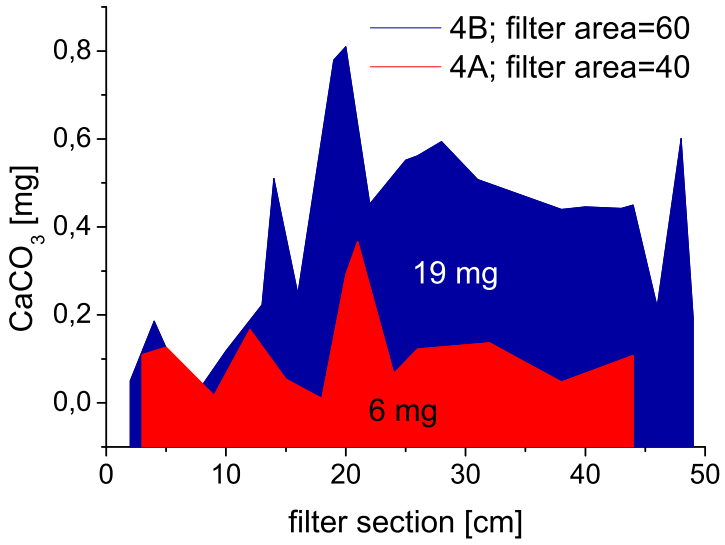

Figure 3.9: *Mass distribution of experiments* $4A$ *and* $4B$ *differing in filter surface area. The numbers inside the graph indicate the total mass of calcite precipitated within a period of* 28 *days.*

(B) Channel atmosphere

Fig. 3.10 shows the mass distribution of experiments $6A$ and $7A$, differing in channel atmosphere. For exp. $7A$, carried out under laboratory atmosphere, a p_{CO_2}-gradient is lacking because the feed solutions were equilibrated with the same atmosphere. Thus, calcite precipitation results solely from the initial supersaturation of the solution.
From Fig. 3.10 it can be deduced that during the first $2-3$ cm both experiments exhibit the same amount of precipitation. However, while for exp. $6A$, carried out under N_2-atmosphere, calcite precipitation decreases stepwise along the channel, exp. $7A$, which was conducted under laboratory atmosphere, shows an abrupt decrease around 8 cm resulting in a total amount of calcite, which is less then half of the total calcite mass precipitated in exp. $6A$. Approx. 15% of this mass difference result from a slightly different amount of solution pumped through the channel (0.1 ml/min for exp. $7A$ and 0.12 ml/min for exp. $6A$). However, the main mass differences can be explained by the fact that even if the initial supersaturation of the solution is the same for both experiments, different processes occur along the channel. For the N_2-atmosphere and the related p_{CO_2}-gradient between the solution and the channel atmosphere CO_2 will degas from the solution, which is generally connected with an increase of the SI_{CaCO_3}. CO_2-degassing will decelerate the decrease of the SI_{CaCO_3} resulting from calcite precipitation. In case of exp. $6A$, conducted under N_2-atmosphere, this process will thus lead to a greater amount of calcite in comparison to exp. $7A$.

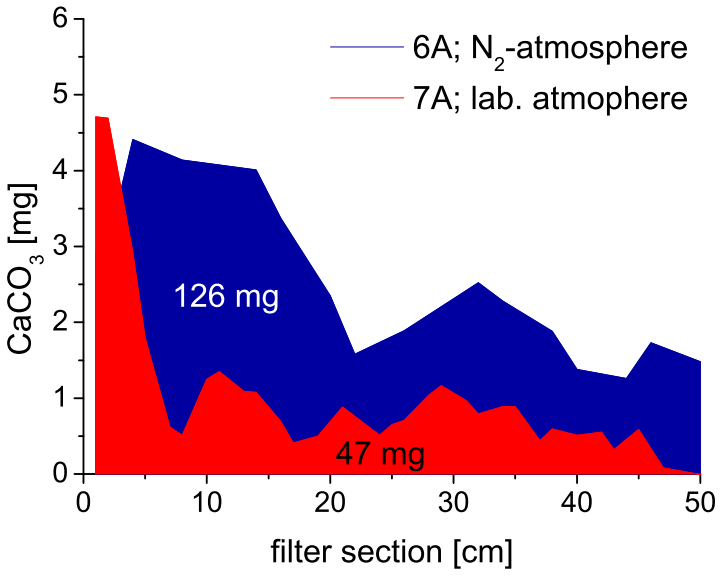

Figure 3.10: *Mass distribution of experiments* $6A$ *and* $7A$ *differing in channel atmosphere. The numbers inside the graph indicate the total mass of calcite precipitated within a period of* 28 *days.*

(C) Temperature

Temperature is the parameter, which is the dominating factor with respect to the total amount of calcite precipitation on the channel (Fig. 3.11). A difference of $13°C$ results in a calcite mass increase of a factor 100 for the experiment carried out under warmer conditions.

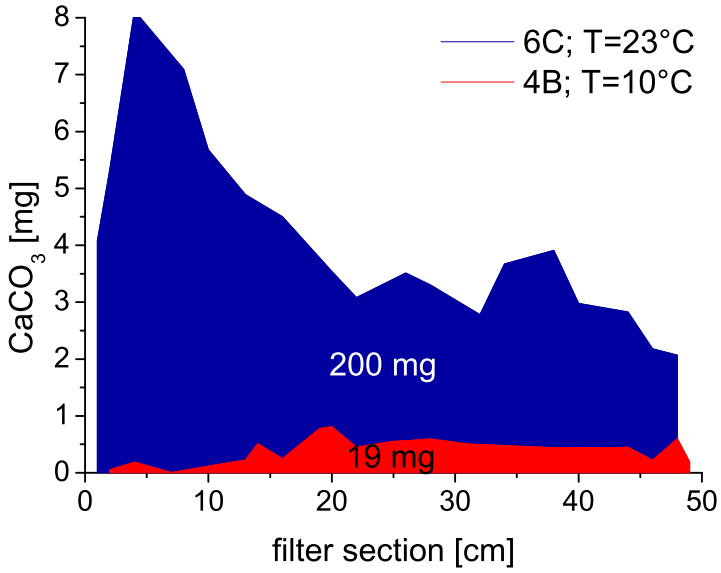

Figure 3.11: *Mass distribution of experiments* $4B$ *and* $6C$ *differing in temperature. The numbers inside the graph indicate the total mass of calcite precipitated within a period of* 28 *days.*

Fig. 3.12 shows the total amount of precipitated calcite normalised to the maximum possible calcite precipitation in percent, plotted versus the initial SI_{CaCO_3} for laboratory experiments $4-6$. The maximum amount of calcite, which theoretically can be precipitated, is calculated with PHREEQC and depends on the initial ion concentration as well as the ambient p_{CO_2}. From Fig. 3.12 can be deduced that the percentage of $CaCO_3$-precipitation strongly depends on temperature showing a more or less constant value for experiments carried out at $23°C$. However, the experiments conducted at $10°C$ seem to show a slight tendency to a greater percental amount with increasing SI_{CaCO_3} but the number of data is too small to generalise this assumption.

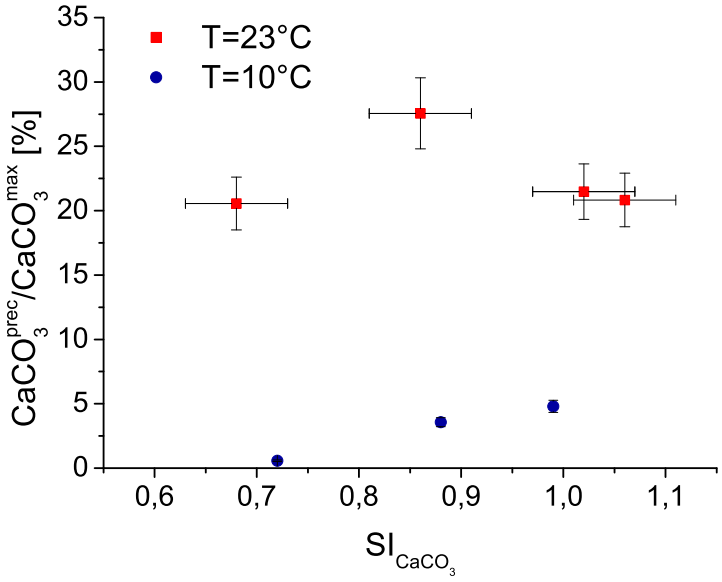

Figure 3.12: *Percental relation between total amount of precipitated calcite and maximum possible calcite mass calculated with PHREEQC plotted versus SI_{CaCO_3} for experiments carried out at different temperatures.*

The observed temperature dependent calcite precipitation is related to the temporal evolution of Ca^{2+} in the solution, which can be expressed by an exponential decrease (Buhmann and Dreybrodt (1985b), Fig. 3.13)[3]:

$$[Ca^{2+}](t) = [Ca^{2+}]_{eq} + ([Ca^{2+}]_0 - [Ca^{2+}]_{eq}) \cdot e^{-\frac{t}{\tau}}, \tag{3.4}$$

where $[Ca^{2+}]_{eq}$ represents the equilibrium calcium concentration and $[Ca^{2+}]_0$ is equal to the initial calcium concentration. While $[Ca^{2+}]_{eq}$ only depends on the ambient p_{CO_2}, $[Ca^{2+}]_0$ shows a slight dependence on temperature due to the chemical properties of calcium. For higher temperatures less calcium ions are dissolved in comparison to lower temperatures. This can be expressed by a SI_{CaCO_3}-temperature-relation of approx. -0.1 per $10°C$. However, $[Ca^{2+}]_0$ is similar for experiments $6C$ and $4B$. Hence the temperature effect included in the data results from temperature dependent chemical rates. The term τ in Eq. (3.4) describes the conversion time from HCO_3^- to CO_2 as the rate limiting step in the precipitation process and can be expressed by:

$$\tau = \frac{d}{a}, \tag{3.5}$$

where $d = V/A$ is the film thickness in cm and a is a kinetic constant in cm/s. The kinetic constant a represents a proportionality factor between the calcite precipitation rate and the

[3]Since for every Ca^{2+}-ion lost from the solution a $CaCO_3$-molecule evolves, calcite precipitation can be illustrated by the reciprocal curve of fig. 3.13 under the simplified assumption that every $CaCO_3$-molecule immidiately precipitates after formation.

available calcium concentration in the solution, and depends mainly on temperature and film thickness (Dreybrodt (1999), Baker et al. (1998)). For higher temperatures the conversion time τ decreases, hence leading to enhanced calcite precipitation.

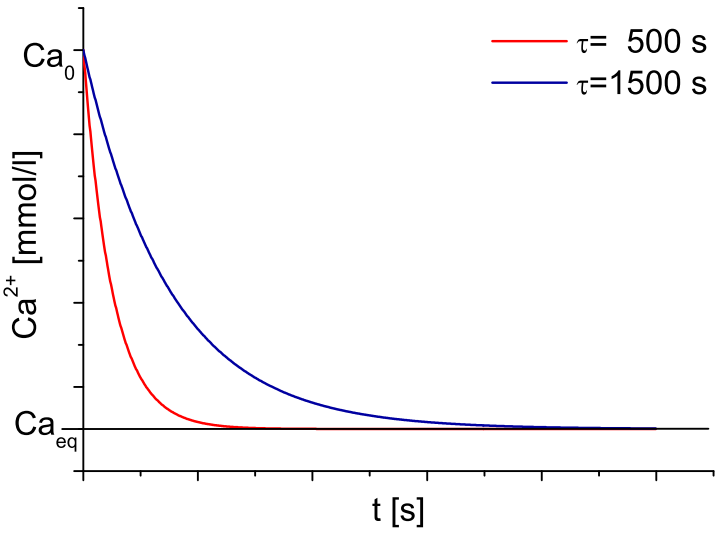

Figure 3.13: *Temporal evolution of Ca^{2+} for two different conversion rates τ (deduced from Baker et al. (1998)). Ca_0 represents the initial calcium concentration, and Ca_{eq} indicates the equilibrium calcium concentration, which is p_{CO_2}-dependent.*

For the laboratory experiments τ can be determined theoretically by the observed decrease of $CaCO_3$. For every precipitated $CaCO_3$-molecule, one Ca^{2+}-ion is lost from the solution. If plotting the Ca^{2+}-decrease logarithmically against the time obtained from the solution flow speed, the slope s of the linear fit of $\frac{(\Delta ln([Ca^{2+}])}{\Delta t}$ yields τ with $\tau = -\frac{1}{s}$. However, in practice the determination of τ with the described method is difficult because the Ca^{2+}-evolution turns out to be more complex than expected from Fig. 3.13. This is explained in detail in the following section.

(D) SI_{CaCO_3} OF INITIAL SOLUTION

Fig. 3.14 shows the effects of initial SI_{CaCO_3} on the calcite mass distribution. It is self-evident that a higher degree of supersaturation, which is accompanied with a higher initial concentration of Ca^{2+}-ions, will lead to a larger amount of calcite precipitation. This is also confirmed by Fig. 3.13.

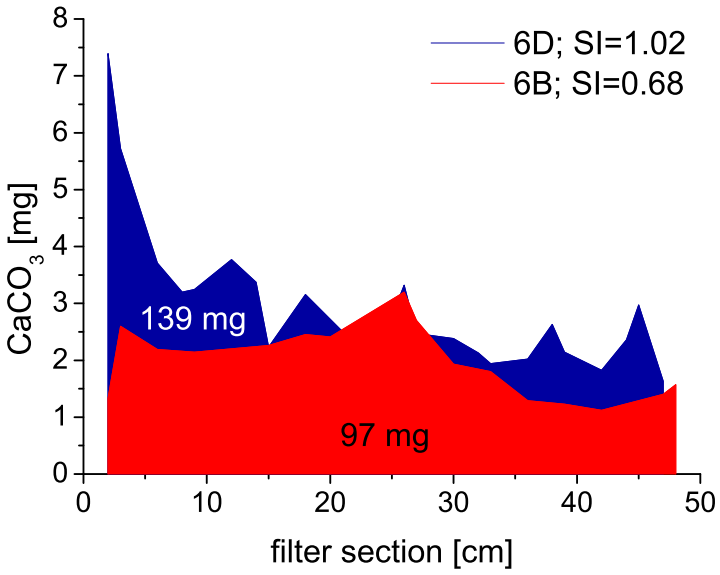

Figure 3.14: *Mass distribution of experiments* $6B$ *and* $6D$ *differing in initial* SI_{CaCO_3}*. The numbers inside the graph indicate the total mass of calcite precipitated within a period of* 39 *days.*

Furthermore, for all experiments an interesting effect could be observed, which is associated with the initial degree of supersaturation. For a relatively high initial supersaturation ($SI_{CaCO_3} \geq 1$) maximum calcite precipitation occurs right at the beginning or on the first few centimeters of the glass fibre stripe. With a lower initial SI_{CaCO_3} the maximum precipitation rate is shifted to later sections, around 20-25 *cm* (Fig. 3.15). This correlation is possibly linked to the crystallisation mechanisms, which depend on the SI_{CaCO_3} (see chapter 2). If the initial solution offers a high degree of supersaturation ($SI_{CaCO_3} \gtrsim 1$), homogeneous calcite nucleation might occur, which means that calcite crystals emerge from the solution itself. Otherwise, if the initial SI_{CaCO_3} is below the limit of homogeneous nucleation, less calcite will precipitate at the beginning of the channel. With progressive degassing of CO_2, the SI_{CaCO_3} will increase until the range of homogeneous nucleation is reached where maximum calcite precipitation occurs. This maximum is subsequently followed by a decrease of SI_{CaCO_3} due to further calcite precipitation.

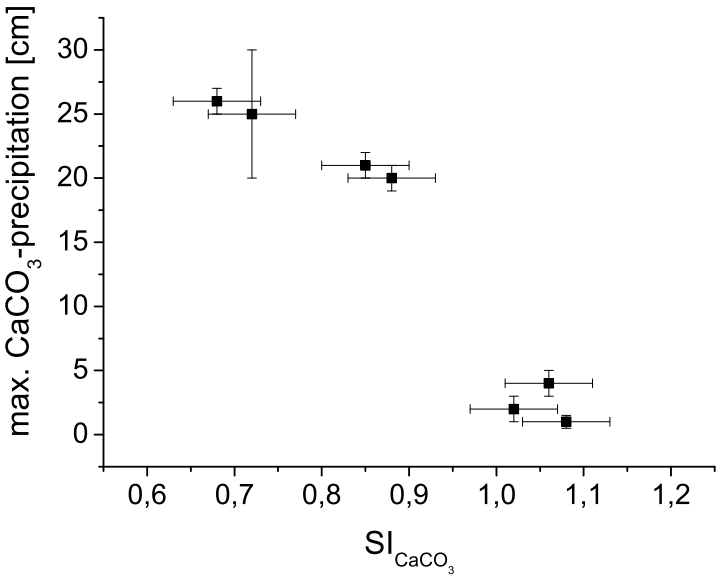

Figure 3.15: *Position of maximum calcite precipitation on the glass fibre stripe versus* SI_{CaCO_3} *for experiments with a constant flow velocity of* 6.6 *min.*

However, for the experiments with a high initial SI_{CaCO_3}, where maximum calcite precipitation occurs at the beginning, τ was calculated with the method described in the previous section. Here τ was determined for experiments $6D$ ($T = 23°C$) and $5B$ ($T = 10°C$) (Fig. 3.16).

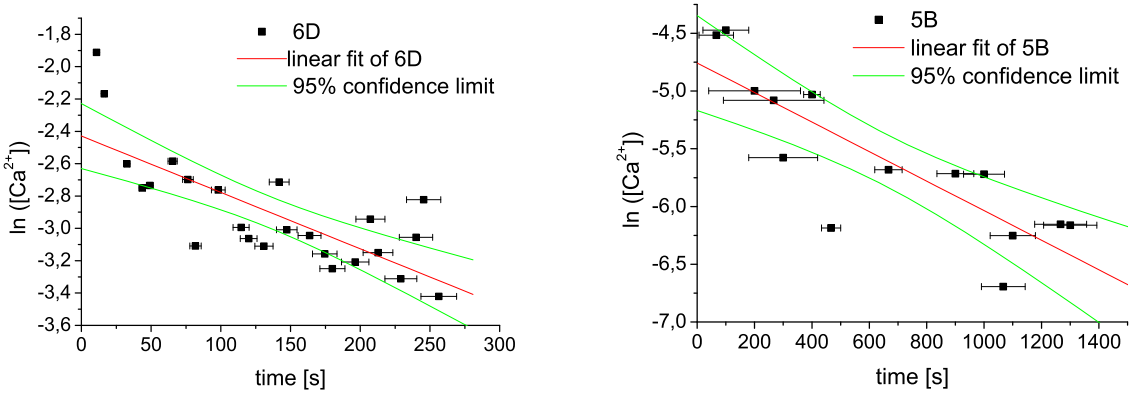

Figure 3.16: *Temporal* Ca^{2+}*-decrease along the channel, plotted logarithmically for experiments* $6D$ *(left) and* $5B$ *(right).* τ *can be determined by the slope* s *with* $\tau = -(1/s)$.

Values for τ can easily be deduced from the slopes of the linear data fit. The difficulty of this approach lies not only in the large uncertainty of the linear fit due to the partially large

deviations of the single measurement points but also in the imprecise estimation of the flow velocity (see section 3.3.5 in chapter 3). For the flow velocity an average value was applied leading to large uncertainties particularly for the experiments with low drip rates (exp. $5B$). However, as a result the calculation of τ yields 287 ± 40 s for exp. $6D$ carried out at $23°C$ and 780 ± 200 s for exp. $5B$ carried out at $10°C$.

To sum up: factors, which influence calcite precipitation are the available surface area, p_{CO_2}, temperature and the initial SI_{CaCO_3}. A larger surface provides a larger area for calcite crystallisation. The ambient p_{CO_2} defines the rate of CO_2-degassing, thus, directly influencing the SI_{CaCO_3}. A dominant factor in calcite precipitation is the temperature. Higher temperatures enhance the chemical rates, hence resulting in an increased calcite precipitation.

3.4.3 $\delta^{13}C$ and $\delta^{18}O$ evolution along the channel

In this chapter the results of the stable isotopes (i.e., $\delta^{13}C$ and $\delta^{18}O$) for the calcite precipitated on the channel and under varying experiment conditions are presented. In total the dependence of isotope development on 4 different parameter settings was studied. Tab. 3.5 gives an overview of the individual experiments.

	Experiments	Varied parameter
(A)	$4A$-$4B$-$5B$	flow velocity (residence time)
(B)	$6A$-$7A$-$7B$	channel atmosphere (p_{CO_2})
(C)	$4B$-$6C$	temperature
(D)	$6A$-$6B$	SI_{CaCO_3} of initial solution

Table 3.5: *Overview of the experiments and the according parameters, which were varied. The values of these parameters are specified in the single plots of Fig. 3.17-3.25.*

In the following figures the relative isotopic enrichment is shown for $\delta^{13}C$ and $\delta^{18}O$, respectively, versus the single filter segments or path length of the glass fibre stripe (in total 50 *cm*). Additionally, $\delta^{18}O$ is plotted versus $\delta^{13}C$ to reveal potential correlations between the two isotopes. According to the Hendy-test, both an enrichment along the channel and a correlation between $\delta^{13}C$ and $\delta^{18}O$ indicates kinetic isotope fractionation. The data points in the $\delta^{18}O(\delta^{13}C)$-plots are fitted linearly if possible whereas the obvious outliers were excluded from the fitting. The obtainend slopes $\Delta(\delta^{18}O)/\Delta(\delta^{13}C)$ can then be interpreted in terms of different parameter settings. Regarding the individual data points in the plots it is obvious that the data often do not show a continuous increase along the channel. Rather many of the data points are more or less subject to fluctuations whereas single outliers interrupt the general trend of enrichment. Sometimes it even seems that the data are shifted segmentally (e.g., exp. $4B$ between 10 *cm* and 12 *cm*, Fig. 3.17). In this case most of the outliers of the data set appear parallel in both $\delta^{13}C$ and $\delta^{18}O$.
Because more or less pronounced discontinuities could also be detected for the calcite precipitation along the channel (section 4.3.4), the outliers in the isotope data set are presumed to be related to different precipitation rates. Another reason for outliers in the data set could be the formation of single macrocrystals, which protrude from the solution or cause turbulent flow leading to locally differing CO_2-degassing. Another possibility for the observed variations are related to the fact that calcite crystals tend to precipitate on the surface of the glass fibre stripe as well as on the subsurface with possibly small differences in flow characteristics and flow velocities. To test for the influence of these processes the stable isotope values, three filter segments were horizontally splitted and analysed seperately[4]. The results of this test are discussed in section (C).
In summary, the variations in the data set result from a combination of different effects (see also section 3.3.5 in chapter 3). Furthermore, one has to keep in mind that the single isotope data points are averaged over the length of the filter segments, which could also contribute to uncertainties. However, despite of the fluctuations in the data set a general enrichment can be observed for all experiments.

[4]separate measurements for filter segments 3 and 12; for filter segment 23 only the subsurface of the filter segment was measured

(A) Flow velocity

Figs. 3.17-3.19 show the results for different solution flow velocities. As expected, the experiment with the lowest solution flow velocity (exp. $5B$) shows the greatest enrichment along the channel within the same distance. However, exp. $4A$ with the fastest flow rate exhibits the lowest enrichment (Fig. 3.17). The flow velocities are associated with the solution residence time on the channel. In case of a fast flow rate, less CO_2 can degas from the solution along its way on the channel in comparison to a lower flow rate. The more CO_2 degases from the solution the more lighter isotopes get lost from the solution. Hence, the solution gets isotopically enriched with time.
If the *cm*-axis is replaced by a time axis by applying the measured flow velocity (fig. 3.18), the data precipitated within the first 300 s (exp. $4A$, $4B$ and two points of $5B$) clearly show a linear increase. Subsequently, the enrichment decreases whereas the relatively high uncertainities associated with the low flow velocities have to be considered. For this reason the time axis of exp. $5B$ is possibly more compressed in reality due to the poorly estimated flow rate. Nevertheless, the evolution of the data points in Fig. 3.18 could be described by a exponentially satiable increase whereas it seems that the isotope equilibrium is not yet reached after 1500 s.
In Fig. 3.19 $\delta^{18}O$ is plotted versus $\delta^{13}C$. The data of all three experiments show a similar development within the errors independent of the flow velocity. The linear interpolated slopes range between 0.6 and 0.75.

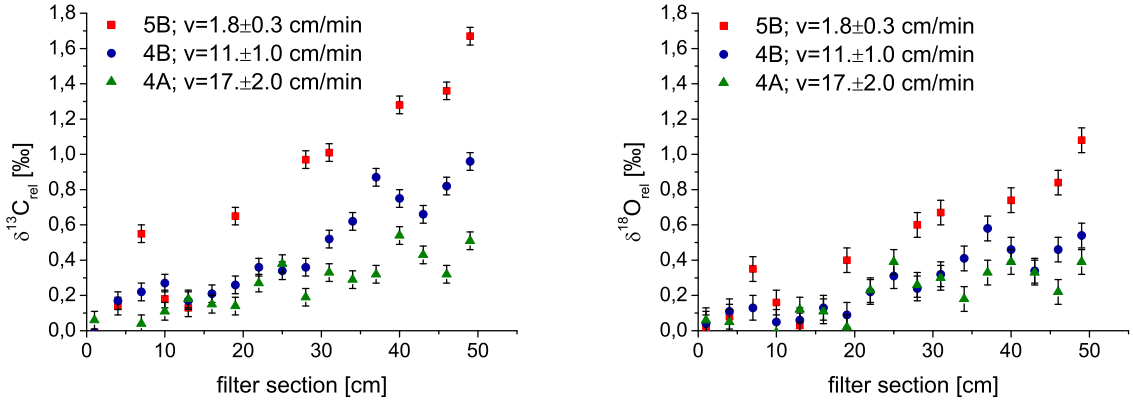

Figure 3.17: *$\delta^{13}C$ (left)- and $\delta^{18}O$ (right)-enrichment along the channel for experiments with different flow velocities v. Values for v are indicated in the plot.*

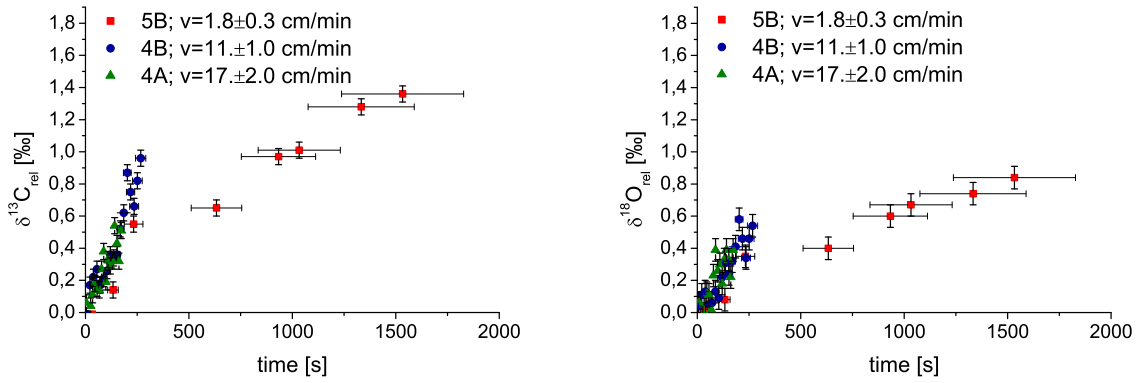

Figure 3.18: *Temporal $\delta^{13}C$ (left)- and $\delta^{18}O$ (right)-enrichment for experiments with different flow velocities v. Values for v are indicated in the plot.*

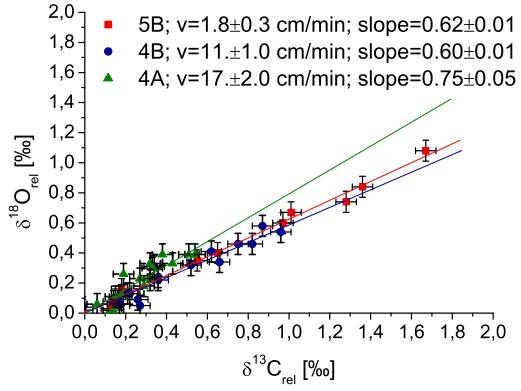

Figure 3.19: *Isotope correlation $\delta^{18}O(\delta^{13}C)$ for experiments with different flow velocities v. Values for v and for the linear interpolated slope $\Delta(\delta^{18}O)/\Delta(\delta^{13}C)$ are indicated in the plot.*

(B) CHANNEL ATMOSPHERE

It is an interesting question if it is necessary to provide a strong p_{CO_2}-gradient in the laboratory experiments like it is the fact in real cave systems forcing the solution to degas CO_2 or if a certain degree of the initial supersaturation alone is adequate. In principle, the supersaturated solution prepared for the experiments simulates the condition of the drop after impinging on the stalagmite where the solution is supersaturated due to prior CO_2-degassing but more or less in equilibrium with cave p_{CO_2} (Dreybrodt (2008)).
Thus, an experiment was carried out in which the nitrogen atmosphere was replaced by laboratory atmosphere (i.e., air with $p_{CO_2} \approx 480\ ppm$). For one of the experiments the laboratory atmosphere was humidified (exp. $7A$) while for another experiment no gas at all was infiltrated into the gas distributor (exp. $7B$), thus, providing only the regular refrigerator atmosphere to test for possible gas exchange and evaporation effects.

While for calcite precipitation a different mass evolution along the filter was observed for the different atmospheric settings (see section 4.3.4), this effect seems to have no influence on the isotopic evolution. From Figs. 3.20 and 3.21 no significant difference in the isotopic enrichment is visible for the experiments carried out under laboratory atmosphere and N_2-atmosphere, respectively. Normally, one would expect a larger isotopic enrichment for exp. $6A$ conducted under a higher p_{CO_2}-gradient, which leads to an increased CO_2-degassing. Instead, the observed similarities in the isotopic enrichment of exp. $6A$ and $7A$ may result from a slightly different flow velocity (6.6 cm/min in case of exp. $6A$ and 5.5 cm/min in case of exp. $7A$). Like it was shown in the previous section, a lower flow velocity, which is represented by exp. $7A$, leads to a larger isotopic enrichment along the channel. This characteristic presumably compensates the effect by the different p_{CO_2}-gradients.

Generally, in case of the laboratory experiments calcite precipitation is mainly driven by the initial supersaturation as it is assumed for natural stalagmite formation. Nevertheless, CO_2-degassing seems to play a decisive role for experiments with low initial SI_{CaCO_3}, a fact also pointed out in section 4.3.4. In this case CO_2-degassing dominates at the beginning until a certain limit of initial supersaturation for specific crystallisation mechanisms is reached. Then precipitation of calcite keeps pace with CO_2 loss. Unfortunately, no experiment was conducted under both conditions (i.e., a laboratory atmosphere and a low initial SI_{CaCO_3}) to generalise the mentioned assumptions.

Another feature, which is noticeable especially for the $\delta^{13}C$ evolution (Fig. 3.20, left) is the general enrichment trend. Particularly in the case of exp. $7A$ the $\delta^{13}C$ enrichment seems to show not a linear increase but rather a stepwise increase. Furthermore, a decreasing slope with increasing distance from top can be observed. However, it is questionable if this trend can be taken for granted within the errors. Although the functional characteristics cannot be verified due to the small data density, the observed trend generally implies that the system slowly approaches isotopic equilibrium.

Exp. $7B$, carried out under dry atmosphere, shows less enrichment in total in comparison to the humidified experiments, although one would expect a larger enrichment at least for $\delta^{18}O$ due to evaporation effects, forcing the lighter isotopes to degas in the form of water vapour. However, these characteristics are not observed in the data (Fig. 3.20, right). Either the degree of evaporation is too low to have a significant effect on the isotopic composition or, more plausibly, the degased CO_2 is not transported away, hence leading to isotope exchange

between the solution and the atmosphere. This would also affect the carbon isotopes, and could, thus, serve as an explanation for the observed lower enrichment of both $\delta^{13}C$ and $\delta^{18}O$ (Fig. 3.20, left).

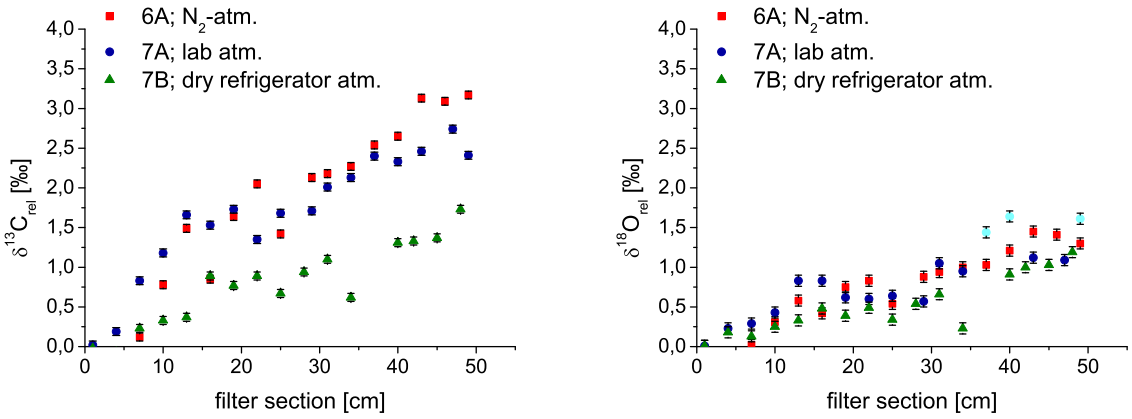

Figure 3.20: *$\delta^{13}C$ (left)- and $\delta^{18}O$ (right)-enrichment along the channel for experiments with different channel atmospheres indicated in the plot.*

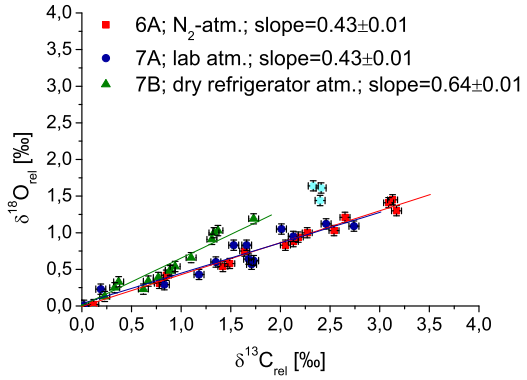

Figure 3.21: *Isotope correlation $\delta^{18}O(\delta^{13}C)$ for experiments with different channel atmospheres indicated in the plot.*

(C) Temperature

It is obvious from Fig. 3.22 that a variation in temperature has a strong effect on the amount of enrichment along the channel. A temperature difference of $13°C$ results in a 6 times higher $\delta^{13}C$-enrichment and a 4 times higher $\delta^{18}O$-enrichment. This great variability is also reflected by the observed slope of $\Delta(\delta^{18}O)/\Delta(\delta^{13}C)$ (Fig. 3.23). Generally, it can be concluded that the temperature has the largest effect on the isotope enrichment in comparison to the other parameters. This can be explained by the strong temperature dependence of the reaction times or conversion rates of the chemical processes involved in calcite precipitation. In this context an important process is the conversion from HCO_3^- to CO_2. At high temperatures the conversion usually proceeds faster and because this process represents the rate limiting step for calcite precipitation, more calcite is precipitated for the experiment conducted at $23°C$ resulting in greater loss of CO_2 leading to an enrichment of the heavier isotopes within the solution and hence within the calcite.

In Figs. 3.22 and 3.23 the light blue points indicate the values measured for the glass fibre subsurface. In case of $\delta^{13}C$ the values from surface and subsurface differ by approx. $0.5‰$. However, the shift is not consistent but rather shows opposite signs for both measurements. The shift in $\delta^{18}O$ is only $0.1‰$ but $\delta^{18}O$ usually shows a less pronounced enrichment.
The difference between the isotope values confirms the assumption that different processes (i.e., related to flow velocity and/or CO_2-degassing) occur at the glass fibre surface and subsurface. Hence, the isotope values represent an average over surface- and subsurface values.

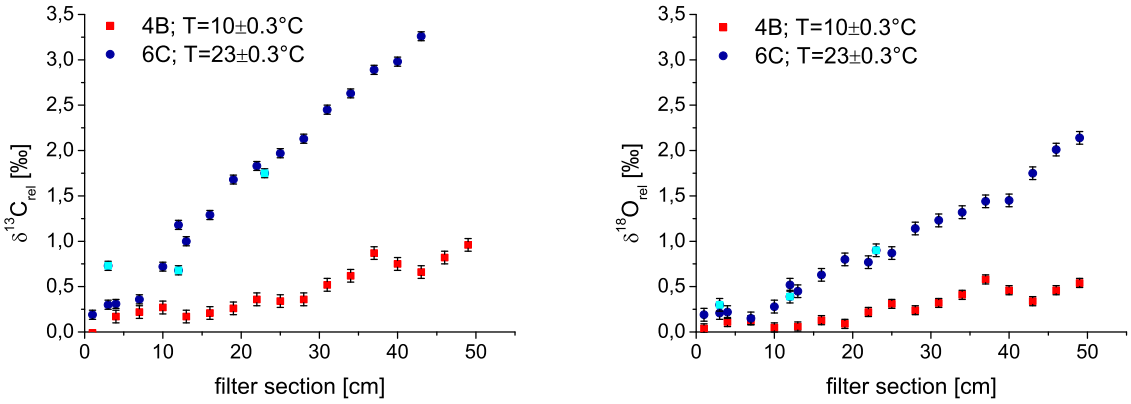

Figure 3.22: *$\delta^{13}C$ (left)- and $\delta^{18}O$ (right)-enrichment along the channel for experiments with different temperatures which are indicated in the plot. The light blue points represent values measured on the glass fibre subsurface.*

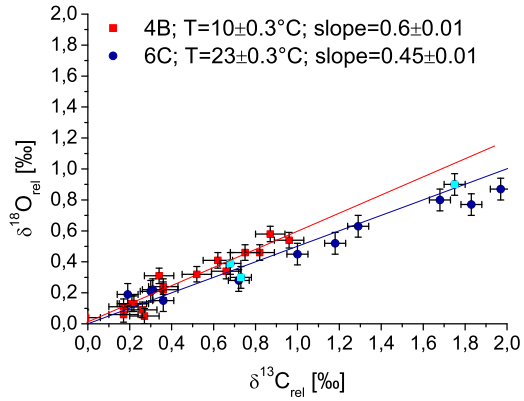

Figure 3.23: *Isotope correlation $\delta^{18}O(\delta^{13}C)$ for experiments with different temperatures which are indicated in the plot. The light blue points represent values measured on the glass fibre subsurface.*

(D) SI_{CaCO_3} of initial solution

Figs. 3.24 and 3.25 display experiments $6A$ and $6B$ differing in their initial solution compositions, and hence their initial SI_{CaCO_3}.
It is obvious that in case of $\delta^{13}C$ (Fig. 3.24, left) the isotope values show a greater total enrichment for the solution with the higher degree of supersaturation. This result is coherent with the greater amount of calcite precipitation in case of higher initial SI_{CaCO_3}. Because the equilibrium ion concentration of Ca^{2+} or HCO_3^-, depending only on the p_{CO_2} in the channel atmosphere, is equal for both experiments, exp. $6A$, which has the higher initial ion concentrations is farther away from equilibrium. Thus, more calcite precipitates within the same time period, in comparison to exp. $6B$ with the lower initial ion concentrations, equivalent with a greater loss of CO_2. However for $\delta^{18}O$ (Fig. 3.24, right) exp. $6A$ and $6B$ show a similar enrichment within the range of errors indicating that the effect seems to be too low for $\delta^{18}O$ to be noticeable.

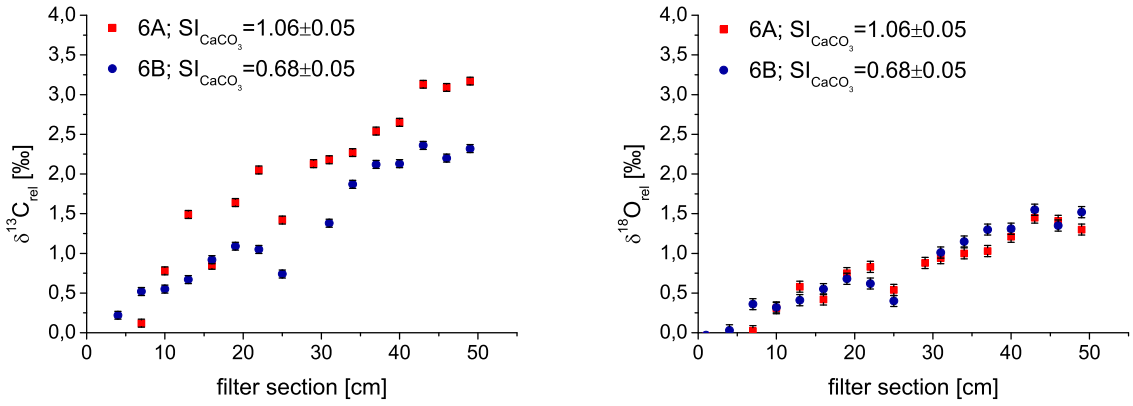

Figure 3.24: *$\delta^{13}C$ (left)- and $\delta^{18}O$ (right)-enrichment along the channel for experiments with different initial ion concentrations expressed as SI_{CaCO_3}. Values for SI_{CaCO_3} are indicated in the plot.*

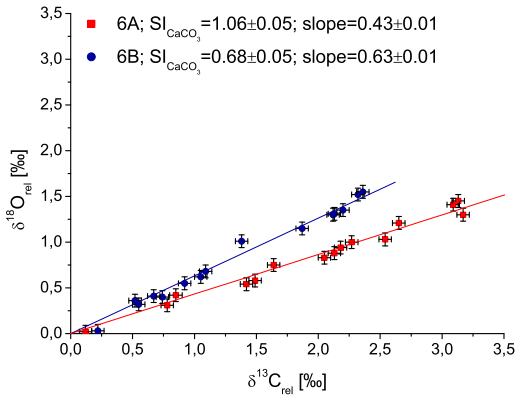

Figure 3.25: *Isotope correlation $\delta^{18}O(\delta^{13}C)$ for experiments with different initial ion concentrations expressed as SI_{CaCO_3}. Values for SI_{CaCO_3} are indicated in the plot.*

3.4.4 Fractionation Factors

In the framework of the laboratory experiments isotope values were measured not only for the precipitated calcite but also for the initially mixed solution, which allows the calculation of the fractionation between the two phases. Within the solution the main part of C-atoms is bound in HCO_3^-. Thus, the fractionation factor in case of $\delta^{13}C$ is indicated as $\alpha_{CaCO_3-HCO_3^-}$ or, as a more descriptive value, expressed by the enrichment $\epsilon_{CaCO_3-HCO_3^-}$ with $\epsilon = (\alpha - 1) \cdot 1000$. In case of $\delta^{18}O$ the enrichment factor $\epsilon_{CaCO_3-H_2O}$ is specified between calcite and water, which represents the main source of O-atoms. With respect to calcite as the solid phase the values of the calcite first precipitated on the filter were used for the determination of ϵ [5].
The absolute isotope values of the precipitated calcite range from $-5‰$ to $-0.5‰$ in case of $\delta^{13}C$ and from $-10‰$ to $-8.5‰$ in case of $\delta^{18}O$. Here the isotope values of the first precipitated calcite on the filter show a clear dependence on temperature (a difference of $1.8‰$ between $10°C$ and $23°C$; $0.5‰$ in case of $\delta^{13}C$).

In the following, the fractionation factors derived from the laboratory experiments are compared to equilibrium fractionation factors obtained from the literature. Many papers were published since the late 1960s dealing with the theoretical and experimental determination of the equilibrium fractionation factors between the different species and phases involved in calcite chemistry. Various authors (e.g., Bottinga (1968), Deines et al. (1974), Kim and O'Neil (1997), Mook (2000)) presented equations for the temperature dependence of the fractionation factors. Tabs. 3.6 and 3.7 summarise some of these relations together with the related determination method. Listed are those enrichment factor relations, which were recently published and/or are most frequently used for isotope calculations.

author	$\epsilon_{CaCO_3-HCO_3^-}$	T-range [°C]	method
Deines et al. (1974)	$\frac{95.000}{T_K^2} + 0.9$	?	linear regression analyses of thitherto empirical data
Romanek et al. (1992)	1 (constant value)	$10 - 40$	open system chemostat technique
Mook (2000)	$-\frac{4232}{T_K} + 15.1$	$0 - 40$	evaluation of the original experiment data of Rubinson and Clayton (1969) and Emrich et al. (1970)

Table 3.6: *Carbon enrichment factors for $\epsilon_{CaCO_3-HCO_3^-}$ from various authors determined by different methods for different temperature ranges.*

[5] If the isotope values for the first precipitated calcite were not available, they were linearly interpolated.

author	$\epsilon_{CaCO_3-H_2O}$	T-range [°C]	method
Kim and O'Neil (1997)	$\frac{18.030}{T_K} - 32.42$	$10 - 40$	'classical method' (bubbling N_2 through a bicarbonate solution)
Mook (2000)	$\frac{19.668}{T_K} - 37.32$	$0 - 40$	combination of different enrichment factors (Friedman and O'Neil (1977), Brenninkmeijer et al. (1983))
Coplen (2007)	$\frac{17.400}{T_K} - 28.6$	$13 - 40$	calibration at Devils Hole (Nevada) as a 'natural laboratory' in combination with data from Kim and O'Neil (1997)

Table 3.7: *Oxygen enrichment factors for $\epsilon_{CaCO_3-H_2O}$ from various authors determined by different methods for different temperature ranges.*

In Fig. 3.26 the isotope enrichment resulting from Tabs. 3.6 and 3.7 are compared with the data obtained from the laboratory experiments.

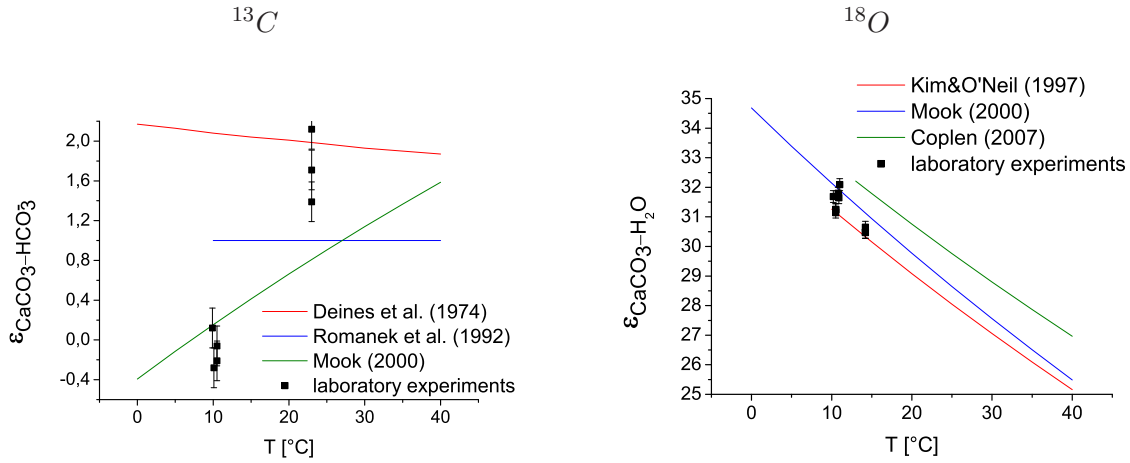

Figure 3.26: *Comparison between enrichment factors obtained from literature and from the laboratory experiments. $\epsilon_{CaCO_3-HCO_3^-}$ is indicated in VPDB and $\epsilon_{CaCO_3-H_2O}$ is indicated in VSMOW.*

$\delta^{13}C$: $\epsilon_{CaCO_3-HCO_3^-}$

From Fig. 3.26 (left) it is clearly observable that the temperature dependent $\epsilon_{CaCO_3-HCO_3^-}$ published by Deines et al. (1974), Romanek et al. (1992) and Mook (2000) differ significantly from each other. The data of Deines et al. (1974) and Romanek et al. (1992) show only a slight or no temperature-dependence at all, while Mook (2000) predicts an $\epsilon_{CaCO_3-HCO_3^-}$-increase of 1.5‰ within a temperature range of $30°C$. For example, for a temperature of $10°C$ the $\epsilon_{CaCO_3-HCO_3^-}$-value calculated by Mook (2000) is equal to 0.1‰, whereas Deines et al. (1974) predict a value of 2‰. This difference is problematic with regard to the interpretation of the results of the laboratory experiments depending on the choice of fractionation factors.

In case of the laboratory experiments equilibrium fractionation is not assumed. However, the results are nevertheless compared to the literature values, which reflect different temperature dependencies for $\epsilon_{CaCO_3-HCO_3^-}$. For $T = 10°C$ the experiment data agree with the results from Mook (2000), even if most of the data points plot below the theoretical curve. However, the experiment data reflect the tendency of the curve of Mook (2000) expressed by a strong increase of $\epsilon_{CaCO_3-HCO_3^-}$ with temperature. Furthermore, the experiment data show a greater fractionation for $23°C$ in comparison to the curve of Mook (2000). A linear approximation of the temperature dependence of the experiment data yields: $\epsilon_{CaCO_3-HCO_3^-} = 1.6 + 0,15 \cdot T_C$. For high temperatures ($23°C$) the experiment data are rather consistent with the curve of Deines (1974) within errors.

$\delta^{18}O$: $\epsilon_{CaCO_3-H_2O}$

In case of $\delta^{18}O$ the curves obtained from the literature all show a relatively similar behaviour. Likewise to $\delta^{13}C$, for a temperature of $10°C$ the experiment data agree with the curve of Mook (2000). Some data points around $12°C$ also correspond to the curve of Kim and O'Neil (1997), which is rather similar. Unfortunately, no experiment data exist for the enrichment factor of $23°C$. It would have been interesting if the developing of the experiment data for higher temperatures would agree with the literature data. Nevertheless, a linear approximation of the experiment data yields: $\epsilon_{CaCO_3-H_2O} = 34.4 - 0,27 \cdot T_C$ (VSMOW). This dependency is similar to the relations obtained from literature.

In general, it is noticeable that the data from the experiments agree in wide ranges with the equilibrium isotope enrichment factors obtained from literature within the errors. The data show the best fit with relations determined by Mook (2000). An exception is the enrichment factor $\epsilon_{CaCO_3-HCO_3^-}$ for $23°C$, for which the data points indicate a relatively high enrichment which does not agree with Mook (2000). This discrepancy could be related to poorly determined literature values for $\epsilon_{CaCO_3-HCO_3^-}$ which is affirmed by the great differences between the relations published by different authors. However, for high temperatures kinetic effects may dominate the precipitation mechanisms leading to kinetic enrichment factors which differ from the fractionation factors determined for equilibrium conditions (Mickler et al. (2006)). In this respect the value of $\epsilon_{CaCO_3-HCO_3^-}$ for $23°C$ obtained from the experiments would be an indication of the magnitude of the kinetic enrichment. Interestingly, for low temperatures around $10°C$ this effect seems to be too small to show a significant influence on the enrichment factor indicating equilibrium fractionation.

3.4.5 Comparison with numerical models

In this chapter the experiment results are compared to numerical models. The parameter settings from the experiments serve as input parameters for a forward model allowing a direct comparison between calculated and experimentally determined results. Deviations between data points and model curves can either be explained by errors within the experiment or with uncertainties in the model. These uncertainties strongly depend on the choice of parameters, and some of those respond very sensibly to slight changes leading to large differences in the model results. In this context it would be beneficial to set as much parameters fixed as possible to reduce the degrees of freedom in the model.

The numerical model used here is based on Mühlinghaus (2008). This model calculates the growth and isotopic composition of stalagmites, and the focus is on the reconstruction of temperature and drip rate of stalagmites grown under kinetic conditions. For the calculations presented here the model was simplified (i.e., excluding mixing effects between the single drops). In contrast, the model describes the chemical evolution of a single drop flowing along the channel. Here a Rayleigh fractionation process is assumed, which is generally described in chapter 2. The fractionation of the isotope and molecule ratios can be described by:

$$\frac{R(t)}{R_0} = \left(\frac{[HCO_3^-](t)}{[HCO_3^-]_0} \right)^{(\alpha-1)} \tag{3.6}$$

The temporal evolution of the bicarbonate is analogous to the calcium evolution (see also Eq. (3.4) in section 4.3.4):

$$[HCO_3^-](t) = [HCO_3^-]_{eq} + ([HCO_3^-]_0 - [HCO_3^-]_{eq}) \cdot e^{-\frac{t}{\tau}}, \tag{3.7}$$

where $[HCO_3^-]_{eq}$ represents the equilibrium bicarbonate concentration depending on the ambient p_{CO_2} and temperature and $[HCO_3^-]_0$ is equal to the initial bicarbonate concentration. The conversion time, τ, with $\tau = \frac{d}{a}$, which strongly depends on temperature was already calculated based on the calcite mass decrease for experiments conducted at different temperatures (see section 4.3.4). Furthermore, values for τ are indirectly indicated in Dreybrodt (1999) and Baker et al. (1998), who used the models of Buhmann and Dreybrodt (1985a) and Buhmann and Dreybrodt (1985b) to calculate precipitation rates. Amongst other things, they plotted the temperature dependence of the kinetic constant a [6] for three different film thicknesses and a constant p_{CO_2} of 300 ppm (see Fig. 2 in Baker et al. (1998)). Because the mathematical function is not included in his paper, the dependence of a from the film thickness was linearly interpolated for the relevant temperatures used in the experiments whereas the effect from p_{CO_2} is assumed to be small (Fig. 3 in Baker et al. (1998)). The interpolation for $10°C$ and $23°C$ and the associated functions are shown in Fig. 3.27. The resulting τ-values for a film thickness of 0.04 ± 0.005 cm are 1190 ± 35 s for a temperature of $10°C$ and 487 ± 20 s for a temperature of $23°C$, respectively.

[6] here the term 'a' is used for the kinetic constant instead of 'α' like in Baker to avoid confusion with the fractionation factors also denoted as 'α'.

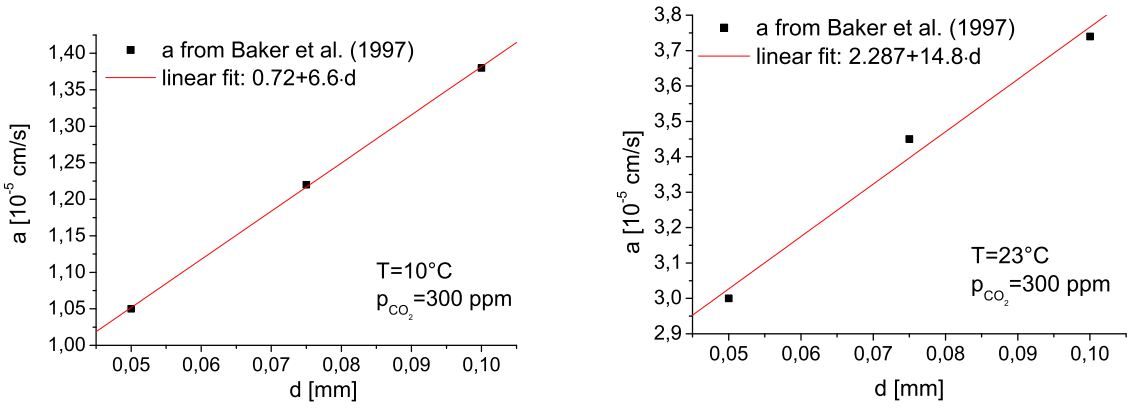

Figure 3.27: *Kinetic constant a versus the film thickness d, interpolated from* Baker et al. (1998) *for a temperature of* $10°C$ *(left) and* $23°C$ *(right).*

As input parameters for the model, temperature, the initial HCO_3^--concentration as well as the initial $\delta^{13}C$- and $\delta^{18}O$-values of the single experiments were used. The absolute isotope values are not relevant because all isotope values are related to the initial value and expressed as relative isotope enrichment.
Implemented in the model as fixed parameters are the p_{CO_2} of the channel atmosphere which was set to 10 *ppm*, and the film thickness d, determined with 0.04 *cm*. Even though the p_{CO_2} inside the channel has not been measured, it is expected that through the constant flow and exchange of nitrogen the p_{CO_2} is insignificantly small. A p_{CO_2} of 10 *ppm* provides a good estimation in this case, at least matching the assumed order of magnitude. Within this range no significant differences should become apparent in the model.

Variable parameters in the model are, (a) the conversion time, τ, (b) the equilibrium fractionation factors, α, and (c) the buffering time, b, between the water and the bicarbonate reservoir in case of $\delta^{18}O$.

(a) The conversion time, τ, controls the precipitation rate with the slow reaction $H^+ + HCO_3^- \rightarrow H_2O + CO_2$. In section 4.3.4, τ was determined by the calcite mass decrease of experiments $6D$ $(23°C)$ and $5B$ $(10°C)$. The experiments yield 287 ± 40 for $23°C$ and 780 ± 200 for $10°C$. In comparison the τ-values deduced from Baker et al. (1998) with the method described earlier in this chapter are 487 ± 20 for $23°C$ and 1190 ± 35 for $10°C$.
Taking both τ-values for both temperatures into account including the errors, τ ranges from 600 *s* -1200 *s* for $10°C$ to 250 *s* -500 *s* for $23°C$. For this reason, models were tested with different τ-values in the mentioned range.

(b) The combined equilibrium fractionation factor, α, which is also included in the Rayleigh-equation (Eq. (3.6)) is also not constant, which was pointed out in detail in section 3.4.4 where different fractionation factors from the literature were compared. The model applies a combined fractionation factor as it is for example used by Mickler et al. (2004). The word 'combined' in related to the fact that within the Rayleigh-fractionation several individual fractionation processes occuring between the different phases, are included.

In case of $\delta^{13}C$ the combined fractionation factor, α, is defined as

$$\alpha_{carbon} = \frac{1}{2}(\alpha_{CO_2-HCO_3^-}) + \frac{1}{2}(\alpha_{CaCO_3-HCO_3^-}).$$

For $\delta^{18}O$ an additional term for H_2O is included leading to

$$\alpha_{oxygen} = \frac{2}{6}(\alpha_{CO_2-HCO_3^-}) + \frac{3}{6}(\alpha_{CaCO_3-HCO_3^-}) + \frac{1}{6}(\alpha_{H_2O-HCO_3^-}),$$

whereas the factors multiplicated with the terms are chosen with respect to the proportion of oxygen amount in each product. As a model input for the fractionation factor $\alpha_{CaCO_3-HCO_3^-}$ here the values from the experiments were used whereas in case of $\delta^{18}O$ the fractionation factor $\alpha_{CaCO_3-HCO_3^-}$ is a sum of $\alpha_{H_2O-HCO_3^-} + \alpha_{CaCO_3-H_2O}$. For the fractionation factors not determined within the laboratory experiments, literature relations from Beck et al. (2005) and Mook (2000) were used in the model.

(c) In case of $\delta^{18}O$ the buffering time or exchange time, b, between the oxygen in the water and the bicarbonate is not well determined in literature. In the classical paper of Hendy (1971) b is estimated as 1500 s for $10°C$ and 680 s for $20°C$ for a pH-range around 8. If assuming a linear dependence, b is calculated with 434 s for $23°C$. However, these values comprise a great uncertainty but nevertheless are used in recently published papers concerning model calculations (Dreybrodt (2008), Scholz et al. (2009), Mühlinghaus et al. (2009)). Here, b can be estimated by implementing the best fit parameters found for $\delta^{13}C$ into the model input of $\delta^{18}O$, finally adjusting b to the experiment data.

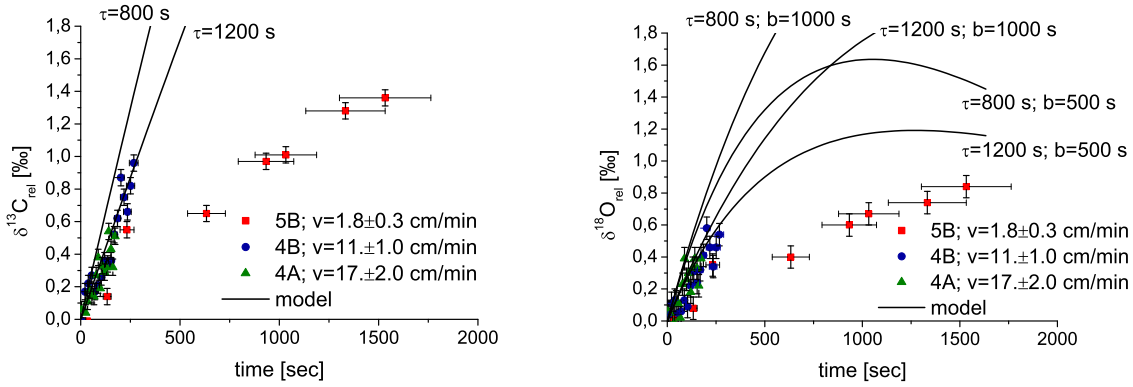

Figure 3.28: *Experiment results for varying flow velocites plotted together with model results for varying values of τ and b.*

Fig. 3.28 shows the experiment results for varying flow velocities and for a constant temperature of $10°C$ (analogous to Fig. 3.18). In addition, the model results are included here as black lines. The best fit is obtained for $\tau = 1200$, which represents the upper limit within

the most probable τ-values indicated before. However, only the first 250 s of the data are fitted by the model. Afterwards, the experiment data show a decrease in the enrichment with almost exponentially satiable characteristics whereas the model rather exhibits a linear behaviour, at least in the case of $\delta^{13}C$. However, for $\delta^{18}O$ the models offer curved lines whereas the degree of bending depends strongly on the buffering time, b. For $\tau = 1200\ s$ and $b = 500\ s$ the generel trend of the data is traced by the model, although the total enrichment of the model is obviously higher in magnitude.
Of course, the offset between model and data could be related to the fixed parameters, d and p_{CO_2}. For the film thickness, d, a decrease would lead to a faster conversion rate, τ, resulting in a greater total enrichment. Higher values for d would lead to a smaller enrichment but are basically ruled out because neither in experimental measurements nor in theoretical calculations, d exceeded a value of 0.04 cm. A lower total enrichment also could be reached, if the ambient p_{CO_2}would be increased. However, this would also affect the other model outputs.

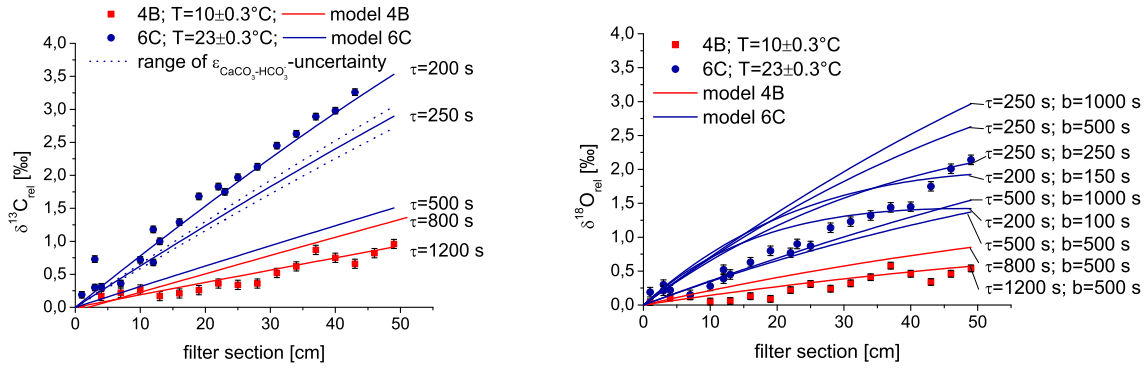

Figure 3.29: *Experiment results for varying temperatures plotted together with model results for varying values of τ, α and b.*

Fig. 3.29 shows the experiments carried out at different temperatures together with the model results. For $10°C$ the data for $\delta^{13}C$ as well as for $\delta^{18}O$ can be fitted well using $\tau = 1200\ s$ and $b = 500\ s$. For a temperature of $23°C$ no set of parameters can be found, which fits both $\delta^{13}C$ and $\delta^{18}O$. In case of $\delta^{13}C$ the model can be adjusted to the data if τ is equal to 200 s but this parameter value would be below the limit of expected τ-values possibly indicating that the temperature dependent variables in the model have to be considered to be erroneous.
Because the experimentally determined values of α show variations for the same temperature, the range of measurement values was exemplarily tested for their influence in the model. The dotted curves in Fig. 3.29 (left) point out the uncertainty if using the whole range of experimentally determined fractionation factors. In contrast to the other parameters, it can be seen that they have a less significant influence on the model variablility.
With respect to $\delta^{18}O$ different model parameter settings (τ and b) were tested for $23°C$. The resulting curves from the different parameter combinations are plotted in Fig. 3.29 (right). A τ-value of 200 s, which fits the data in case of $\delta^{13}C$, would lead to a higher enrichment with

respect to the experimental data if using a buffering parameter below 150 s. Values of b equal or above 500 s are implausible due to the fact that the buffering time for $23°C$ should be less than in the case of $10°C$, for which the model shows the best fits for $b = 500$ s. Furthermore, it is obvious for the $\delta^{18}O$-plot that for small values of τ and b (i.e., below approx. 250 s) the models more and more show a curved feature whereas the data rather imply a linear distribution. However, no model parameter setting can be found, which exactly fits the data enrichment of $\delta^{18}O$ in case of $23°C$. This leads to the conclusion that for high temperatures a so far unconsidered kinetic term could be possible, which is not included in the models. Nevertheless, it has to be kept in mind that the model assumptions are simplified and that effects like mixture between the single drops, excluded here, could also effect the isotope enrichment.

3.5 Conclusion

Generally, the theoretical models react very sensitive on slight changes of the parameters τ and b. Hence, it is important to determine the temperature dependent values as accurate as possible. Within laboratory experiments the τ-value was obtained by the calcite mass decrease along the channel. As a result, the experimentally determined τ-values are by a factor of 1.5 smaller in comparison to the literature values (Baker et al. (1998)). For the experiments carried out with $10°C$, the best model results were obtained applying the theoretical predicted values. In contrast, for the experiments conducted under the high temperature ($23°C$), the model calculated with the experimental determined τ-value rather reflects the high enrichment trend of the data.
Also in case of the buffering parameter b, the values obtained from literature (Hendy (1971)) do not fit the data adequately. The best fits are obtained if the models are calculated with b-values, which are approx. by a factor 3 smaller than the literature values.

Tab. 3.8 gives an overview of the different values for τ and b, obtained from i) laboratory experiments (determination of τ by calcite mass decrease), ii) literature (Baker et al. (1998) in case of τ and Hendy (1971) in case of b, respectively), and iii) theoretical models fitting the experiment data (Mühlinghaus (2008)).

	$10°C$	$23°C$
$\tau_{calcite\,mass\,decrease}$ $[s]$	780 ± 200	287 ± 40
τ_{Baker} $[s]$	1190 ± 35	487 ± 20
τ_{model} $[s]$	1200 ± 100	200 ± 10
b_{Hendy} $[s]$	1500	434
b_{model} $[s]$	500 ± 50	120 ± 30

Table 3.8: *Overview and comparison of τ- and b-values obtained from laboratory experiments, from literature (Baker et al. (1998) and Hendy (1971), respectively) and from the numerical models.*

The fact that both τ and b determined by the experiments are below the theoretical predicted values, leads to the conclusion that at least in case of high temperatures the chemical reactions may occur faster than expected.

For a general comparison of the experiment data the slopes $\Delta(\delta^{18}O)/\Delta(\delta^{13}C)$ of experiments $4A$, $4B$, $5B$, $6A$, $6B$, $6C$ and $7A$ were divided into distinct ranges (0.75, $0.6 - 0.63$, $0.43 - 0.45$). For the individual ranges the main experiment parameters (e.g., temperature, flow velocity and SI_{CaCO_3}) were investigated in terms of similar characteristics. Tab. 3.9 gives an overview of the linearly interpolated slopes plotted in Fig. 3.30 and the related experiments together with a qualitative classification of the parameters. Here, the parameter values are divided in high ($+$), middle ($\circ$) and low ($-$) (related quantitative values are specified in the caption in Tab. 3.9).

slope	experiment	T	v	SI_{CaCO_3}
0.75	$4A$	$-$	$+$	$\circ$
	$4B$	$-$	$\circ$	$\circ$
$0.6 - 0.63$	$5B$	$-$	$-$	$+$
	$6B$	$+$	$\circ$	$-$
	$6A$	$+$	$\circ$	$+$
$0.43 - 0.45$	$7A$	$+$	$\circ$	$+$
	$6C$	$+$	$\circ$	$\circ$

Table 3.9: *Qualitative comparison between slopes* $\Delta(\delta^{18}O)/\Delta(\delta^{13}C)$ *and experiment parameters with the following nomeclature for temperature, solution flow velocity and saturation index:*
$+ : T = 23°C;\ v = 17\ s;\ SI_{CaCO_3} \geq 1$
$\circ : v = 11\ s;\ SI_{CaCO_3}$ *between* 0.8 *and* 1
$- : T = 10°C;\ v = 1.8\ s;\ SI_{CaCO_3} < 0.7$

As a common feature for the slope-range around 0.4 all experiments exhibit a high temperature. The largest slope of 0.75 is equal to the experiment with the fastest flow velocity. The intermedium slope is characterised by experiments with low temperatures besides experiment $6B$, which instead offers a low SI_{CaCO_3} as a differing feature.

In his paper of 2006 Mickler et al. (2006) calculated the $\Delta(\delta^{18}O)/\Delta(\delta^{13}C)$-slopes for the two extreme cases of 'complete isotope buffering' and 'no buffering' (Fig. 6 in his paper) by a Rayleigh distillation model. In case of complete isotope buffering a horizontal slope results, indicating that CO_2 hydration and hydroxilation reactions are fast in comparison to the calcite precipitation, hence, leading to an oxygen isotopic equilibrium between bicarbonate and water. If no hydration and hydroxilation reactions are present, i.e., if the oxygen content of the bicarbonate is not buffered by the water reservoir, the slope of $\Delta(\delta^{18}O)/\Delta(\delta^{13}C)$ reaches maximum. However, this endmember condition in unrealistic. In natural systems or in the laboratory one would expect an intermediate slope depending mainly on temperature and solution flow speed.

Similarly to Mickler et al. (2006) the two limiting values were calculated with the model of Mühlinghaus (2008). Fig. 3.30 gives an overview of the $\Delta(\delta^{18}O)/\Delta(\delta^{13}C)$-slopes obtained from the experiments including the resulting values for the buffering limits. It can be observed that the isotope slopes resulting from the experiments are between the two extreme cases of 'no buffering' and 'complete buffering'. For $23°C$ the data is buffered approx. 65% whereas for $10°C$ the data is only buffered up to approx. 33%, if the model assumptions are correct.

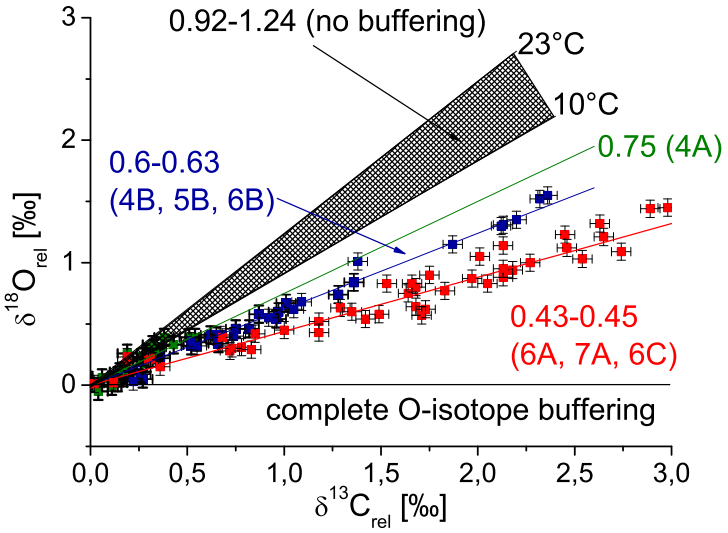

Figure 3.30: *Overview of the isotope correlation $\delta^{18}O(\delta^{13}C)$ for most of the laboratory experiments in comparison with the expected slopes for the extreme cases of 'no buffering' and 'complete buffering'.*

Chapter 4

Cave experiments

4.1 General

The laboratory experiments described in the previous chapter were carried out within the framework of the DAPHNE-research group[1], subproject 1: 'Synthetic Carbonates'. Also included in DAPHNE is a subproject focusing on cave monitoring (subproject 2). The main focus of this subproject is to understand how the cave environments respond to climatic changes above the cave. Within this subproject two cave systems (Grotta di Ernesto, northern Italy and Bunkerhöhle, north-western Germany) are monitored with respect to cave climate (i.e., temperature, humidity and CO_2-partial pressure), drip water composition (i.e., isotopes, ion-concentration) and soil conditions above the cave (i.e., soil water composition, CO_2-partial pressure). Furthermore, selected stalagmites were removed from the caves for a detailed analysis.
The long-term monitoring of the water samples is carried out in intervals of one month. Included in the monitoring program is the analysis of the drip water composition, i.e., stable isotopes and composition of minor and trace elements and the determination of drip intervals at several drip sites. Additionally, watch glasses were put beneath active drip sites to collect modern precipitates.
Sampling of modern calcite is useful to investigate the actual precipitation mechanisms. Mickler et al. (2004) and Banner et al. (2007), for example, used glass plates affixed at the top of stalagmites to study seasonal variations in growth rate and isotopic composition. In situ cave experiments as a nondestructive sampling method enables the determination of the actual fractionation between the precipitated calcite and the feeding drip water. In this manner, it can be tested if calcite is precipitated in isotopic equilibrium with the drip water or if kinetic isotope fractionation occurs.

In this context, channel experiments (glass channels with a glass fibre stripe inside) were set up beneath active drip sites. In contrast to the usage of flat glass plates or watch glasses, the channel experiments provide the possibility to study the temporal evolution of the precipitated calcite along the channel.

[1]DAPHNE=dated speleothems archives of the paleoenvironment; research project funded by DFG

Channel experiments were conducted in the Bunkerhöhle and also in the nearby B7-Höhle. The two cave systems are located close to Iserlohn (Sauerland) and are part of the karstified upper devonian massive limestone.

In total, 4 glass channels were put underneath active drip sites for a time period of $100-300$ days. It was difficult to find an adequate location for the channels because in contrast to glass plates, which can be put directly on top of the stalagmites, the channel systems need a fixation such as a tripod. The channels were preferentially put underneath stalactites, where the correlating stalagmites were already cut off.

4.2 Bunkerhöhle

4.2.1 Location

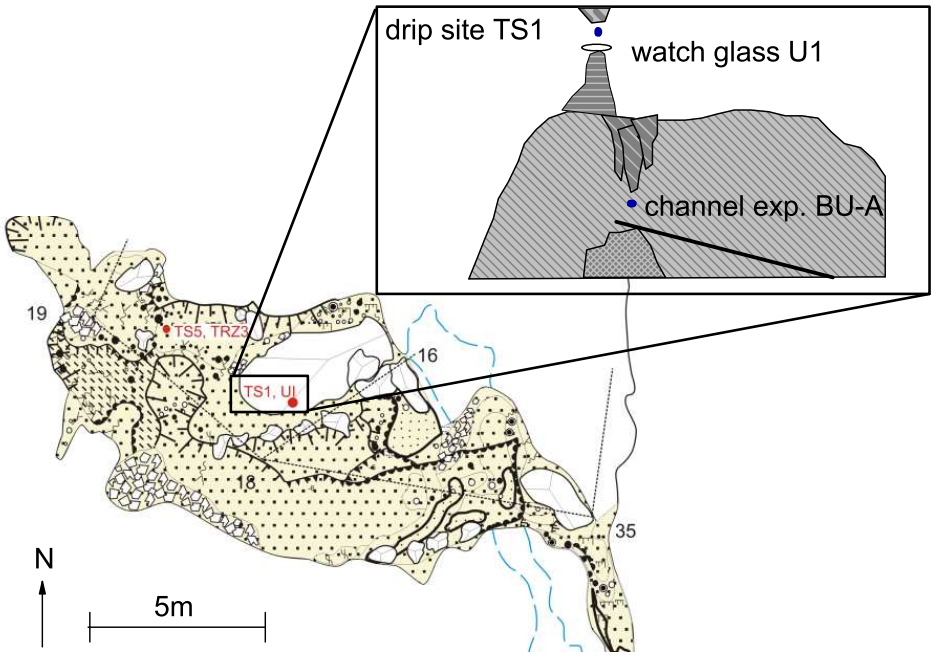

Figure 4.1: *Map of Bunker-Höhle, chamber* 1 *and sketch of the set-up of experiment BU-A.*

The Bunkerhöhle (map in Fig. 4.1) is divided in a strongly ventilated entrance area followed by two larger moderatly ventilated chambers separated by narrow passages. The temperature in Bunkerhöhle is $10.5°C$ in average, and the CO_2-partial pressure ranges from 610 *ppm* to 870 *ppm* depending on the seasonal conditions. Detailed descriptions of monitoring results can be found in Schröder-Ritzrau et al. (2009) and Fohlmeister (2008).

Channel experiment $BU-A$ was placed in chamber 1 close to monitoring drip site $TS1$ (Fig. 4.1), which is characterised by extremely high drip rates in the range of a few seconds.

Unfortunately, it was not possible to install the channel system directly below $TS1$ because the related stalagmite was connected to a sinter wall. Instead, the channel was set up at the bottom of the sinter shoulder approx. 1 to 2 meters away from the actual point of drip water impinge. Fig. 4.1 shows a sketch of the formation at $TS1$, illustrating the drip water path: First, the drip water sips onto watch glass $U1$, which serves as a sampler for modern calcite. Subsequently, the water flows alongside a sinter shoulder before finally reaching the top of the glass channel set up with an inclination of approx. $10° - 20°$.

Channel experiment $BU - B$ was directly set up underneath drip site $TS2$ in chamber 2. Unfortunately not enough calcite for isotope analysis was precipitated within a period of 4 month. Neither the drip interval nor the SI_{CaCO_3} give reason for the sparse calcite precipitation at this site.

Tab. 4.1 lists the actual monitoring data for drip sites $TS1$ and $TS2$. The data represent mean values for the period, in which the channels were placed inside the cave (i.e., 4 month). The standard deviations are included in the table to point out the fluctuation range. The values of drip site $TS1$ are related to water samples taken immediately whereas in case of $TS2$ the water is sampled over a period of one month. Hence, in the latter case, degassing and precipitation already could have influenced pH and isotopic composition of the water due to its long residence time in the sampling vessel. This was confirmed by comparative measurements, showing an enrichment of the long-time drip water samples of up to $2-3‰$ in $\delta^{13}C$ in comparison to the immediately taken drip water samples. A detailed list of data from Bunkerhöhle can be found in Appendix B.

	TS1	SD	TS2	SD
dT [sec]	3.4	2.5	30	0
pH	8.02	0.07	8	0.03
Ca^{2+} [mg/l]	93	6.6	79	3.3
HCO_3^- [mg/l]	215	10.9	139	13.6
SI_{CaCO_3}	0.7		0.5	
$\delta^{13}C$ [‰]	−11.5	0.7	−7.8	0.3
$\delta^{18}O$ [‰]	−8.4	0.1	−8.3	0.1

Table 4.1: *Drip water values for $TS1$ and $TS2$ averaged over the measurement period (april-august). Additionally, the standard deviations of the mean values are indicated.*

4.2.2 Calcite crystals

After removing the channels from the caves, the calcite crystals were analysed with SEM and compared to the crystals grown in the laboratory or on watch glasses.

Generally, crystal habits are primarily controlled by the degree of supersaturation of the solution (Gonzáles et al. (1992)). The higher the SI_{CaCO_3}, the more complex the crystal morphology. Even though the SI_{CaCO_3} of the cave drip water is generally lower than the SI_{CaCO_3} adjusted in the laboratory experiments, the observed crystal habits shows contrary characteristics. In comparison to the rhombohedral crystals observed in the laboratory (Figs. 3.7 and 3.8 in chapter 3), which mostly exhibit cubic shapes with flat surfaces, the calcite

precipitated in the cave rather exhibit hexagonal crystals (scalenoeder, prisms, or mixtures of both) with a rough surface structure including holes and small cracks. Hence, the differences in crystal habit are certainly related to the different purity of the drip solutions. The solutions used in the laboratory exclude minor and trace elements (e.g., Mg^{2+}, Sr^{2+}, Ba^{2+}), clay, and organic material, which all influence the crystallisation process and morphological development of calcite crystals in a different manner (e.g., Paquette and Reeder (1995), Fernandez-Diaz et al. (1996), Jimenez-Lopez et al. (2003), Taylor and Chafetz (2004)).

Fig. 4.2 shows SEM-pictures of calcite crystals precipitated on watch glass $U1$ at drip site $TS1$ (Fig. 4.2, left) compared to crystals obtained from in situ channel experiments (Fig. 4.2, right). The crystals precipitated on the glass fibre stripe are generally smaller and exhibit a rougher surface without clear crystal faces. The observed differences are possibly related to the drip water evolution. First, the drop impinges from the cave ceiling onto the watch glass with its clean surface. At this stage the drip water is assumed to possess the highest degree of supersaturation with respect to calcite leading to large, homogeneous crystals. Before dripping onto the channel, the solution flows along the sinter shoulder. Hence, particles of clay and mud probably infiltrate into the drip solution, maybe influencing characteristics of crystal growth. Furthermore, the degree of supersaturation has already diminished along the flow path, which may also control the crystal shape.

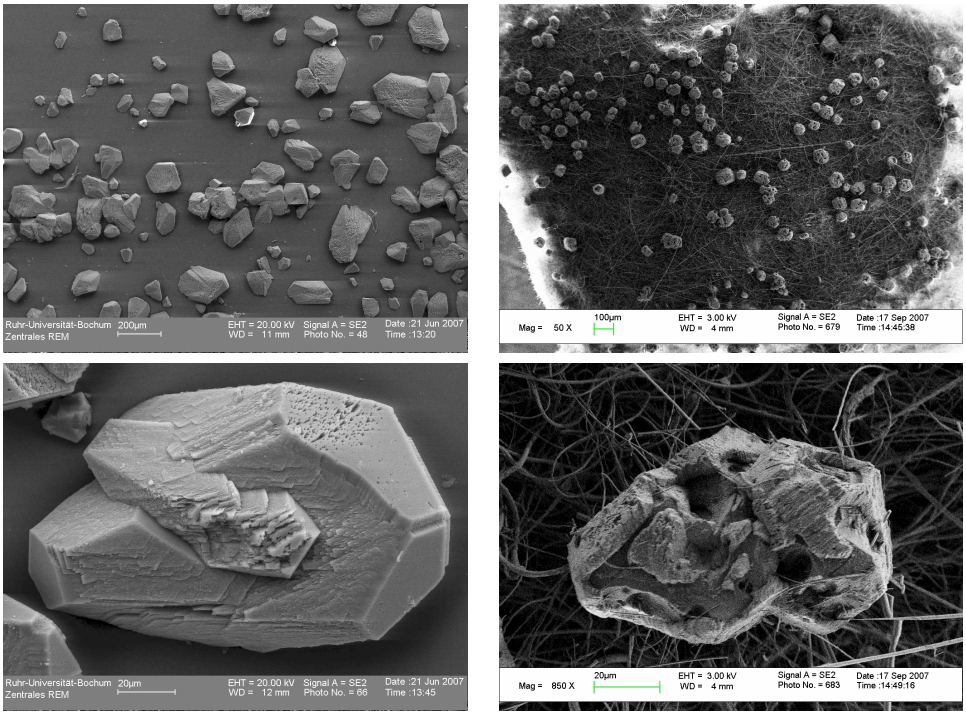

Figure 4.2: *SEM-pictures of calcite crystals precipitated in Bunkerhöhle on watch glass $U1$ at drip site $TS1$ (left) and on the glass fiber stripe of channel experiment $BU - A$ (right).*

4.2.3 Calcite precipitation along the channel

Experiment $BU - A$ was set up in Bunkerhöhle for a period of 113 days (April to August). Within this time, between 1 mg/cm^2 and 9 mg/cm^2 calcite was precipitated on the filter resulting in an integrated mass of 127 mg analogous to 1.12 mg/d. Within this time, 25% less calcite was precipitated on the watch glass. The difference in the precipitation amount of calcite may be caused by the difference in surface and geometry of the watch glass and the slightly curved glass fibre stripe on the channel. Furthermore, the glass fibre stripe on the channel promotes heterogeneous nucleation.

The mass development along the filter is shown in Fig. 4.3. It is noticeable that the amount of precipitated calcite decreases by approx. 80% in relation to the initial value at 10 cm. A similar decrease within the first few centimeters was observed for laboratory experiment $7A$, which was conducted under laboratory atmosphere, and calcite precipitation was, thus, solely driven by the initial supersaturation of the feed solution. For natural stalagmites, supersaturation is expected to be highest at or nearby the point of drip water impinge. After flowing along the sinter shoulder the supersaturation of the drip water with respect to calcite be close to equilibrium. Nevertheless, it could be observed that after the second impinge (i.e., onto the channel) still a great amount of calcite is precipitated close to the point of impinge. Hence, it can be concluded that the solution has not yet reached equilibrium.

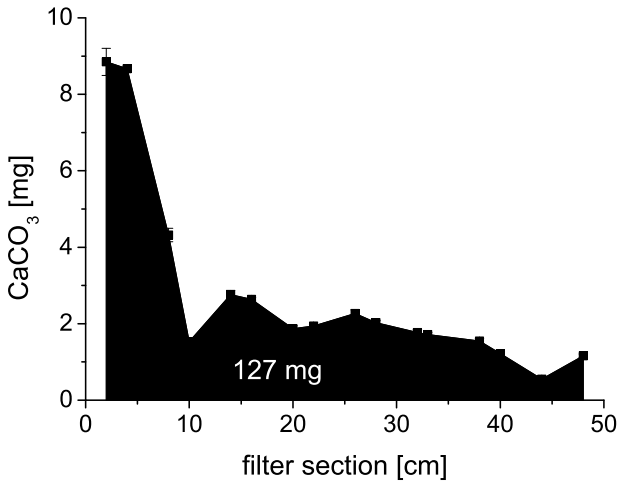

Figure 4.3: *Mass distribution of in situ experiment $BU - A$.*

4.2.4 $\delta^{13}C$ and $\delta^{18}O$ evolution along the channel

Fig. 4.4 shows the isotopic evolution for channel experiment $BU-A$. During the removement of the glass fibre stripe a small fissure between 30 cm and 35 cm was detected. Consequences of this asperity can be observed in the $\delta^{13}C$-values (Fig. 4.4, left). $\delta^{13}C$-values at the location of the fissure are significantly higher interrupting the continuous isotope enrichment trend. In contrast, no similar outliers can be observed for $\delta^{18}O$ except for a small shift around 30 cm.

Generally, $\delta^{18}O$ (Fig. 4.4, right) shows only a marginal enrichment along the channel. During the last 20 *cm* the isotope values are nearly constant indicating that the oxygen isotope equilibrium has been reached. In contrast, the $\delta^{13}C$-values increase until the end of the channel. The mentioned isotope characteristics lead to a moderate slope (0.27 ± 0.05) in the linear interpolation of $\Delta(\delta^{18}O)/\Delta(\delta^{13}C)$ (see Fig. 4.5). It can be concluded that the oxygen isotopes are almost completely buffered by the water reservoir.

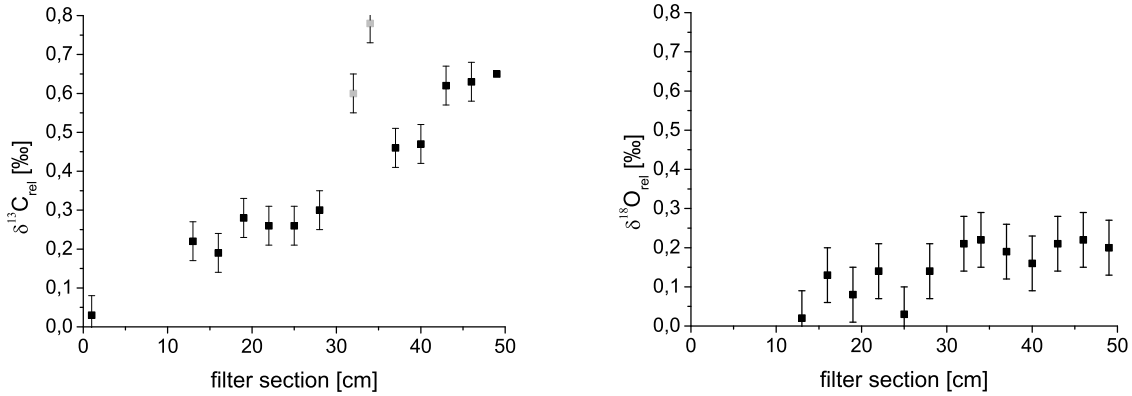

Figure 4.4: *$\delta^{13}C$ (left) and $\delta^{18}O$ (right) evolution for in situ experiment $BU - A$. Between* 30 *cm and* 35 *cm the glass fibre stripe was ripped lengthwise indicated by light grey values in the isotopic values.*

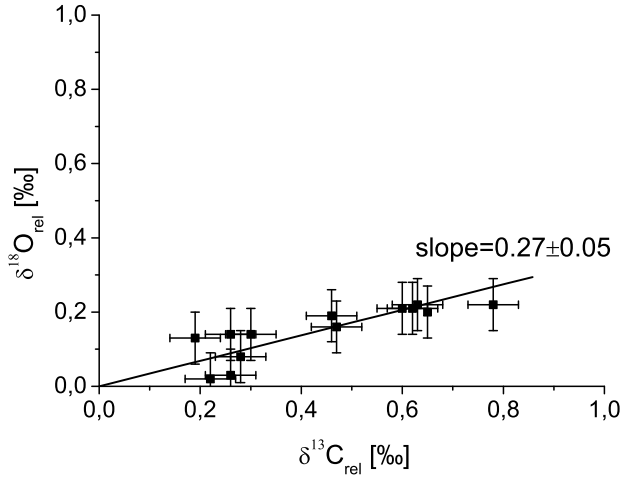

Figure 4.5: *Isotope correlation $\delta^{18}O(\delta^{13}C)$ for in situ experiment $BU - A$. The data are linearly interpolated.*

In Fig. 4.6, $\delta^{13}C$- and $\delta^{18}O$-values from Fig. 4.4 are plotted together with the isotope range of the monitored drip water ($TS1$) and the isotope values determined for the watch glass calcite ($U1$). For better comparison, the value range is related to the drip water data measured within the season between April and August. In case of the watch glass calcite the values in the plot refer to the season between May and September and represent integrated values over the summer season. The range of values result from several isotope measurements carried out along the radius of the watch glass whereas no trend could be observed for a larger enrichment with increasing radius. Additionally, in Fig. 4.6 the range of equilibrium fractionation between the drip water and the calcite is plotted, using the whole range of fractionation factors documented in literature (see section 3.4.4 in chapter 3). In case of $\delta^{13}C$, both the monitored drip water and the fractionation factors offer a wide range. Hence, it can not definitely be decided if the precipitated calcite is consistent with equilibrium fractionation. In case of $\delta^{18}O$, the fractionation factors also cover a wide range, but the drip water exhibits only a narrow range of isotope values. It can be observed that the oxygen isotope values of the calcite precipitated on the watch glass is more enriched then expected from the range of equilibrium fractionation factors. This leads to the assumption that kinetic effects such as fast CO_2-degassing or other effects like evaporation play a significant role at this drip site. Similar results were described by Mickler et al. (2004) who sampled watch glass calcite in cave systems on Barbados. For several drip sites they observed that in case of $\delta^{13}C$ most of the calcite isotope data fit within the range of used fractionation factors. In contrast, the $\delta^{18}O$-values were in the most cases consistently 2.3‰ higher than expected for isotope equilibrium. Mickler et al. give two explanations for the observed shift. On the one hand they explain the discrepancy with poorly determined equilibrium values $\alpha_{CaCO_3-HCO_3^-}$ for $\delta^{18}O$, referring to the values determined by Usdowski and Hoefs (1993). On the other hand they do not exclude a kinetically driven change of $\alpha_{CaCO_3-HCO_3^-}$ due to an increase in the calcite precipitation rate.
There is a general correlation between drip water discharge and the deviation of the predicted $\delta^{18}O_{CaCO_3}$ (based on $\delta^{18}O_{drip\,water}$) from the measured $\delta^{18}O_{CaCO_3}$. For $TS1$, Schröder-Ritzrau et al. (2009) showed, that in the month with the highest drip rate, the predicted and measured $\delta^{18}O$-values are similar. In contrast for months with lower drip rates the predicted values are below the measured values.

Besides the isotopic shift between the drip water and the watch glass calcite, an additional shift exists between the isotope values of the watch glass calcite and the calcite precipitated on the channel (i.e., 3.1‰ for $\delta^{13}C$ and 0.6‰ for $\delta^{18}O$ [2]). This shift is most likely related to the great distance between the watch glass and the channel. After the impinge on the watch glass the drip water flows along the sinter shoulder until it reaches the bottom of the shoulder and drips onto the upper part of the channel. Along the flow path the drip water continuously looses CO_2 leading to an increasing isotope enrichment within the solution and, hence, the precipitated calcite.

[2] In case of $\delta^{18}O$ the first measured filter section is identical with 11 cm.

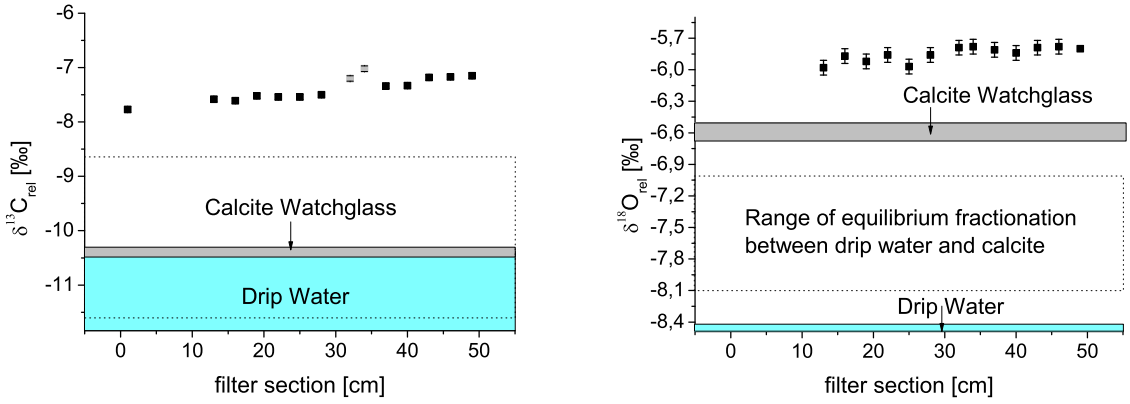

Figure 4.6: *Combined plot, showing the results of TS1 in Bunkerhöhle: $\delta^{13}C$ (left) and $\delta^{18}O$ (right) for in situ experiment BU − A together with the isotope range of the drip water and the watch glass calcite. The dotted rectangles indicate the range of the theoretical equilibrium fractionation values (whole range calculated with fractionation factors from literature) between the drip water and the calcite.*

4.3 B7-Höhle

4.3.1 Location

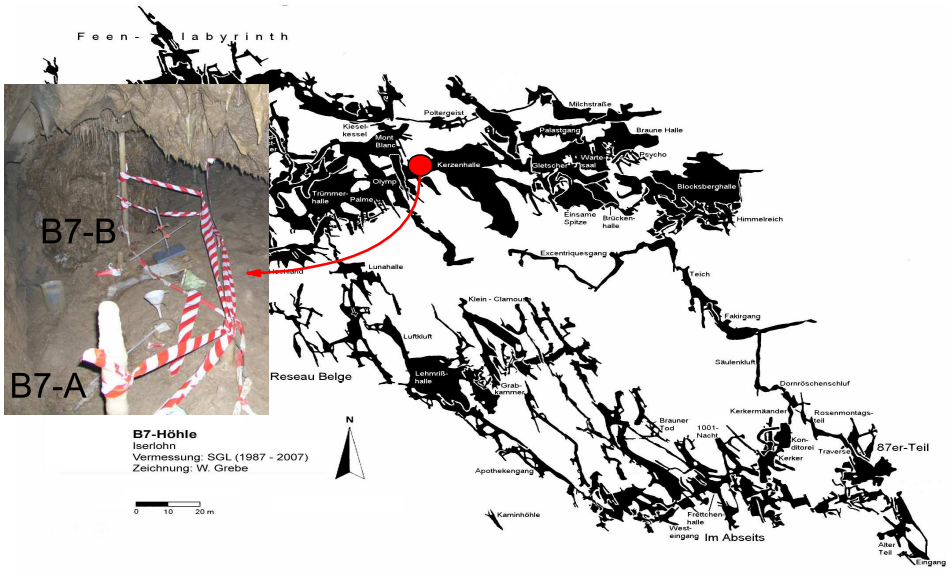

Figure 4.7: *Map of B7-Höhle and picture of the set-up of experiments B7-A and B7-B in the northern part of the cave (interconnection of 'Kerzenhalle' and 'Olymp').*

In addition to exp. $BU - A$, carried out in Bunkerhöhle, two channel experiments were set up in the nearby B7-Höhle for a time period of 9 months (25.04.'07-02.02.'08). Fig. 4.7 shows a map of B7-Höhle together with a picture of the channel experiments indicated as $B7 - A$ and $B7 - B$. The two experiments were placed in the northern part of B7-Höhle, in the interconnection of 'Kerzenhalle' and 'Olymp'.
This part of the cave was discovered in 1988 and is described in detail in Niggemann (2000). The rock cover at this part of the cave is approx. 50 m, and the host rock basically represents devonian limestone. The air temperature in Kerzenhalle measured in 1997 was 9.4 ± 0.1°C (annual mean). The average of the mean annual outside temperature between 1981 and 1996 was 9.85°C (unpublished data of the Deutsche Wetter-Dienst Essen). In 2007 the mean annual temperature has increased about approx. 0.5°C (Niggemann, pers. comm.), which is also confirmed by a temperature measurement in Kerzenhalle during the removal of the experiments.
The CO_2-concentration of the cave air was not measured but the cave systems in Sauerland usually have a p_{CO_2}, which is $2 - 10$ times higher than the atmospheric p_{CO_2} with highest values in late summer and early autumn (Pust (1990)). The relative humidity in these cave systems exceeds 95% in the majority of cases, so that evaporation can be neglected.

The glass channels were put at the former locations of stalagmites $STAL-B7-6$ and $STAL-B7-7$, which were explored by Niggemann (2000), who also carried out the monitoring of the corresponding drip water in the period between 1997 and 1999. The two drip sites are within a short distance of each other (i.e., 1 m - 2 m) and are fed by small macaroni-stalactites located at heights above ground between 50 cm and 100 cm . Channel B7-A was placed at the former location of $STAL-B7-7$. Due to the very low drip rate at this site a funnel on a wire construction was used to centralise the drip onto the top of the channel (Fig. 4.8, left). The channel itself was put on a flagstone formerly used as a surface for calcite precipitation analysis. Hence, the channel had only a low inclination presumably leading to a rather low flow velocity. The other channel experiment $B7-B$ was fixed with a tripod at the former location of $STAL-B7-6$ (Fig. 4.8, right).

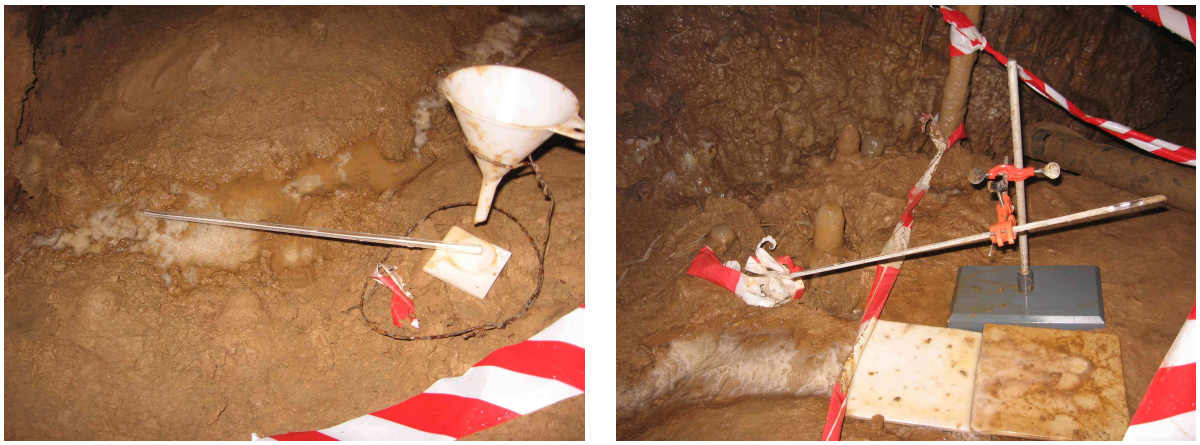

Figure 4.8: *Close-ups of the experiment set-ups in B7-Höhle: $B7-A$ (left) was placed at the former location of $STAL-B7-7$and $B7-B$ (right) according to the former location of $STAL-B7-6$, both investigated by Niggemann et al. (2003).*

4.3.2 Comparison with previous data

From the campaign of Niggemann (2000) in the late 1990s already a lot of data are available for the drip waters as well as for the stalagmites and modern calcite. Tab. 4.2 lists some selected data values of drip sites $B7-A$ and $B7-B$. The values are related to the drip water and to the actual calcite precipitate. Unfortunately, during removal of $B7-A$ no drip water samples were taken. A detailed list of data from B7-Höhle can be found in Appendix B.

Stalagmite $STAL-B7-7$ had a length of 62 cm and was still actively growing during drip water monitoring. The indicated values of $\delta^{13}C_{speleothem}$ and $\delta^{18}O_{speleothem}$ in Tab. 4.2 refer to the top of the stalagmite. The nearby $STAL-B7-6$ had a total length of 20 cm. Unfortunately, the isotopic composition of $STAL-B7-7$ was not analysed. Instead, $\delta^{13}C$- and $\delta^{18}O$-values were determined for the recent calcite, which was precipitated on the PET-flasks after two months of water sampling.

	STAL-B7-7	B7-A		STAL-B7-6	B7-B
	Niggemann	this work		Niggemann	this work
drip interval [sec]	$\overline{271} \pm 23$	-		$\overline{3.2} \pm 0.4$	$3-5$
$length_{stalagmite}$ [cm]	62	-		20	-
$length_{stalactite}$ [cm]	20	-		3	-
$Ca^{2+}_{drip\,water}$ [mg/l]	$\overline{110} \pm 13$	-		$\overline{122} \pm 24$	131 ± 8
$Mg^{2+}_{drip\,water}$ [mg/l]	$\overline{11.8} \pm 0.04$	-		$\overline{9.24} \pm 1.07$	7.14 ± 0.35
Mg/Ca	$\overline{0.108} \pm 0.024$	-		$\overline{0.078} \pm 0.012$	0.055
$HCO^{-}_{3\,drip\,water}$ [mg/l]	$\overline{213} \pm 14$	-		$\overline{263} \pm 12$	309 ± 10
$pH_{drip\,water}$	$\overline{7.65} \pm 0.08$	-		$\overline{7.43} \pm 0.1$	7.53 ± 0.05
$\delta^{13}C_{drip\,water}$	-9.13	-		-12.2	-14.2 ± 0.1
$\delta^{18}O_{drip\,water}$	$\overline{-8.37} \pm 0.22$	-		$\overline{-8.43} \pm 0.35$	-
actual growth rate $[\mu m/a]$	55	-		70	-
$\delta^{13}C_{speleothem}$	-9.75	-9.5 ± 0.1		-11.6	12.6 ± 0.2
$\delta^{18}O_{speleothem}$	-6.28	-5.65 ± 0.15		-5.76	5.8 ± 0.1

Table 4.2: *Results of drip water and speleothem samplings: Values of* $STAL-B7-7$ *and* $STAL-B7-6$ *were measured by Niggemann between 1997 and 1999 and respresent the annual mean. The* $\delta^{13}C_{drip\,water}$ *values of* $STAL-B7-7$ *and* $STAL-B7-6$ *were measured once (07.01.1999). Samples for* $B7-A$ *and* $B7-B$ *were taken during removal of the experiments (02.02.2008).* $\delta^{13}C_{speleothem}$ *and* $\delta^{18}O_{speleothem}$ *refer to the top of the stalagmite in case* $STAL-B7-7$ *and to the calcite deposited on a PET-flask in case of* $STAL-B7-6$*. For* $B7-A$ *and* $B7-B$ $\delta^{13}C_{speleothem}$ *and* $\delta^{18}O_{speleothem}$ *represent the values of the topmost calcite precipitated on the channel (interpolation).*

The saturation index of the drip water with respect to calcite varies independently of the season between 0.1 and 0.4 for both drip sites. Hence, the solution is $1-2.5$ times supersaturated and, therefore, calcite precipitation can be expected for the whole time of the year. Other cations and anions within the drip water, which are not listed in Tab. 4.2, but which are in the order of several ppm are Na^{+}, Cl^{-}, NO^{3-} and SO^{4-}. K^{+} and Sr^{2+} only exist in traces and are below 1 ppm.

It is obvious from Tab. 4.2 that the values obtained from Niggemann (2000) and the values measured within this campaign agree more or less within the range of errors, although, nearly 9 years lie between the sampling. An exception is $\delta^{13}C_{drip\,water}$, which offers a difference of 2‰ between $STAL-B7-6$ and $B7-B$. The more enriched value in case of $STAL-B7-6$ is possibly related to the sampling technique. The PET-flasks were collected every two weeks or every month. In this manner, ongoing degassing of CO_2 along with calcite precipitation leads to an increase in the stable isotope values especially in $\delta^{13}C$. The discrepancy is also observable in $\delta^{13}C_{speleothem}$ with a difference of 1‰ between the calcite precipitation of $STAL-B7-6$ and $B7-B$. The possibility that the original $\delta^{13}C$-content of the drip water has changed during the last 9 years due to changes in vegetation, or the drip water flow path is unlikely. Rather the difference results from seasonal variations in $\delta^{13}C_{drip\,water}$, which could fluctuate up to 5‰ (e.g., this was observed for drip waters in Bunkerhöhle).

4.3.3 Calcite crystals

After a period of 9 months both glass fibre stripes were partly or in their whole length calcified. In the upper part of channel $B7-B$ even a little stalagmite or flow stone has grown, which is displayed in Fig. 4.9. It formed at the point of drip water impinge, lying longitudinally in the channel with a length of 2.7 *cm* and exhibits a cylindrical form representing the diameter of the glass channel.

Figure 4.9: *Little flow stone grown during* 9 *month in the upper part of the glass channel in experiment* $B7-B$*. The white fabric visible at the subsurface represents a part of the glass fibre stripe.*

Besides the calcite crystals on the glass fibre stripe, which were macroscopically visible, also clay particles were present on the filter, sometimes observable as brown tracks of a few centimeters length. On some sections of glass fibre stripe $B7-B$ fine, cobweb-like and black hairy structures could be detected, which subsequently were examined under stereo microscope and SEM. Some selected microscope pictures are displayed in Fig. 4.10.

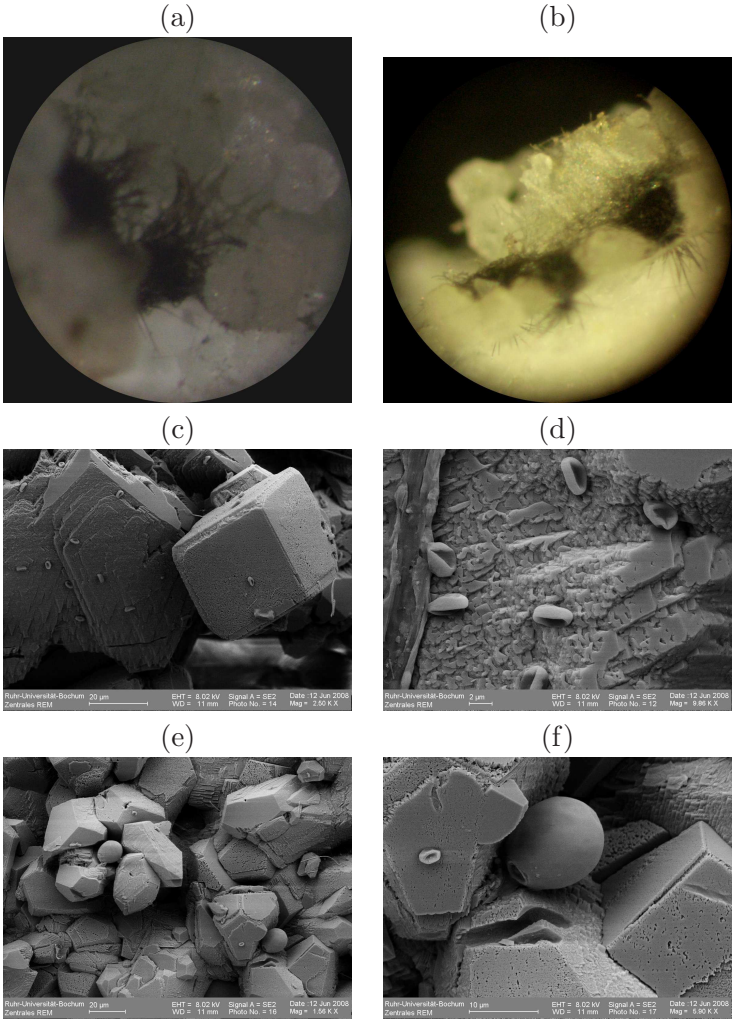

Figure 4.10: *Microscope pictures of channel experiment $B7-B$, section* 13. *(a)-(b): Stereo microscope pictures showing black hairy structures which may indicate some kind of spores or fungi. (c)-(f): high resolution SEM-pictures of section* 13.

Pictures (a) and (b) are light microscope photos of filter section 13 showing the black structures, which are embedded in the precipitated calcite. In pictures (d)-(f), several SEM-micrographs show the related microstructures on the affected filter section. Here, two kind of structures can be differentiated:

1.) flat, ringlike structures with an impression in the centre, sometimes partly incorporated into the calcite crystals ((c) and (d) in Fig. 4.10).

2.) olive-shaped structures with a diameter of approx. 10 μm, which offer a small opening or round cap at one side ((e) and (f) in Fig. 4.10).

If the two mentioned structures are somehow connected to each other, for example, if the smaller structure is a part of the large round structure, is questionable. Most likely the observed structures are of organic origin, but an exact classification of the potential mi-

croorganisms is hardly possible. Generally, speleothems often exhibit various kinds of microorganisms such as fungi, algae, and bacteria. However, the extent of microbial interactions in speleothems is uncertain (Northup and Lavoie (2001)). It is assumed that the structures observed in the cave experiments basically represent some kind of fungi, spores or pollen. D. Riechelmann did also find evidence for organic matter on some watch glass samples. The structures on the watch glasses were similar to the small structures observed on the filter, but they were additionally covered by a filamentous netting supporting the assumption of fungoids. On some SEM-pictures it seems that the structures 'destroy' the calcite leading to holes on the crystal surface. From geomicrobiological studies it is known that microorganisms can contribute to calcite precipitation in a constructive as well as in a destructive manner, often on the same substrate (Cacchio et al. (2004)). For example, some bacteria and fungi can promote calcite precipitation by increasing the bicarbonate concentration through oxidation and reduction processes, hence, increasing the supersaturation with respect to calcite (Barton and Northup (2007)). Furthermore, microbial structures like fungal hyphae may act as nucleation sites for calcite crystallisation (Went (1969)). Unfortunately, it is unknown, if, and to what extent microorganisms influence the isotope composition of the calcite.

4.3.4 Calcite precipitation along the channel

Because the channel systems were place for 282 days in total in B7-cave, a lot of calcite precipitated within this time especially at site $B7-B$ associated with a high drip interval. Fig. 4.11 shows the calcite mass distributions for experiment $B7-A$ and $B7-B$. Also included in Fig. 4.11 is the mass of the little flow stone in the upper part of $B7-B$, holding a value of approx. 1 g.

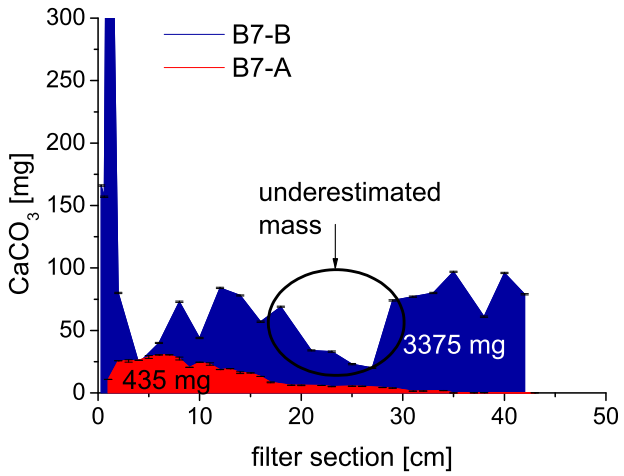

Figure 4.11: *Mass distribution of in situ experiments $B7-A$ and $B7-B$. The black circle indicates sections, where much of the glass fibre stripe got stuck at the channel, which underestimates the true mass of calcite.*

It can be observed that in case of $B7-A$ the mass reduces from 25 mg in the upper part of the glass fibre stripe to a few μg after a distance of 35 cm. The small amount of calcite precipitated in the bottom part of $B7-A$ leads to the conclusion that by the time the drip water is already in equilibrium. This could have been enhanced by a low flow velocity, which is assumed for $B7-A$ due to the small inclination of the channel. Furthermore, the mass distribution of $B7-A$ shows a mass peak at approx. 7 cm, and not, like expected, at the point of drip water impinge (1 cm). For the laboratory experiments an analogous behaviour was observed for those experiments, which offered a low initial SI_{CaCO_3}. This effect was explained by cristallographic characteristics (see section 4.3.4 in chapter 3). Hence, for the cave this observation supports the possibility that not all excess CO_2 in the drip water was lost due to the impinge. Rather the CO_2-degassing rate dominates in the beginning of precipitation until the precipitation rate keeps pace with the degassing, i.e., when the SI_{CaCO_3} has reached a certain limit, which coincides with the point of maximum precipitation.
In contrast, the mass distribution for $B7-B$ shows no clear trend besides the strong mass decrease in the beginning caused by the flow stone. The mass values strongly fluctuate. Here, a lot of calcite was stuck on the channel itself, e. g., to a large extent between 20 cm and 30 cm. This results in an underestimation of the calcite mass (indicated in Fig. 4.11).

Generally, it is possible to calculate the maximum amount of calcite precipitation for a given solution composition, temperature and CO_2-partial pressure with a rate equation program within PHREEQC. As initial values for the cation- and anion concentration the measured drip water values of $B7-B$ were used together with a fixed p_{CO_2} of 1000 ppm (reasonable value for the cave air). As a result of the solution composition, the pH-value (7.5), and the temperature (9.5°C), the initial SI_{CaCO_3} is calculated as 0.3. If the solution finally has reached equilibrium with the cave p_{CO_2}, and the drip water is saturated with respect to calcite ($SI_{CaCO_3}=0$), the calculated total precipitation of calcite amounts to 148 mg/l. Because this is an endmember calculation no information is given about time constants, which basically depend on the rate of degassing and calcite precipitation. To determine the maximum possible amount of calcite precipitation for experiment $B7-B$, it is necessary to know the amount of drip water flowing along the channel whithin the measuring period. With a drip volume of 0.075 ml (measured by S. Niggemann) and a mean drip interval of 3.3 s, approx. 530 l of water flew along the channel within 9 month. This means, that 78 g of calcite theoretically could have been precipitated on the channel but in fact only 5 g of calcite were measured on the glass fibre stripe. Prior calcite precipitation along the stalactite which fed the channel with drip water is not considered here. It can be concluded that less than 10% of possible calcite actually precipitated on the channel. In case of $B7-A$ the calculations could not been carried out due to the lacking drip water data.
For cave systems the CO_2-degassing rate is expected to dominate over the precipitation rate (Appelo and Postma (2005)). In summary, if a drop appears at the cave ceiling in the beginning the rate of CO_2-degassing will dominate the process. Initially the SI_{CaCO_3} will increase until the precipitation of calcite keeps pace with the loss of CO_2. If the solution is finally in equilibrium with cave p_{CO_2}, calcite will still be precipitated resulting in a decrease in the $SI_{Calcite}$ until the solution is also in equilibrium with respect to calcite.

4.3.5 $\delta^{13}C$ and $\delta^{18}O$ evolution along the channel

The isotopic evolution on the channel for in situ experiments $B7-A$ and $B7-B$ is shown in Figs. 4.12 and 4.13. For both channels the isotope values strongly fluctuate. Only for $\delta^{13}C$ in case of $B7-A$ a clear enrichment is observed along the channel. For all other isotope developments leaps and shifts exist in-between the data. For $B7-A$, $\delta^{18}O$ is highly variable, particularly in the upper part of the glass fibre stripe (Fig. 4.12, right). Adjacent values vary in a systematical manner up and down around 0.5‰. The $\delta^{13}C$-values of $B7-B$ show a recurring pattern with a smooth increase of 0.5‰ and an abrupt decrease to initial values.

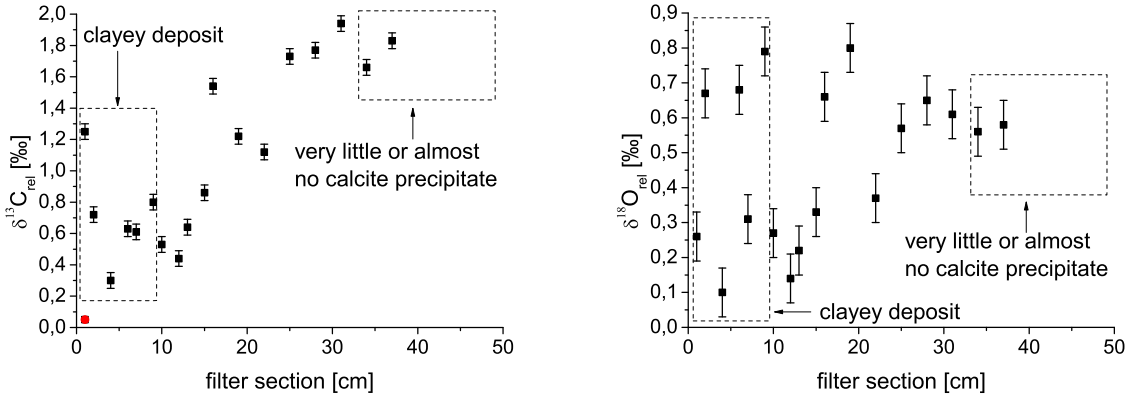

Figure 4.12: *Isotope development of $\delta^{13}C$ (left) and $\delta^{18}O$ (right) along the channel for in-situ experiment $B7-A$. The red value is related to the top of STAL-B7-7 (Niggemann (2000)).*

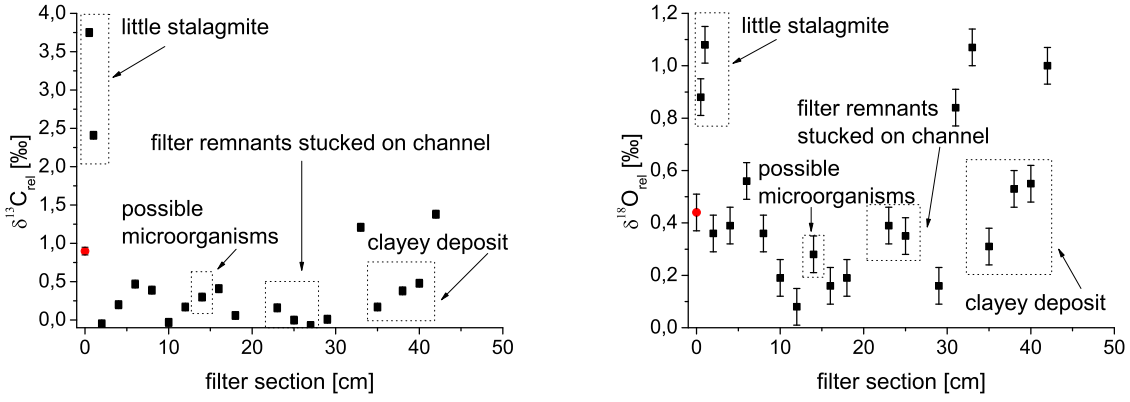

Figure 4.13: *Isotope development of $\delta^{13}C$ (left) and $\delta^{18}O$ (right) along the channel for in-situ experiment $B7-B$. The red value is related to the top of the PET-flask set out at the site of STAL-B7-6 (Niggemann (2000)).*

Additionally indicated in Figs. 4.12 and 4.13 are some visual characteristics of the glass fibre stripe, like sections with clayey deposit, or sections offering other structures of potentially organic origin. Sometimes these 'morphological' characteristics seem to correlate with shifts in the data. For example in case of $\delta^{13}C$ ($B7-A$), the gap between 9 cm and 10 cm coincides with the end of a brown clayey deposit on the glass fibre stripe. In case of $\delta^{18}O$ ($B7-B$), the glass fibre stripe section possibly affected by microorganisms (section 14) offers a slight shift in the isotope value. Why the mentioned effects cause these variations in the isotope values or why the shifts are sometimes restricted to $\delta^{13}C$ or $\delta^{18}O$ is not clear. Possibly, drip water from another source sips on the glass fibre stripe along the channel , which could also have produced the brown lumps and clayey deposits observed in $B7-A$ and $B7-B$, respectively and would explain the shift to more depleted, or even the initial values if the drip water composition is the same. Another reason for the variability in the data could be related to a diffuse flow path of the drip water along the channel, induced, for example, by lumps of clay or the progressive growth of the calcite crystals on the glass fibre stripe surface leading to a local increase or decrease of the flow velocity and even of the film thickness affecting the degassing rate of CO_2.

One of the most noticeable points in case of $B7-B$ is the fact that there is a massive shift between the isotope values of the grown flow stone on top of the glass channel and the calcite precipitated along the glass fibre stripe (see Fig. 4.13). In case of $\delta^{13}C$ the difference ranges from 1.5‰ to 3‰ and for $\delta^{18}O$ the values differ between 0.5‰ and 0.7‰. Why the compact flow stone is enriched relatively to the laminary covered calcite on the glass fibre stripe can not be explained easily. Probably again crystallisation effects play a significant role here.

Comparing the absolute isotope values of the precipitated calcite between experiments $B7-A$ and $B7-B$, it turns out, that the mean values differ in 3‰ in case of $\delta^{13}C$ and 0.5‰ in case of $\delta^{18}O$. Since the two drip sites feeding $B7-A$ and $B7-B$ are in a short distance to each other (approx. 1 m), it is expected that the drip water compositition is similar for both sites. However, a difference of 3‰ was also observed for $\delta^{13}C_{drip\,water}$ between both sites (see Tab. 4.2). This deviation may result from a combination of the different drip intervals (271 s in case of $B7-A$; 3 s in case of $B7-B$) and the different length of the corresponding stalactites (20 cm in case of $B7-A$; 3 cm in case of $B7-B$). A longer residence time or a longer flow path, respectively, is associated with a larger amount of CO_2-degassing. The drip water of $B7-A$ should, thus, already be enriched in comparison to $B7-B$ when dripping into the sample flask or onto the channel due to the longer flow path and prior calcite precipitation along the stalactite. $\delta^{18}O$ is not affected in a similar manner because of buffering processes. Furthermore, it cannot be ruled out that the funnel, which was used to centralise the drip water on top of the channel, represents a supporting substrate for calcite precipitation.

4.4 Conclusion

In general, it can be concluded that the isotope results from the cave experiments show more fluctuations in comparison to the laboratory experiments. These different characteristics were expected because unlike the 'clean' laboratory conditions, the conditions in the cave environment underlie various different factors and influences, which complicate the interpretation of drip water and calcite precipiation chemistry. Effects from different parameter settings on the isotope enrichment in the laboratory are clearly discriminable in most cases. The cave system processes are presumably overlied by too many factors. From the cave experiments it can be deduced that the isotope development not only seems to be driven by kinetic degassing and precipiation mechanisms but also by other parameters like the incorporation of organic matter into the calcite, or crystallographic aspects.

In Fig. 4.14, $\delta^{18}O$ is plotted against $\delta^{13}C$ for all three cave experiments showing a correlation in all cases with resulting slopes, which range between 0.25 and 0.48.

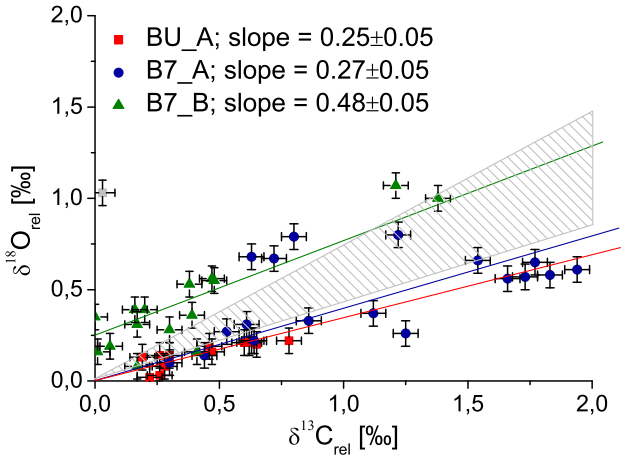

Figure 4.14: *$\delta^{18}O$ versus $\delta^{13}C$ for all three cave experiments (including Bunkerhöhle and B7-Höhle). The shaded area represents the slope range obtained from the laboratory experiments.*

According to the Hendy-test, which predicts a kinetically driven fractionation, if $\delta^{13}C$ and $\delta^{18}O$ show a linear correlation along a growth layer, all cave experiments are supposed to be influenced by kinetics. On the other hand at least drip site $B7-B$ offers an extremely high drip rate with 3 s, rather excluding strong kinetics. This would confirm the fact, that the Hendy-test is a necessary criteria for kinetics but not a sufficient one.

Chapter 5

Summary and outlook

Laboratory experiments were carried out simulating calcite precipitation under cave analogous conditions. Additionally, in situ cave experiments were conducted under active drip sites in two cave systems in Sauerland (Bunkerhöhle and B7-Höhle) to investigate and compare the results to those of the laboratory experiments. The major focus of the experiments was the investigation of the evolution of the stable isotopes $\delta^{13}C$ and $\delta^{18}O$ within the precipitated calcite under varying conditions. Parameters, which were varied within the laboratory experiments were p_{CO_2}, temperature, drip rate and the initial SI_{CaCO_3} of the solution.

All experiments showed an isotopic enrichment along the channel for both $\delta^{13}C$ and $\delta^{18}O$. Furthermore, a positive correlation correlation between both isotopes was observed in all experiments confirming that calcite precipitation occured under kinetic conditions (Hendy (1971)). The amount of isotopic enrichment and the slope of $\Delta(\delta^{18}O)/\Delta(\delta^{13}C)$, which is an indicator for the degree of oxygen isotope buffering, depend on the experimental settings. Generally, lower drip rates, higher temperatures and higher initial supersaturations with respect to calcite resulted in a larger isotopic enrichment along the channel and in an lower slope of $\Delta(\delta^{18}O)/\Delta(\delta^{13}C)$, indicating a larger oxygen isotope buffering. In case of lower drip rates, more CO_2 degasses from the solution. This is accompanied by increasing loss of lighter isotopes from the solution, leading to a larger isotopic enrichment in both the solution and the precipitated calcite. For $\delta^{18}O$ the longer drip interval increases the exchange time between the oxygen isotopes in the bicarbonate and the water reservoir leading to a larger degree of buffering. Higher temperatures enhance the chemical reaction rates affecting both the calcite precipitation and the buffering.

For experiments conducted under high drip rates (i.e.,$< 20\ s$) and low temperatures ($10°C$), the $\delta^{13}C$ evolution along the channel could be verified by theoretical models (Mühlinghaus (2008)). However, the $\delta^{18}O$ enrichment can only be described by the model if a buffering value, which is one third of the value indicated in Hendy (1971) is used. A similar relation could be observed for higher temperatures ($23°C$). This suggests a faster isotope exchange reaction rate than theoretically predicted by Hendy (1971). Since the literature values have never been experimentally validated, they could theoretically be erroneous. Another reason for the observed discrepancy might be related to processes, which are not included in the model. Thus, future experiments should be conducted to systematically determine the temperature dependent buffering time.

Furthermore, the experiment data showed an extremely large isotopic enrichment for high temperatures ($23°C$). Models only fit these values using a half as large conversion time, τ, between the bicarbonate and the CO_2 in the solution than theoretically predicted (Dreybrodt (1999), Baker et al. (1998)). The calcite mass decrease along the channel observed in the experiments yields a τ, which is similar to the τ obtained from the model confirming the characteristics at high temperatures. Similarly as in the case of the buffering value, the observed difference between the theoretically predicted and the τ value determined within the experiments allows two interpretations. Either the theoretically calculated value for τ is wrong, or other effects play a significant role, which result in a decrease of the conversion time in case of high temperatures, hence leading to a greater amount of calcite precipitation.

Another parameter, which resulted in a larger value for high temperatures than expected, is the carbon isotopic enrichment factor between the bicarbonate in the solution and the precipitated calcite, $\epsilon_{CaCO_3-HCO_3^-}$. From the laboratory experiments a linear approximation yields $\epsilon_{CaCO_3-HCO_3^-} = 1.6 + 0.15 \cdot T_C$ (valid in the range of $10°C - 23°C$). This value is again different from the value found in literature (Mook (2000)). The enrichment factor observed in the experiments for $23°C$ was approx. $1.5‰$ higher than the predicted value. This discrepancy could result from the fact that the experiments include kinetic fractionation processes whereas the theoretical values are determined for equilibrium fractionation. However, it is an interesting fact, that the experiments carried out at $10°C$ agree with the equilibrium fractionation factor in case of $\delta^{13}C$. The observed characteristic confirmes the assumption that other significant effects influence calcite precipitation and the isotopic evolution at higher temperatures, which are not included in models yet. In future laboratory experiments the observed effects should be verified and further investigated. Processes occuring at high temperatures are relevant for the interpretation of stalagmites from subtropical or tropical cave systems grown at higher temperatures.

Other effects, which are not considered in numerical models but might potentially be of importance with respect to isotope values observed in natural speleothems, are related to calcite crystallisation mechanisms. For example the in situ cave experiments revealed a relation between crystallisation processes and the absolute isotope values. It could be observed that different forms of calcite showed extremely differing isotope values. A compact piece of calcite with cylindrical shape, precipitated in the upper part of the channel showed a large enrichment (factor 10) in comparison to the calcite precipitated along the lower part of the channel.
Furthermore, the laboratory experiments showed a correlation between the initial SI_{CaCO_3} of the solution and the calcite mass distribution along the channel. Maximum $CaCO_3$ precipitation in the beginning of the channel occured only if the SI_{CaCO_3} was close to 1, the limit for homogeneous nucleation (Kunz and Stumm (1984)). For different values the maximum of calcite precipitation shifted along the channel, i.e., the lower the initial SI_{CaCO_3} the later the maximum was reached. Thus, the mass distribution along the channel is an indicator for the different processes leading to calcite precipitation. For a low initial SI_{CaCO_3}, first CO_2-degassing is dominant coupled with an increase in SI_{CaCO_3}. After a certain limit of SI_{CaCO_3} is reached, which is presumably connected with homogeneous nucleation, calcite precipitation dominates accompanied by a decrease of SI_{CaCO_3}.
Similar observations were also made in the situ cave experiments. For example in cave experiment $B7 - A$, the maximum of calcite precipitation occured at 7 cm. This leads to the

conclusion that the impinge of the drop does not lead to a complete CO_2 equilibration within the solution. If equilibrium with cave CO_2 had already been reached, the calcite mass would decrease along the channel right from the start, independently from the SI_{CaCO_3}.

All cave experiments showed indications for kinetic isotope fractionation even in case of the fast dripping site $BU - A$. This confirms the observation of Mickler et al. (2006) that most stalagmite samples used for paleoclimatic interpretation are influenced by kinetics. In this respect further investigation of the kinetic processes in terms of numerical models in combination with experimental studies are of great importance.

Appendix A

Data from laboratory experiments

exp.	duration [days]	temperature [°C]	pump rate [ml/min]	drip rate [sec]	flow velocity [cm/min]	pH	Ca^{2+} [mg/l]	HCO_3^- [mg/l]	SI	$\delta^{13}C$ [‰]	$\delta^{18}O$ [‰]	notes
1A	31	14,2	0,027	40	2,500	8,62	51	192	1,08	-6,85	-8,4	
1B	31	14,2	0,1	10,8	9,000	8,51	51	192	0,98	-5,36	-8,5	for two weeks only NaHCO3
1D	31	14,2	0,2	5,4	18,000	8,48	52	200	0,98	-5,25	-8,55	
2A	29	10,8	0,1	10,8	9,000	8,35	55	166	0,76		-8,51	
2B	29	11	0,1	10,8	9,000	8,35	54	166	0,76		-8,47	
2D	29	10,9	0,1	10,8	9,000	8,35	55	166	0,76		-8,51	VE-metal-wire as channel material
4A	28	10,5	0,12	9	17	8,54	43	174	0,85	-4,14	-8,62	filter width = 0,4 cm
4B	28	10,5	0,12	9	11	8,55	45	174	0,88	-3,96	-8,60	
4C	28	10,5	0,12			8,52	68	157	0,97	-4,81	-8,55	plexiglass channel
5B	61	10,1	0,02	60	1,8	8,55	58	183	0,99	-3,73	-8,48	
5D	31	9,9	0,12	9	11	8,46	47	139	0,72	-4,69	-8,54	
6A	28	23	0,12	9	11	8,53	51	166	1,06	-3,52		air bubble in d13C-water-sample
6B	39	23	0,12	9	11	8,52	29	113	0,68	-5,71		
6C	28	23	0,12	9	11	8,16	61	200	0,86	-5,44		
6D	39	23	0,12	9	11	8,63	39	157	1,02	-4,68		
7A	27	23	0,1	10,8	9	8,45	60*	181	1,08	-3,58		humidified CO2-atmosphere
7B	27	23	0,096	10,8	9	8,42	60*	157	1	-4,72		no air exchange in gas distributor
err.:		0,3	5%	5%	max. 15%	0,05	4%	8	0,05	0,1	0,08	

drip volume: 0,03 ml

filter length: 50 cm; filter width: 0,6 cm (besides exp. 4A)

imprecise experiment conditions

* theoretical values

Experiment 1A

filter seg. [cm]	$\delta^{13}C$ [‰]	$\delta^{13}C_{rel}$ [‰]	$\delta^{18}O$ [‰]	$\delta^{18}O_{rel}$ [‰]
6	-3,68	0,42	-8,35	0,25
9	-3,82	0,28	-8,44	0,16
12	-3,67	0,43	-8,38	0,22
16	-3,37	0,73	-8,11	0,49
19	-3,23	0,87	-8,05	0,55
22	-3,07	1,03	-7,86	0,74
26	-3,11	0,99	-7,92	0,68
29	-2,66	1,44	-7,65	0,95
32	-2,73	1,37	-7,57	1,03
36	-2,66	1,44	-7,78	0,82
39	-2,31	1,79	-7,48	1,12
42	-2,04	2,06	-7,27	1,33
46	-2,18	1,92	-7,18	1,42
49	-1,93	2,17	-7,34	1,26

filter seg. [cm]	$CaCO_3$ [mg]	err
0	0,27	0,011
5	0,03	0,001
20	0,31	0,012
30	0,53	0,021
40	0,77	0,031
50	0,39	0,015

Experiment 1B

filter seg. [cm]	$\delta^{13}C$ [‰]	$\delta^{13}C_{rel}$ [‰]	$\delta^{18}O$ [‰]	$\delta^{18}O_{rel}$ [‰]
2	-3,41	5,79	-8,61	14,67
6	-3,58	9,79	-8,77	18,67
9	-3,58	12,79	-8,75	21,67
12	-3,51	15,79	-8,75	24,67
16	-3,49	19,79	-8,74	28,67
19	-3,14	22,79	-8,50	31,67
22	-3,43	25,79	-8,57	34,67
26	-3,29	29,79	-8,58	38,67
29	-3,22	32,79	-8,55	41,67
32	-2,80	35,79	-7,91	44,67
36	-2,86	39,79	-8,28	48,67
39	-3,00	42,79	-8,38	51,67
42	-2,90	45,79	-8,37	54,67
46	-2,77	49,79	-8,33	58,67
49	-2,75	52,79	-8,25	61,67

filter seg. [cm]	$CaCO_3$ [mg]	err
2	0,2239	0,05
6	0,355	0,05
9	0,38275	0,05
12	0,58275	0,05
16	0,6105	0,05
19	0,29	0,05
22	0,0045	0,05
26	0,2105	0,05
29	0,119	0,05
32	0,755	0,05
36	0,555	0,05
39	0,455	0,05
42	0,255	0,05
46	0,255	0,05
49	0,555	0,05

Experiment 1D

filter seg. [cm]	$\delta^{13}C$ [‰]	$\delta^{13}C_{rel}$ [‰]	$\delta^{18}O$ [‰]	$\delta^{18}O_{rel}$ [‰]
2	-3,70	0,12	-8,90	0,02
6	-3,36	0,46	-8,86	0,06
9	-3,64	0,18	-8,85	0,07
12	-3,49	0,33	-8,78	0,14
16	-3,39	0,43	-8,80	0,12
19	-3,28	0,54	-8,75	0,17
22	-3,46	0,36	-8,50	0,42
26	-3,21	0,61	-8,45	0,47
29	-2,93	0,89	-8,55	0,37
32	-2,86	0,96	-8,63	0,29
39	-2,80	1,02	-8,21	0,71
42	-2,65	1,17	-8,15	0,77
46	-2,53	1,29	-8,53	0,39
49	-2,78	1,04	-8,42	0,50

filter seg. [cm]	$CaCO_3$ [mg]	err
5	0,73	0,029
20	0,83	0,033
30	0,95	0,038
40	0,72	0,029
50	0,39	0,015

Experiment 2A

filter seg. [cm]	$\delta^{13}C$ [‰]	$\delta^{13}C_{rel}$ [‰]	$\delta^{18}O$ [‰]	$\delta^{18}O_{rel}$ [‰]
3	-5,90	-1,45	-8,41	-0,81
7	-8,12	-3,67	-6,83	0,77
10	-4,25	0,20	-7,90	-0,30
14	-3,86	0,59	-7,04	0,56
17	-3,58	0,87	-7,39	0,21
21	-3,56	0,89	-7,22	0,38
24	-3,43	1,02	-7,24	0,36
28	-3,32	1,13	-7,28	0,32
32	-3,28	1,17	-7,09	0,51
35	-3,03	1,42	-7,08	0,52
38	-2,25	2,20	-6,50	1,10
42	-2,88	1,57	-7,10	0,50
45	-2,47	1,98	-6,82	0,78
49	-2,71	1,74	-6,93	0,67

filter seg. [cm]	$CaCO_3$ [mg]	err
14	0,23	0,05
17	0,22	0,05
21	1,22	0,05
24	0,51	0,05
28	0,35	0,05
31	1,07	0,05
35	0,49	0,05
38	0,27	0,05
42	0,21	0,05
45	0,49	0,05
49	0,31	0,05
51	1,91	0,05

Experiment 2B

filter seg. [cm]	$\delta^{13}C$ [‰]	$\delta^{13}C_{rel}$ [‰]	$\delta^{18}O$ [‰]	$\delta^{18}O_{rel}$ [‰]
6	-4,36	-0,63	-6,71	
10	-3,44	0,29	-7,37	-0,09
14	-3,27	0,46	-7,13	0,15
17	-3,02	0,71	-7,21	0,07
21	-3,06	0,67	-7,18	0,10
24	-3,05	0,68	-7,14	0,14
28	-2,67	1,06	-7,13	0,15
31	-2,75	0,98	-7,23	0,05
35	-2,59	1,14	-7,05	0,23
38	-2,46	1,27	-7,11	0,17
42	-2,29	1,44	-7,10	0,18
45	-2,19	1,54	-7,03	0,25
49	-1,97	1,76	-6,96	0,32
51	-2,15	1,58	-7,01	0,27

filter seg. [cm]	$CaCO_3$ [mg]	err
7	0,0595	0,05
10	0,19	0,05
14	0,2185	0,05
17	0,2805	0,05
21	0,3895	0,05
24	0,26469	0,05
28	0,3675	0,05
31	0,7525	0,05
35	0,35275	0,05
38	0,61275	0,05
42	0,995	0,05
45	0,83888	0,05
49	1,00	0,05
51	0,97887	0,05

Experiment 2D

filter seg. [cm]	$\delta^{13}C$ [‰]	$\delta^{13}C_{rel}$ [‰]	$\delta^{18}O$ [‰]	$\delta^{18}O_{rel}$ [‰]
3	-3,77	0,53	-7,47	0,27
6	-5,44	-1,14	-8,78	-1,04
10	-3,09	1,21	-7,23	0,51
14	-3,19	1,11	-7,15	0,59
17	-2,77	1,53	-4,21	3,53
21	-1,71	2,59	-6,37	1,37
24	-1,73	2,57	-5,80	1,94
28	-0,97	3,33	-5,58	2,16
31	-1,01	3,29	-6,42	1,32
35	-3,43	0,87	-7,56	0,18
38	-3,36	0,94	-7,63	0,11
41	-3,15	1,15	-7,52	0,22
45	-3,17	1,13	-7,44	0,30
48	-2,80	1,50	-7,30	0,44
50	-2,60	1,70	-7,13	0,61

filter seg. [cm]	$CaCO_3$ [mg]	err
3	0,17725	0,05
7	0,10112	0,05
10	0,265	0,05
14	0,32888	0,05
17	0,095	0,05
21	0,015	0,05
24	0,095	0,05
28	0,20725	0,05
31	0,13888	0,05
35	1,08	0,05
38	0,7428	0,05
42	1,58	0,05
45	0,72725	0,05
49	0,41112	0,05
51	0,46888	0,05

Experiment 4A

filter seg. [cm]	$\delta^{13}C$ [‰]	$\delta^{13}C_{rel}$ [‰]	$\delta^{18}O$ [‰]	$\delta^{18}O_{rel}$ [‰]
1	-4,14	0,06	-8,19	0,06
4	-4,25	-0,05	-8,20	0,05
7	-4,16	0,04	-8,30	-0,05
10	-4,09	0,11	-8,26	-0,01
13	-4,02	0,18	-8,13	0,12
16	-4,05	0,15	-8,14	0,11
19	-4,06	0,14	-8,23	0,02
22	-3,93	0,27	-8,02	0,23
25	-3,82	0,38	-7,86	0,39
28	-4,01	0,19	-7,99	0,26
31	-3,87	0,33	-7,95	0,30
34	-3,91	0,29	-8,07	0,18
37	-3,88	0,32	-7,92	0,33
40	-3,66	0,54	-7,86	0,39
43	-3,77	0,43	-7,92	0,33
46	-3,88	0,32	-8,03	0,22
49	-3,69	0,51	-7,86	0,39

filter seg. [cm]	$CaCO_3$ [mg]	err
3	0,11	0,05
5	0,127	0,05
9	0,017	0,05
12	0,167	0,05
15	0,054	0,05
18	0,01	0,05
20	0,292	0,05
21	0,367	0,05
24	0,067	0,05
26	0,123	0,05
32	0,137	0,05
38	0,048	0,05
44	0,108	0,05
50	0,525	0,05

Experiment 4B

filter seg. [cm]	$\delta^{13}C$ [‰]	$\delta^{13}C_{rel}$ [‰]	$\delta^{18}O$ [‰]	$\delta^{18}O_{rel}$ [‰]
1	-4,18	-0,01	-8,27	0,04
4	-4,00	0,17	-8,20	0,11
7	-3,95	0,22	-8,18	0,13
10	-3,90	0,27	-8,26	0,05
13	-4,00	0,17	-8,25	0,06
16	-3,96	0,21	-8,18	0,13
19	-3,91	0,26	-8,22	0,09
22	-3,81	0,36	-8,09	0,22
25	-3,83	0,34	-8,00	0,31
28	-3,81	0,36	-8,07	0,24
31	-3,65	0,52	-7,99	0,32
34	-3,55	0,62	-7,90	0,41
37	-3,30	0,87	-7,73	0,58
40	-3,42	0,75	-7,85	0,46
43	-3,51	0,66	-7,97	0,34
46	-3,35	0,82	-7,85	0,46
49	-3,21	0,96	-7,77	0,54

filter seg. [cm]	$CaCO_3$ [mg]	err
2	0,05	0,002
4	0,186	0,05
7	0,003	0,05
8	0,04	0,002
10	0,118	0,05
13	0,223	0,05
14	0,51	0,021
16	0,248	0,05
19	0,779	0,05
20	0,81	0,032
22	0,452	0,05
25	0,552	0,05
26	0,562	0,05
28	0,594	0,05
31	0,508	0,05
32	0,83	0,033
37	0,041	0,05
38	0,44	0,018
40	0,446	0,05
43	0,442	0,05
44	0,45	0,018
46	0,219	0,05
48	0,601	0,05
49	0,192	0,05

Experiment 4C

filter seg. [cm]	$\delta^{13}C$ [‰]	$\delta^{13}C_{rel}$ [‰]	$\delta^{18}O$ [‰]	$\delta^{18}O_{rel}$ [‰]
1	-4,12	0,06	-7,79	0,38
4	-4,14	0,04	-8,15	0,02
7	-3,92	0,26	-8,00	0,17
10	-4,00	0,18	-8,05	0,12
13	-3,87	0,31	-7,96	0,21
16	-3,61	0,57	-7,89	0,28
19	-3,75	0,43	-7,93	0,24
22	-3,48	0,70	-7,67	0,50
25	-3,31	0,87	-7,76	0,41
28	-2,70	1,48	-7,33	0,84
31	-3,55	0,63	-7,80	0,37
34	-3,74	0,44	-7,82	0,35
37	-3,39	0,79	-7,73	0,44
40	-3,06	1,12	-7,54	0,63
43	-3,22	0,96	-7,70	0,47
46	-3,00	1,18	-7,46	0,71
49	-2,51	1,67	-7,22	0,95

filter seg. [cm]	$CaCO_3$ [mg]	err
2	0,40	0,016
8	0,24	0,010
14	0,06	0,002
20	0,19	0,008
26	0,15	0,006
32	0,08	0,003
38	0,23	0,009
44	0,21	0,009
48	0,12	0,005

Experiment 5B

filter seg. [cm]	$\delta^{13}C$ [‰]	$\delta^{13}C_{rel}$ [‰]	$\delta^{18}O$ [‰]	$\delta^{18}O_{rel}$ [‰]
1	-4,02	-0,01	-7,67	0,02
4	-3,87	0,14	-7,61	0,08
7	-3,46	0,55	-7,34	0,35
10	-3,83	0,18	-7,53	0,16
13	-3,88	0,13	-7,66	0,03
19	-3,36	0,65	-7,29	0,40
28	-3,04	0,97	-7,09	0,60
31	-3,00	1,01	-7,02	0,67
40	-2,73	1,28	-6,95	0,74
46	-2,65	1,36	-6,85	0,84
49	-2,34	1,67	-6,61	1,08

filter seg. [cm]	$CaCO_3$ [mg]	err
2	0,546	0,022
8	0,571	0,023
9	0,3375	0,05
12	0,311	0,05
14	0,189	0,008
20	0,327	0,013
26	0,103	0,004
27	0,1705	0,05
32	0,165	0,007
33	0,16406	0,05
38	0,062	0,002
39	0,0963125	0,05
44	0,106	0,004
48	0,105	0,004

Experiment 5D

filter seg. [cm]	$\delta^{13}C$ [‰]	$\delta^{13}C_{rel}$ [‰]	$\delta^{18}O$ [‰]	$\delta^{18}O_{rel}$ [‰]
10	-4,27	0,30	-7,80	0,29
16	-4,00	0,57	-7,92	0,17
19	-4,11	0,46	-7,95	0,14
28	-3,99	0,58	-7,90	0,19
31	-3,88	0,69	-7,81	0,28
34	-3,73	0,84	-7,73	0,36
43	-3,37	1,20	-7,45	0,64
49	-3,20	1,37	-7,51	0,58

filter seg. [cm]	$CaCO_3$ [mg]	err
8	0,034	0,001
14	0,040	0,002
20	0,154	0,006
26	0,072	0,003
32	0,154	0,006
38	0,084	0,003
44	0,019	0,001
50	0,373	0,015

Experiment 6A

filter seg. [cm]	$\delta^{13}C$ [‰]	$\delta^{13}C_{rel}$ [‰]	$\delta^{18}O$ [‰]	$\delta^{18}O_{rel}$ [‰]
1	-3,69	-0,24	-10,07	-0,04
7	-3,33	0,12	-10,01	0,02
10	-2,67	0,78	-9,72	0,31
13	-1,96	1,49	-9,45	0,58
16	-2,60	0,85	-9,61	0,42
19	-1,81	1,64	-9,28	0,75
22	-1,40	2,05	-9,20	0,83
25	-2,03	1,42	-9,49	0,54
29	-1,32	2,13	-9,15	0,88
31	-1,27	2,18	-9,09	0,94
34	-1,18	2,27	-9,03	1,00
37	-0,91	2,54	-9,00	1,03
40	-0,80	2,65	-8,82	1,21
43	-0,32	3,13	-8,58	1,45
46	-0,36	3,09	-8,62	1,41
49	-0,28	3,17	-8,73	1,30

filter seg. [cm]	$CaCO_3$ [mg]	err
1	2,93	0,05
2	3,02	0,05
4	4,41	0,05
8	4,14	0,05
10	2,99	0,05
14	4,01	0,05
16	3,37	0,05
20	2,35	0,05
22	1,58	0,05
26	1,89	0,05
32	2,52	0,05
34	2,28	0,05
38	1,88	0,05
40	1,38	0,05
44	1,26	0,05
46	1,73	0,05
50	1,48	0,05

Experiment 6B

filter seg. [cm]	$\delta^{13}C$ [‰]	$\delta^{13}C_{rel}$ [‰]	$\delta^{18}O$ [‰]	$\delta^{18}O_{rel}$ [‰]
1	-3,85	-0,26	-10,41	-0,03
4	-3,37	0,22	-10,35	0,03
7	-3,07	0,52	-10,02	0,36
10	-3,04	0,55	-10,06	0,32
13	-2,92	0,67	-9,97	0,41
16	-2,67	0,92	-9,83	0,55
19	-2,50	1,09	-9,70	0,68
22	-2,54	1,05	-9,76	0,62
25	-2,85	0,74	-9,98	0,40
31	-2,21	1,38	-9,37	1,01
34	-1,72	1,87	-9,23	1,15
37	-1,47	2,12	-9,08	1,30
40	-1,46	2,13	-9,07	1,31
43	-1,23	2,36	-8,83	1,55
46	-1,39	2,20	-9,03	1,35
49	-1,27	2,32	-8,86	1,52

filter seg. [cm]	$CaCO_3$ [mg]	err
2	1,33	0,053
3	2,6	0,05
6	2,19	0,05
9	2,144	0,05
15	2,2597	0,05
18	2,454	0,05
20	2,41	0,096
26	3,20	0,128
27	2,70185	0,05
30	1,9305	0,05
33	1,8005	0,05
36	1,2895	0,05
39	1,229	0,05
42	1,12	0,05
47	1,4	0,05
48	1,57	0,063

Experiment 6C

filter seg. [cm]	$\delta^{13}C$ [‰]	$\delta^{13}C_{rel}$ [‰]	$\delta^{18}O$ [‰]	$\delta^{18}O_{rel}$ [‰]
1	-3,76	0,19	-10,32	0,19
3	-3,65	0,30	-10,30	0,21
3	-3,22	0,73	-10,21	0,30
4	-3,64	0,31	-10,29	0,22
7	-3,59	0,36	-10,36	0,15
10	-3,23	0,72	-10,23	0,28
12	-2,77	1,18	-9,99	0,52
12	-3,27	0,68	-10,12	0,39
13	-2,95	1,00	-10,06	0,45
16	-2,66	1,29	-9,88	0,63
19	-2,27	1,68	-9,71	0,80
22	-2,12	1,83	-9,74	0,77
23	-2,20	1,75	-9,61	0,90
25	-1,98	1,97	-9,64	0,87
28	-1,82	2,13	-9,37	1,14
31	-1,50	2,45	-9,28	1,23
34	-1,32	2,63	-9,19	1,32
37	-1,06	2,89	-9,07	1,44
40	-0,97	2,98	-9,06	1,45
43	-0,69	3,26	-8,76	1,75
46	0,20	4,15	-8,50	2,01
49	0,47	4,42	-8,37	2,14

filter seg. [cm]	$CaCO_3$ [mg]	err
1	4,08	0,05
2	5,32	0,05
4	8,12	0,05
8	7,09	0,05
10	5,68	0,05
13	4,89	0,05
14	3,70	0,05
16	4,50	0,05
20	3,54	0,05
22	3,08	0,05
26	3,51	0,05
28	3,30	0,05
32	2,78	0,05
34	3,67	0,05
38	3,91	0,05
40	2,98	0,05
44	2,83	0,05
46	2,18	0,05
48	2,07	0,05

Experiment 6D

filter seg. [cm]	$\delta^{13}C$ [‰]	$\delta^{13}C_{rel}$ [‰]	$\delta^{18}O$ [‰]	$\delta^{18}O_{rel}$ [‰]
1	-3,01	-0,04	-10,29	0,00
4	-2,89	0,08	-10,10	0,19
7	-2,62	0,35	-10,00	0,29
10	-2,43	0,54	-9,90	0,39
13	-2,34	0,63	-9,73	0,56
16	-1,93	1,04	-9,62	0,67
19	-1,73	1,24	-9,48	0,81
22	-1,74	1,23	-9,45	0,84
25	-1,86	1,11	-9,59	0,70
28	-1,75	1,22	-9,62	0,67
31	-1,46	1,51	-9,44	0,85
34	-1,34	1,63	-9,34	0,95
37	-1,05	1,92	-9,18	1,11
40	-0,88	2,09	-9,00	1,29
43	-0,78	2,19	-8,95	1,34

filter seg. [cm]	$CaCO_3$ [mg]	err
2	7,39	0,296
3	5,719	0,05
6	3,7105	0,05
8	3,20	0,128
9	3,246	0,05
12	3,7723	0,05
14	3,37	0,135
15	2,23285	0,05
18	3,156038	0,05
21	2,5028825	0,05
22	2,34	0,093
24	2,230125	0,05
26	3,32	0,133
27	2,4691875	0,05
30	2,3825	0,05
32	2,13	0,085
33	1,940125	0,05
36	2,0225	0,05
38	2,63	0,105
39	2,1414575	0,05
42	1,8236	0,05
44	2,36	0,094
45	2,973416	0,05
47	1,6336	0,05

Experiment 7A

filter seg. [cm]	$\delta^{13}C$ [‰]	$\delta^{13}C_{rel}$ [‰]	$\delta^{18}O$ [‰]	$\delta^{18}O_{rel}$ [‰]
1	-2,67	0,02	-10,19	0,01
4	-2,50	0,19	-9,97	0,23
7	-1,86	0,83	-9,91	0,29
10	-1,51	1,18	-9,77	0,43
13	-1,03	1,66	-9,37	0,83
16	-1,16	1,53	-9,37	0,83
19	-0,96	1,73	-9,58	0,62
22	-1,34	1,35	-9,60	0,60
25	-1,01	1,68	-9,56	0,64
29	-0,98	1,71	-9,63	0,57
31	-0,68	2,01	-9,15	1,05
34	-0,56	2,13	-9,25	0,95
37	-0,29	2,40	-8,76	1,44
40	-0,36	2,33	-8,56	1,64
43	-0,23	2,46	-9,08	1,12
47	0,05	2,74	-9,11	1,09
49	-0,28	2,41	-8,59	1,61

filter seg. [cm]	$CaCO_3$ [mg]	err
1	4,71	0,05
2	4,6914575	0,05
4	2,92	0,05
5	1,7928825	0,05
7	0,62	0,05
8	0,51	0,05
10	1,25	0,05
11	1,349	0,05
13	1,09	0,05
14	1,0776325	0,05
16	0,69	0,05
17	0,406325	0,05
19	0,50	0,05
21	0,8814575	0,05
22	0,76	0,05
24	0,5086875	0,05
25	0,65	0,05
26	0,70665	0,05
28	1,04	0,05
29	1,163	0,05
31	0,97	0,05
32	0,792349	0,05
34	0,89	0,05
35	0,88935	0,05
37	0,44	0,05
38	0,593	0,05
40	0,51	0,05
42	0,553	0,05
43	0,32	0,05
45	0,586159	0,05
47	0,08	0,05
50	-0,007651	0,05

Experiment 7B

filter seg. [cm]	$\delta^{13}C$ [‰]	$\delta^{13}C_{rel}$ [‰]	$\delta^{18}O$ [‰]	$\delta^{18}O_{rel}$ [‰]
1	-3,83	-0,02	-10,15	0,01
4	-3,88	-0,07	-9,98	0,18
7	-3,58	0,23	-10,03	0,13
10	-3,48	0,33	-9,91	0,25
13	-3,44	0,37	-9,83	0,33
16	-2,92	0,89	-9,68	0,48
19	-3,04	0,77	-9,77	0,39
22	-2,92	0,89	-9,67	0,49
25	-3,14	0,67	-9,82	0,34
28	-2,87	0,94	-9,62	0,54
31	-2,71	1,10	-9,50	0,66
34	-3,19	0,62	-9,93	0,23
40	-2,50	1,31	-9,25	0,91
42	-2,48	1,33	-9,16	1,00
45	-2,44	1,37	-9,13	1,03
48	-2,08	1,73	-8,97	1,19

filter seg. [cm]	$CaCO_3$ [mg]	err
1	0,48	0,05
2	5,93	0,05
4	4,00	0,05
7	1,32	0,05
10	1,10	0,05
13	1,12	0,05
16	0,42	0,05
19	0,15	0,05
22	0,22	0,05
25	0,13	0,05
28	0,07	0,05
31	0,30	0,05
34	0,63	0,05

$\delta^{13}C$ (VPDB)

Deines		Romanek		Mook		laboratory experiments		
T [°C]	$\varepsilon_{CaCO3\text{-}HCO3}$	T [°C]	$\varepsilon_{CaCO3\text{-}HCO3}$	T [°C]	$\varepsilon_{CaCO3\text{-}HCO3}$	T [°C]	exp.	$\varepsilon_{CaCO3\text{-}HCO3}$
0	2,17	10	1	0	-0,393318689	9,9	5D	0,12
5	2,13	15	1	5	-0,114812152	10,1	5B	-0,28
10	2,08	20	1	10	0,153858379	10,5	4A	-0,06
15	2,04	25	1	15	0,413204928	10,5	4B	-0,21
20	2,01	30	1	20	0,663704588	10,5	4C	0,63
25	1,97	35	1	25	0,905802448	14,2	1A	-0,42
30	1,93	40	1	30	1,139914234	14,2	1B	-0,38
35	1,90			35	1,366428687	14,2	1D	-0,12
40	1,87			40	1,585709724	23	6B	2,12
						23	6C	1,39
						23	6D	1,71

δ^{18O} (VSMOW)

Kim		Mook		Coplen		laboratory experiments		
T [°C]	$\varepsilon_{CaCO3\text{-}H2O}$	T [°C]	$\varepsilon_{CaCO3\text{-}H2O}$	T [°C]	$\varepsilon_{CaCO3\text{-}H2O}$	T [°C]	exp.	$\varepsilon_{CaCO3\text{-}H2O}$
						10,1	5B	31,69
10	31,26	0	34,68439319	13	32,20726891	10,5	4A	31,24
15	30,15	5	33,39004853	15	31,78521603	10,5	4B	31,16
20	29,08	10	32,14141621	20	30,75527887	10,5	4C	31,25
25	28,05	15	30,93611661	25	29,75988596	10,8	2A	31,8
30	27,06	20	29,77193246	30	28,79732806	10,9	2D	31,65
35	26,09	25	28,64679524	35	27,86600681	11	2B	32,09
40	25,16	30	27,55877288	40	26,96442599	14,2	1A	30,65
		35	26,50605874			14,2	1B	30,47
		40	25,48696152			14,2	1D	30,48

Appendix B

Data from in situ cave experiments

exp.	duration [days]	T [°C]	$CO_{2\ soil}$ [ppm]	$CO_{2\ cave}$ [ppm]	drip rate [s]	pH	Ca^{2+} [mg/l]	Mg^{2+} [mg/l]	K^{+} [mg/l]	Na^{+} [mg/l]	HCO_3^{-} [mg/l]	Cl^{-} [mg/l]	NO^{3-} [mg/l]	SO^{4-} [mg/l]	SI	$\delta^{13}C$ [‰]	$\delta^{18}O$ [‰]
Bu_A	113	10,5			30;108*	8,07**									0,74		
Bu_B	113	10,5			36	8,16; 8,06**					135,11**				0,49	-9,5;-8,5**	
B7_A	282	10													0,36		
B7_B	282	10			3-5	7,53	131	7,14	0,28	8	309				0,46	-14,2	
* value for April (otherwise August) ** sample taken at the end of the channel																	
TS1 (immidiate sampling) - sampling by Dana Riechelmann																	
24.04.		10,8	4470	610	0,4918	7,9	104	3,5	0,22	5	200	12,9	9,8	24,1		-12,35	-8,18
23.05.		10,6	4620	650	1,2766	8,03	90,2	3,3	0,28	5,1	229	12,5	9,2	27,1		-11,84	-8,43
26.06.		10,4	4460	750	3,52941	8,01	86,4	3	0,27	5,1	220	12,6	9,6	29,6		-11,62	-8,49
17.07.		10,4	4580	720	5	8,05	92,5	3	0,24	5,7	218	12,4	9,7	30,2		-10,94	-8,49
14.08.		11	4500	870	6,66667	8,09	91,5	2,8	0,25	5,9	209	12,7	9,9	31,2		-10,68	-8,42
TS2 (samples integrated over one month) - sampling by Dana Riechelmann																	
24.04.		11,1	4470	610	30	8	81,0	4,3	0,37	6,50	118	16,9	2,8	63,2		-7,5	-8,13
23.05.		11,6	4620	650	30	8,035	75,6	4,1	0,38	6,30	139	15,8	2,8	65,8		-7,84	-8,33
26.06.		11,2	4460	750	30	7,97	74,3	4,1	0,38	6,30	135	15,4	3,1	65,1		-8,2	-8,39
17.07.		11,3	4580	720	30	7,97	80,4	4,2	0,39	6,80	148	15,3	2,7	64,4		-7,65	-8,35
14.08.		11,5	4500	870	30	8,04	81,3	4,3	0,37	6,90	153	15,2	2,7	63,9		-7,77	-8,32

Cave experiment BU-A

filter seg. [cm]	$\delta^{13}C$ [‰]	$\delta^{13}C_{rel}$ [‰]	$\delta^{18}O$ [‰]	$\delta^{18}O_{rel}$ [‰]
1	-7,77	0,03	-4,97	1,03
13	-7,58	0,22	-5,98	0,02
16	-7,61	0,19	-5,87	0,13
19	-7,52	0,28	-5,92	0,08
22	-7,54	0,26	-5,86	0,14
25	-7,54	0,26	-5,97	0,03
28	-7,50	0,30	-5,86	0,14
32	-7,20	0,60	-5,79	0,21
34	-7,02	0,78	-5,78	0,22
37	-7,34	0,46	-5,81	0,19
40	-7,33	0,47	-5,84	0,16
43	-7,18	0,62	-5,79	0,21
46	-7,17	0,63	-5,78	0,22
49	-7,15	0,65	-5,80	0,20

filter seg. [cm]	$CaCO_3$ [mg]	err
2	9,02	0,05
4	8,67	0,05
8	1,11	0,05
10	1,53	0,05
14	2,58	0,05
16	2,64	0,05
20	1,74	0,05
22	1,94	0,05
26	1,92	0,05
28	2,03	0,05
33	1,72	0,05
38	1,47	0,05
40	1,22	0,05
44	0,41	0,05
48	0,94	0,05

Cave experiment B7-A

filter seg. [cm]	$\delta^{13}C$ [‰]	$\delta^{13}C_{rel}$ [‰]	$\delta^{18}O$ [‰]	$\delta^{18}O_{rel}$ [‰]
1	-8,55	1,25	-5,64	0,26
2	-9,08	0,72	-5,23	0,67
4	-9,50	0,30	-5,80	0,10
6	-9,17	0,63	-5,22	0,68
7	-9,19	0,61	-5,59	0,31
9	-9,00	0,80	-5,11	0,79
10	-9,27	0,53	-5,63	0,27
12	-9,36	0,44	-5,76	0,14
13	-9,16	0,64	-5,68	0,22
15	-8,94	0,86	-5,57	0,33
16	-8,26	1,54	-5,24	0,66
19	-8,58	1,22	-5,10	0,80
22	-8,68	1,12	-5,53	0,37
25	-8,07	1,73	-5,33	0,57
28	-8,03	1,77	-5,25	0,65
31	-7,86	1,94	-5,29	0,61
34	-8,14	1,66	-5,34	0,56
37	-7,97	1,83	-5,32	0,58

filter seg. [cm]	$CaCO_3$ [mg]	err
1	10,77	0,05
2	25,76	0,05
4	26,13	0,05
6	30,45	0,05
7	30,49	0,05
9	20,44	0,05
10	24,49	0,05
12	18,69	0,05
13	19,42	0,05
15	16,02	0,05
16	13,20	0,05
19	6,12	0,05
22	6,00	0,05
25	5,40	0,05
28	4,31	0,05
31	1,37	0,05
34	1,88	0,05
37	0,06	0,05
43	0,06	0,05

Cave experiment B7-B

filter seg. [cm]	$\delta^{13}C$ [‰]	$\delta^{13}C_{rel}$ [‰]	$\delta^{18}O$ [‰]	$\delta^{18}O_{rel}$ [‰]
1A	-14,2			
1B	-8,75	-1,70	-5,32	0,88
1C	-10,09	3,75	-5,12	1,08
2	-12,55	-0,05	-5,84	0,36
4	-12,30	0,20	-5,81	0,39
6	-12,03	0,47	-5,64	0,56
8	-12,11	0,39	-5,84	0,36
10	-12,53	-0,03	-6,01	0,19
12	-12,33	0,17	-6,12	0,08
14	-12,20	0,30	-5,92	0,28
16	-12,09	0,41	-6,04	0,16
18	-12,44	0,06	-6,01	0,19
23	-12,34	0,16	-5,81	0,39
25	-12,50	0,00	-5,85	0,35
27	-12,57	-0,07	-6,22	-0,02
29	-12,49	0,01	-6,04	0,16
31	-12,66	-0,16	-5,36	0,84
33	-11,29	1,21	-5,13	1,07
35	-12,33	0,17	-5,89	0,31
38	-12,12	0,38	-5,67	0,53
40	-12,02	0,48	-5,65	0,55
42	-11,12	1,38	-5,20	1,00

filter seg. [cm]	$CaCO_3$ [mg]	err
1A	166,00	0,500
1B	157,00	0,500
1C	635,00	0,500
2	80	0,500
4	24	0,500
6	40	0,500
8	73	0,500
10	44	0,500
12	84	0,500
14	78	0,500
16	57	0,500
18	69	0,500
21	34	0,500
23	33	0,500
25	23	0,500
27	20	0,500
29	74,00	0,500
31	77,00	0,500
33	80,00	0,500
35	97,00	0,500
38	61,00	0,500
40	96,00	0,500
42	79,00	0,500

Bibliography

Appelo, C. and Postma, D.: Geochemistry, Groundwater and Pollution, chap. 2,4,5, pp. 33 – 219, A.A. Balkema, 2005.

Arakaki, T. and Mucci, A.: A continuous and mechanistic representation of calcite reaction-controlled kinetics in dilute solutions at 25°C and 1 atm total pressure, Aquatic Geochemistry, 1, 105–130, 1995.

Baker, A., Genty, D., Dreybrodt, W., Barnes, W., Mockler, N., and Grapes, J.: Testing theoretically predicted stalagmite growth rate with recent annually laminated samples: Implications for past stalagmite deposition, Geochimica et Cosmochimica Acta, 62 (3), 393–404, 1998.

Banner, J., Guilfoyle, A., James, E., Stern, L., and Musgrove, M.: Seasonal variations in modern speleothem calcite growth in central Texas, USA, Journal of Sedimentary Research, 77, 615–622, 2007.

Barton, H. and Northup, D.: Geomicrobiology in cave environments: Past, current and future perspectives, Journal of Cave and Karst Studies, 69 (1), 163–178, 2007.

Beck, W., Grossman, E., and Morse, J.: Experimental studies of oxygen isotope fractionation in the carbonic acid system at 15°C, 25°C, and 40°C, Geochimica et Cosmochimica Acta, 69, 3493–3503, 2005.

Bottinga, Y.: Calculation of fractionation factors for carbon and oxygen isotopic exchange in the system calcite-carbon dioxide-water, The Journal Of Physical Chemistry, 72, 800 – 808, 1968.

Brenninkmeijer, C., Kraft, P., and Mook, W.: Oxygen Isotope Fractionation between CO_2 and H_2O, Isotope Geoscience, 1, 181 – 190, 1983.

Buhl, D., Immenhauser, A., Smeulders, G., Kabiri, L., and Richter, D.: Time series δ^{26}Mg analysis in speleothem calcite: Kinetic versus equilibrium fractionation, comparison with other proxies and implications for palaeoclimate research, Chemical Geology, 244, 715–729, 2007.

Buhmann, D. and Dreybrodt, W.: The kinetics of calcite dissolution and precipitation in geologically relevant situations of karst areas - Open system, Chemical Geology, 48, 189 – 211, 1985a.

Buhmann, D. and Dreybrodt, W.: The kinetics of calcite dissolution and precipitation in geologically relevant situations of karst areas - Closed system, Chemical Geology, 53, 109 – 124, 1985b.

Cacchio, P., Contento, R., Ercole, C., Cappuccio, G., Martinez, M. P., and Lepidi, A.: Involvement of microorganisms in the formation of carbonate speleothems in the Cervo Cave (L'Aquila-Italy), Geomicrobiology Journal, 21, 497–509, 2004.

Clark, I. and Fritz, R.: Environmental Isotopes in Hydrogeology, chap. divers, p. divers, CRC, 1997.

Coplen, T.: Calibration of the calcite-water oxygen-isotope geothermometer at Devils Hole, Nevada, a natural laboratory, Geochimica et Cosmochimica Acta, 71, 3948–3957, 2007.

Deines, P., D., L., and Harmon, R. S.: Stable carbon isotope ratios and the existence of a gas phase in the evolution of carbonate ground waters, Geochimica et Cosmochimica Acta, 38, 1147–1164, 1974.

Dreybrodt, W.: Processes in karst systems, chap. Chemistry of the System H_2O-CO_2-$CaCO_3$, pp. 13 – 31, Springer, 1988.

Dreybrodt, W.: Chemical kinetics, speleothem growth and climate, Boreas, 28, 347–356, 1999.

Dreybrodt, W.: Evolution of the isotopic composition of carbon and oxygen in a calcite precipitating $H_2O - CO_2 - CaCO_3$ solution and the related isotopic composition of calcite in stalagmites, Geochimica et Cosmochimica Acta, 72 (19), 4712–4724, 2008.

Dreybrodt, W. and Buhmann, D.: A mass transfer model for dissolution and precipitation of calcite from solutions in turbulent motion, Chemical Geology, 90, 107–122, 1991.

Dreybrodt, W. and Kaufmann, G.: Physics and chemistry of dissolution on subaerialy exposed soluble rocks by flowing water films, Acta Carsologica, 36 (3), 357–367, 2007.

Dreybrodt, W., Eisenlohr, L., Madry, B., and Ringer, S.: Precipitation kinetics of calcite in the system $CaCO_3 - CO_2 - H_2O$: The conversion to CO_2 by the slow process $CO_2 + H_2O \rightleftharpoons H^+ + HCO_3^-$ as a rate limiting step, Geochimica et Cosmochimica Acta, 61, 3897 – 3904, 1997.

Dulinski, M. and Rozanski, K.: Formation of $^{13}C/^{12}C$ isotope ratios in speleothems: A semi-dynamic model, Radiocarbon, 32, 7 – 16, 1990.

Emrich, K., Ehhalt, D. H., and Vogel, J. C.: Carbon isotope fractionation during the precipitation of calcium carbonate, Earth and Planetary Science Letters, 8, 363–371, 1970.

Fairchild, I., Borsato, A., Tooth, A., Frisia, S., Hawkesworth, C., Huang, Y., McDermot, F., and Spiro, B.: Controls of trace element (Sr-Mg) compositions of carbonate cave waters: Implications for speleothem climatic records, Chemical Geology, 166, 255 – 269, 2000.

Fairchild, I., Smith, C., Baker, A., Fuller, L., Spötl, C., Mattey, D., McDermott, F., and E.I.M.F.: Modification and preservation of environmental signals in speleothems, Earth Science Reviews, 75, 105–153, 2006.

Fantidis, J.: Die Variationen des C^{13}- und O^{18}-Gehaltes in Stalaktiten und Stalagmiten und ihre möglichen paläoklimatischen Aussagen, Ph.D. thesis, Ruprecht-Karl-Universität zu Heidelberg, 1969.

Fantidis, J. and Ehhalt, D.: Variations of the carbon and oxygen isotopic composition in stalagmites: Evidence of non-equilibrium isotopic fractionation, Earth and Planetary Science Letters, 10, 136 – 144, 1970.

Fernandez-Diaz, L., Putnis, A., Prieto, M., and Putnis, C.: The role of magnesium in the crystallization of calcite and aragonite in porous medium, Journal of Sedimentary Research, 66, 482–491, 1996.

Fernandez-Diaz, L., Astilleros, J., and Pina, C.: The morphology of calcite crystals grown in a porous medium doped with divalent cations, Chemical Geology, 225, 314 – 321, 2006.

Fleitmann, D., Burns, S., Neff, U., Mudelsee, M., Mangini, A., and Matter, A.: Palaeoclimatic interpretation of high-resolution oxygen isotope profiles derived from annually laminated speleothems from Southern Oman, Quaternary Science Reviews, 23, 935 – 945, 2004.

Fohlmeister, J.: Carbon isotopes in stalagmites and drip water: Tracers of soil processes, Ph.D. thesis, Universität Heidelberg, 2008.

Ford, D. and Williams, P.: Karst Hydrology and Geomorphology, Wiley & Sons, 2007.

Friedman, I. and O'Neil, R.: Compilation of Stable Isotope Fractionation Factors of Geochemical Interest, chap. Data of Geochemistry, pp. KK1 – KK12, US Govt. Print. Office, 1977.

Frisia, S., Borsato, A., Mangini, A., Spötl, C., Madonia, G., and Sauro, U.: Holocene climate variability in Sicily from a discontinous stalagmite record and the Mesolithic to Neolithic transition, Quarternary Research, 66, 388 – 400, 2006.

Gebauer, D., Völkel, A., and Cölfen, H.: Stable prenucleation calcium carbonate clusters, Science, 322, 1819–1822, 2008.

Gewies, S.: Weiterentwicklung von Laborexperimenten zur Untersuchung der Fraktionierung der Sauerstoff- und Kohlenstoffisotope bei der Kalkfällung, Master's thesis, Institut für Umweltphysik der Universität Heidelberg, 2003.

Ghosh, P., Adkins, J., Affek, H., Balta, B., Guo, W., Schauble, E., Schrag, D., and Eiler, J.: $^{13}C -^{18} O$ bonds in carbonate minerals: A new kind of paleothermometer, Geochimica et Cosmochimica Acta, 70, 1439 – 1456, 2006.

Gonzáles, L., Carpenter, S., and Lohmann, K.: Inorganic calcite morphology: Roles of fluid chemistry and fluid flow, Journal of Sedimentary Petrology, 62, 382–399, 1992.

Grasby, S. E.: Naturally precipitating vaterite (μ-$CaCO_3$) spheres: Unusual carbonates formed in an extreme environment, Geochimica et Cosmochimica Acta, 67 (9), 1659–1666, 2003.

Harmon, R., Schwarz, H., Gascoyne, M., Hess, J., and Ford, D.: Studies of cave sediments. Physical and chemical records of palaeoclimate, chap. Palaeoclimate Information From Speleothems: The Present As A Guide To The Past, pp. 199 – 226, Kluwer Academic, 2004.

Hendy, C.: The isotopic geochemistry of speleothems - I. The calculation of the effects of different modes of formation on the isotopic composition of speleothems and their applicability as palaeoclimatic indicators, Geochimica et Cosmochimica Acta, 35, 801 – 824, 1971.

Hendy, C. and Wilson, A.: Palaeoclimatic data from speleothems, Nature, 219, 48 – 51, 1968.

Holland, H., Kirsipu, T., Huebner, J., and Oxburgh, U.: On some aspects of the chemical evolution of cave waters, The Journal of Geology, 72, 36–67, 1964.

Huang, Y. and Fairchild, I.: Partitioning of Sr^{2+} and Mg^{2+} into calcite under karst-analogue experimental conditions, Geochimica et Cosmochimica Acta, 65, 47 – 62, 2001.

Jimenez-Lopez, C., Rodriguez-Navarro, A., Dominguez-Vera, J., and Garcia-Ruiz, J.: Influence of lysozyme on the precipitation of calcium carbonate: A kinetic and morphologic study, Geochimica et Cosmochimica Acta, 67 (9), 1667–1676, 2003.

Johnson, K., Hu, C., Belshaw, N., and Henderson, G.: Seasonal trace-element and stable-isotope variations in a Chinese speleothem: The potential for high-resolution paleomonsoon reconstruction, Earth and Planetary Science Letters, 244, 394 – 407, 2006.

Kim, S. and O'Neil, J.: Equilibrium and nonequilibrium oxygen isotope effects in synthetic carbonates, Geochimica et Cosmochimica Acta, 61, 3461 – 3475, 1997.

Kluge, T.: Fluid inclusions in speleothems as a new archive for the noble gas palaeothermometer, Ph.D. thesis, Ruprecht-Karls-Universität Heidelberg, 2008.

Kralj, D., Brecevic, L., and Nielsen, A.: Vaterite growth and dissolution in aqueous solution, Journal of Crystal Growth, 104, 793–800, 1990.

Kunz, B. and Stumm, W.: Kinetik der Bildung und des Wachstums von Calciumcarbonat, Vom Wasser, 62, 279–293, 1984.

Lebrón, I. and Suárez, D. L.: Kinetics and mechanisms of preciptitation of calcite as affected by P_{CO2} and organic ligands at 25°C, Geochimica et Cosmochimica Acta, 62 (3), 405–416, 1998.

Lee, M. and Bethke, M.: A model of isotope fractionation in reacting geochemical systems, American Journal of Science, 296, 965–988, 1996.

März, R.: Laborexperimente zur Anreicherung der stabilen Isotope C^{13}- und O^{18} in künstlichen Carbonaten als Modell der Stalagmitenbildung , Master's thesis, Ruprecht-Karls-Universität Heidelberg, 2006.

Matthess, G., Frimmel, F., Hirsch, P., Schulz, H. D., and Usdowski, E.: Progress in Hydrogeochemistry, chap. 3, pp. 101–175, Springer, 1992.

Mayewski, P., Rohling, E., and Stager, J.: Holocene climate variability, Quaternary Research, 62, 243 – 255, 2004.

Michaelis, J., Usdowski, E., and Menschel, G.: Partitioning of ^{13}C and ^{12}C on the degassing of CO_2 and the precipitation of calcite - Rayleigh-type fractionation and a kinetic model, American Journal of Science, 285, 318 – 327, 1985.

Mickler, P., Banner, J., Stern, L., Asmerom, Y., Edwards, R., and Ito, E.: Stable isotope variations in modern tropical speleothems: Evaluating equilibrium vs. kinetic isotope effects, Geochimica et Cosmochimica Acta, 68, 4381 – 4393, 2004.

Mickler, P., Stern, L., and Banner, J.: Large kinetic isotope effects in modern speleothems, Geological Society of America, 118, 65 – 81, 2006.

Mook, W.: Environmental Isotopes in the Hydrological Cycle, chap. 3,4,7,9, pp. 31 – 266, IAEA, 2000.

Mühlinghaus, C.: The principles of growth and isotopic fractionation of stalagmites- A numerical model to reconstruct temperature and precipitation records from stalagmites grown under disequilibrium conditions, Ph.D. thesis, University of Heidelberg, 2008.

Mühlinghaus, C., Scholz, D., and Mangini, A.: Modelling fractionation of stable isotopes in stalagmites under disequilibrium conditions, in review, 2009.

Nielsen, A. and Toft, J.: Electrolyte crystal growth kinetics, Journal of Crystal Growth, 67, 278–288, 1984.

Niggemann, S.: Klimabezogene Untersuchungen an spät- bis postglazialen Stalagmiten aus Massenkalkhöhlen des Sauerlandes, chap. 55, pp. 5–129, Bochumer geologische und geotechnische Arbeiten, 2000.

Niggemann, S., Mangini, A., Richter, D. K., and Wurth, G.: A paleoclimate record of the last 17.600 years in stalagmites from the B7 cave, Sauerland, Germany, Quaternary Science Reviews, 22, 555–567, 2003.

Northup, D. E. and Lavoie, K.: Geomicrobiology of caves: A review, Geomicrobiology Journal, 18, 199–222, 2001.

Onac, B.: Cave minerals of the world, chap. Crystallography of Speleothems, pp. 230–236, National Speleological Society, 1997.

Paquette, J. and Reeder, R.: Relationship between surface structure, growth mechanism, and trace element incorporation in calcite, Geochimica et Cosmochimica Acta, 59 (4), 735 – 749, 1995.

Plummer, L. and Busenberg, E.: The solubilities of calcite, aragonite and vaterite in CO_2-H_2O solutions between 0 and 90°, and an evaluation of the aqueous model for the system $CaCO_3$-CO_2-H_2O, Geochimica et Cosmochimica Acta, 46, 1011 – 1040, 1982.

Plummer, L., Wigley, T., and Parkhurst, D.: The kinetics of calcite dissolution in CO_2-water systems at 5 to 60°C and 0.0 to 1 atm CO_2, American Journal of Science, 278, 179–216, 1978.

Pust, J.: Untersuchung zur Systematik, Morphologie und Ökologie der in westfälischen Höhlen vorkommenden aquatischen Höhlentiere, Abh. Westf. Museum f. Naturkunde, 1990.

Roberts, M., Smart, P., Hawkesworth, C., Perkins, W., and Pearce, N.: Trace element variations in coeval Holocene speleothems from GB Cave, southwest England, The Holocene, 9 (6), 707 – 713, 1999.

Romanek, C. S., Grossman, E. L., and Morse, J. W.: Carbon isotopic fractionation in synthetic aragonite and calcite: Effects of temperature and precipitation rate, Geochimica et Cosmochimica Acta, 56, 419 – 430, 1992.

Romanov, D., Kaufmann, G., and Dreybrodt, W.: $\delta^{13}C$ profiles along growth layers of stalagmites: Comparing theoretical and experiemntal results, Geochimica et Cosmochimica Acta, 72 (2), 438–448, 2008.

Rubinson, M. and Clayton, R.: Carbon-13 fractionation between aragonite and calcite, Geochimica et Cosmochimica Acta, 33, 997 – 1002, 1969.

Salomons, W. and Mook, W.: Handbook of environmental isotope geochemistry, chap. Isotope Geochemistry of Carbonates in the Weathering Zone, pp. 239 – 264, 1986.

Scholz, D. and Hoffmann, D.: ^{230}Th/U-Dating of Fossil Reef Corals and Speleothems, Quaternary Science Journal, 57, 52–77, 2008.

Scholz, D., Mühlinghaus, C., and Mangini, A.: Modelling the evolution of $\delta^{13}C$ and $\delta^{18}O$ in the solution layer on stalagmite surfaces, in review, 2009.

Schröder-Ritzrau, A., Riechelmann, D., Scholz, D., Spötl, C., Richter, D., and Mangini, A.: Monitoring Bunker Cave (Iserlohn-Letmathe, NRW, Germany): Methods and preliminary results, submitted to the journal of Hydrology, 2009.

Self, C. and Hill, C.: How speleothems grow: An introduction to the ontogeny of cave minerals, Journal of Cave and Karst Studies, 65(2), 130 – 151, 2003.

Spötl, C. and Mangini, A.: Stalagmite from the Austrian Alps reveals Dansgaard-Oeschger events during isotope stage 3: Implications for the absolute chronology of Greenlandice cores, Earth and Planetary Science Letters, 203, 507 – 518, 2002.

Taylor, P. and Chafetz, H.: Floating rafts of calcite crystals in cave pools, Central Texas, U.S.A.: Crystal habit vs. saturation state, Journal of Sedimentary Research, 74 (3), 328–341, 2004.

Turner, J.: Kinetic fractionation of carbon-13 during calcium carbonate precipitation, Geochimica et Cosmochimica Acta, 46, 1183–1191, 1982.

Usdowski, E. and Hoefs, J.: Oxygen isotope exchange between carbonic acid, bicarbonate, carbonate and water: A re-examination of the data of McCrea (1950) and an expression for the overall partitioning of oxygen isotopes between the carbonate species and water, Geochimica et Cosmochimica Acta, 57, 3815 – 3818, 1993.

Vollweiler, N., Scholz, D., Mühlinghaus, C., Mangini, A., and Spötl, C.: A precisely dated climate record for the last 9 kyr from three high alpine stalagmites, Spannagel Cave, Austria, Geophysical Research Letters, 33, L20 703, 2006.

Wang, Y., Cheng, H., Lawrence Edwards, R., Kong, X., Shao, X., Chen, S., Wu, J., Jiang, X., Wang, X., and Zhisheng, A.: Millenial- and orbital-scale changes in the East Asian monsoon over the past 224.000 years, Nature, 451, 1090–1093, 2008.

Went, F.: Fungi associated with stalactite growth, Science, 166, 385–386, 1969.

Wiedner, E.: Laborexperimente zur kinetischen Fraktionierung stabiler Isotope bei der Sinterbildung, Ph.D. thesis, Ruprecht-Karls-Universität Heidelberg, 2004.

Wiedner, E., Scholz, D., Mangini, A., Polag, D., Mühlinghaus, C., and Segl, M.: Investigation of the stable isotope fractionation in speleothems with laboratory experiments, Quaternary International, 187 (1), 15–24, 2008.

Xie, S., Huang, Y., J., H., Cai, C., Collins, Y., and Baker, M.: Lipid distribution in a subtropical southern China stalagmite as a record of soil ecosystem response to paleoclimate change, Quaternary Research, 60, 340–347, 2003.

List of Figures

2.1 *Scheme, basically illustrating the formation of speleothems.* 6

2.2 *Percentage of carbonate species as a function of pH (from Clark and Fritz (1997)).* . 8

2.3 *Crystal growth in dependence of the saturation state (modified after Nielsen and Toft (1984)).* 12

3.1 *Picture (left) and sketch (right) of the experiment set-up used to precipitate synthetic carbonates under controlled conditions in the laboratory.* 17

3.2 *Picture of the u-shaped glass channel with the glass fibre stripe inside. Four temperature sensors attached at the undersurface of the glass channel were used for spatial and temporal temperature control during the experiment.* 18

3.3 *Comparison between the cave system (left) and the laboratory set-up (right).* 19

3.4 *Experimental determination of the flow velocity for two different pump rates (three tests in each case).* 21

3.5 *Average cation content of the initial solution used calcite precipititation.* 25

3.6 *SEM-pictures of the calcite precipitated on the glass fiber stripe in laboratory experiment 1: top: experiment 1A (section 43); middle: experiment 1C (left: section 18, right: section 48), bottom: experiment 1D (section 8).* 27

3.7 *SEM-pictures of the calcite precipitated on the glass fibre stripe in laboratory experiment 4B (section 5).* 28

3.8 *SEM-pictures of the calcite precipitated on the glass fibre stripe in laboratory experiment 4B (section 47).* 28

3.9 *Mass distribution of experiments* $4A$ *and* $4B$ *differing in filter surface area. The numbers inside the graph indicate the total mass of calcite precipitated within a period of* 28 *days.* 31

3.10 *Mass distribution of experiments* $6A$ *and* $7A$ *differing in channel atmosphere. The numbers inside the graph indicate the total mass of calcite precipitated within a period of* 28 *days.* 32

3.11 *Mass distribution of experiments* $4B$ *and* $6C$ *differing in temperature. The numbers inside the graph indicate the total mass of calcite precipitated within a period of* 28 *days.* 33

3.12 *Percental relation between total amount of precipitated calcite and maximum possible calcite mass calculated with PHREEQC plotted versus SI_{CaCO_3} for experiments carried out at different temperatures.* 34

3.13 *Temporal evolution of Ca^{2+} for two different conversion rates τ (deduced from Baker et al. (1998)). Ca_0 represents the initial calcium concentration, and Ca_{eq} indicates the equilibrium calcium concentration, which is p_{CO_2}-dependent.* 35

3.14 *Mass distribution of experiments $6B$ and $6D$ differing in initial SI_{CaCO_3}. The numbers inside the graph indicate the total mass of calcite precipitated within a period of 39 days.* 36

3.15 *Position of maximum calcite precipitation on the glass fibre stripe versus SI_{CaCO_3} for experiments with a constant flow velocity of 6.6 min.* 37

3.16 *Temporal Ca^{2+}-decrease along the channel, plotted logarithmically for experiments $6D$ (left) and $5B$ (right). τ can be determined by the slope s with $\tau = -(1/s)$.* . . . 37

3.17 *$\delta^{13}C$ (left)- and $\delta^{18}O$ (right)-enrichment along the channel for experiments with different flow velocities v. Values for v are indicated in the plot.* 40

3.18 *Temporal $\delta^{13}C$ (left)- and $\delta^{18}O$ (right)-enrichment for experiments with different flow velocities v. Values for v are indicated in the plot.* 41

3.19 *Isotope correlation $\delta^{18}O(\delta^{13}C)$ for experiments with different flow velocities v. Values for v and for the linear interpolated slope $\Delta(\delta^{18}O)/\Delta(\delta^{13}C)$ are indicated in the plot.* 41

3.20 *$\delta^{13}C$ (left)- and $\delta^{18}O$ (right)-enrichment along the channel for experiments with different channel atmospheres indicated in the plot.* 43

3.21 *Isotope correlation $\delta^{18}O(\delta^{13}C)$ for experiments with different channel atmospheres indicated in the plot.* 43

3.22 *$\delta^{13}C$ (left)- and $\delta^{18}O$ (right)-enrichment along the channel for experiments with different temperatures which are indicated in the plot. The light blue points represent values measured on the glass fibre subsurface.* 44

3.23 *Isotope correlation $\delta^{18}O(\delta^{13}C)$ for experiments with different temperatures which are indicated in the plot. The light blue points represent values measured on the glass fibre subsurface.* 45

3.24 *$\delta^{13}C$ (left)- and $\delta^{18}O$ (right)-enrichment along the channel for experiments with different initial ion concentrations expressed as SI_{CaCO_3}. Values for SI_{CaCO_3} are indicated in the plot.* 46

3.25 *Isotope correlation $\delta^{18}O(\delta^{13}C)$ for experiments with different initial ion concentrations expressed as SI_{CaCO_3}. Values for SI_{CaCO_3} are indicated in the plot.* 46

3.26 *Comparison between enrichment factors obtained from literature and from the laboratory experiments. $\epsilon_{CaCO_3-HCO_3^-}$ is indicated in VPDB and $\epsilon_{CaCO_3-H_2O}$ is indicated in VSMOW.* 48

3.27 *Kinetic constant a versus the film thickness d, interpolated from* Baker et al. (1998) *for a temperature of $10°C$ (left) and $23°C$ (right).* 51

3.28 *Experiment results for varying flow velocites plotted together with model results for varying values of τ and b.* 52

3.29 *Experiment results for varying temperatures plotted together with model results for varying values of τ, α and b.* 53

3.30 *Overview of the isotope correlation $\delta^{18}O(\delta^{13}C)$ for most of the laboratory experiments in comparison with the expected slopes for the extreme cases of 'no buffering' and 'complete buffering'.* 56

4.1 *Map of Bunker-Höhle, chamber 1 and sketch of the set-up of experiment BU-A.* . . . 58

4.2 *SEM-pictures of calcite crystals precipitated in Bunkerhöhle on watch glass $U1$ at drip site $TS1$ (left) and on the glass fiber stripe of channel experiment $BU-A$ (right).* 60

4.3 *Mass distribution of in situ experiment $BU-A$.* 61

4.4 *$\delta^{13}C$ (left) and $\delta^{18}O$ (right) evolution for in situ experiment $BU-A$. Between 30 cm and 35 cm the glass fibre stripe was ripped lengthwise indicated by light grey values in the isotopic values.* 62

4.5 *Isotope correlation $\delta^{18}O(\delta^{13}C)$ for in situ experiment $BU-A$. The data are linearly interpolated.* 62

4.6 *Combined plot, showing the results of $TS1$ in Bunkerhöhle: $\delta^{13}C$ (left) and $\delta^{18}O$ (right) for in situ experiment $BU-A$ together with the isotope range of the drip water and the watch glass calcite. The dotted rectangles indicate the range of the theoretical equilibrium fractionation values (whole range calculated with fractionation factors from literature) between the drip water and the calcite.* 64

4.7 *Map of B7-Höhle and picture of the set-up of experiments B7-A and B7-B in the northern part of the cave (interconnection of 'Kerzenhalle' and 'Olymp').* 65

4.8 *Close-ups of the experiment set-ups in B7-Höhle: $B7-A$ (left) was placed at the former location of $STAL-B7-7$ and $B7-B$ (right) according to the former location of $STAL-B7-6$, both investigated by Niggemann et al. (2003).* 66

4.9 *Little flow stone grown during 9 month in the upper part of the glass channel in experiment $B7-B$. The white fabric visible at the subsurface represents a part of the glass fibre stripe.* 68

4.10 *Microscope pictures of channel experiment $B7-B$, section 13. (a)-(b): Stereo microscope pictures showing black hairy structures which may indicate some kind of spores or fungi. (c)-(f): high resolution SEM-pictures of section 13.* 69

4.11 *Mass distribution of in situ experiments $B7-A$ and $B7-B$. The black circle indicates sections, where much of the glass fibre stripe got stuck at the channel, which underestimates the true mass of calcite.* 70

4.12 *Isotope development of $\delta^{13}C$ (left) and $\delta^{18}O$ (right) along the channel for in-situ experiment $B7-A$. The red value is related to the top of STAL-B7-7 (Niggemann (2000)).* 72

4.13 *Isotope development of $\delta^{13}C$ (left) and $\delta^{18}O$ (right) along the channel for in-situ experiment $B7-B$. The red value is related to the top of the PET-flask set out at the site of STAL-B7-6 (Niggemann (2000)).* 72

4.14 *$\delta^{18}O$ versus $\delta^{13}C$ for all three cave experiments (including Bunkerhöhle and B7-Höhle). The shaded area represents the slope range obtained from the laboratory experiments.* 74

List of Tables

3.1 *Parameter ranges used in the laboratory experiments and observed for the monitoring caves of the DAPHNE research project (Bunkerhöhle in Sauerland/Germany and Grotta di Ernesto in northern Italy).* 20

3.2 *Listing and description of experiment samples and measured parameters. The following sample nomenclature was applied: x = number of experiment (1-7); y = part experiment (A-D); n = number of glass fibre stripe section (1-50)* 23

3.3 *Overview of investigated parameters and the corresponding analysis methods. Also given are the required sample amount and the measurement error.* 23

3.4 *Overview of the respective experiments compared to each other and the differing parameters. The related quantities of these parameters are specified in the single plots of fig. 3.9-3.14. All parameters not depicted in the plot are constant for both displayed experiments.* 30

3.5 *Overview of the experiments and the according parameters, which were varied. The values of these parameters are specified in the single plots of Fig. 3.17-3.25.* 39

3.6 *Carbon enrichment factors for* $\epsilon_{CaCO_3-HCO_3^-}$ *from various authors determined by different methods for different temperature ranges.* 47

3.7 *Oxygen enrichment factors for* $\epsilon_{CaCO_3-H_2O}$ *from various authors determined by different methods for different temperature ranges.* 48

3.8 *Overview and comparison of* τ*- and b-values obtained from laboratory experiments, from literature (Baker et al. (1998) and Hendy (1971), respectively) and from the numerical models.* 54

3.9 *Qualitative comparison between slopes* $\Delta(\delta^{18}O)/\Delta(\delta^{13}C)$ *and experiment parameters with the following nomeclature for temperature, solution flow velocity and saturation index:*
$+ : T = 23°C;\ v = 17\ s;\ SI_{CaCO_3} \geq 1$
$\circ : v = 11\ s;\ SI_{CaCO_3}$ *between* 0.8 *and* 1
$- : T = 10°C;\ v = 1.8\ s;\ SI_{CaCO_3} < 0.7$ 55

4.1 *Drip water values for* $TS1$ *and* $TS2$ *averaged over the measurement period (april-august). Additionally, the standard deviations of the mean values are indicated.* . . . 59

4.2 *Results of drip water and speleothem samplings: Values of* $STAL-B7-7$ *and* $STAL-B7-6$ *were measured by Niggemann between 1997 and 1999 and respresent the annual mean. The* $\delta^{13}C_{drip\,water}$ *values of* $STAL-B7-7$ *and* $STAL-B7-6$ *were measured once (07.01.1999). Samples for* $B7-A$ *and* $B7-B$ *were taken during removal of the experiments (02.02.2008).* $\delta^{13}C_{speleothem}$ *and* $\delta^{18}O_{speleothem}$ *refer to the top of the stalagmite in case* $STAL-B7-7$ *and to the calcite deposited on a PET-flask in case of* $STAL-B7-6$*. For* $B7-A$ *and* $B7-B$ $\delta^{13}C_{speleothem}$ *and* $\delta^{18}O_{speleothem}$ *represent the values of the topmost calcite precipitated on the channel (interpolation).* 67

Danksagung

Als erstes möchte ich mich bei meinem Betreuer Prof. Dr. Augusto Mangini bedanken, der mir die Möglichkeit zu dieser Arbeit im Bereich der Paläoklimaforschung gegeben hat, stets zu hilfreichen Diskussionen bereit war und mir außerdem die Bestellung eines Weinkühlschranks genehmigt hat.

Desweiteren danke ich der Zweitgutachterin dieser Arbeit, Prof. Dr. Margot Isenbeck-Schröter für die konstruktiven Diskussionen und den Einführungskurs in das Programm PHREEQC.

Im Rahmen der Arbeit möchte ich mich auch herzlich bedanken bei Dr. Monika Segl aus Bremen für die Isotopenmessungen am Calcit, bei Prof. Dr. Christoph Spötl aus Innbruck für die Isotopenmessung an den Lösungen und bei Andrea für die Kationenmessungen. Außerdem vielen Dank an Dana Riechelmann für die REM-Messung in Bochum und an Andrea Seehuber für die Möglichkeit und die Hilfe bei der Messung am REM des chemischen Institutes der Universität Heidelberg.

Ein großer Dank gilt Denis, Christian, Jens und Andrea für die stets anregenden Diskussionen und vor allem einen herzlichen Dank für das Korrekturlesen der Arbeit.

Vielen Dank auch an Ricardo März für die Einführung in die Laborexperimente.

Weiterer Dank hier auch an Tobias, Dana und Dr. Silvia Frisia für wichtige Diskussionen zur Calcitmorphologie und zu den 'ominösen Höhlenpilzen'.

Ebenfalls bedanken möchte ich mich bei Dr. Stephan Niggemann und Dana Riechelmann für die spannenden Höhlenexkursionen und in dem Sinne auch einen großen Dank an Tobias, der unter großen Strapazen meine Experimente aus der B7-Höhle herausgeholt hat und danke an Martin, ohne dessen helfende Hände ich heute noch in der B7-Höhle sitzen würde.

Vielen Dank auch Jens, Christian und Markus für die Hilfen in LaTeX, welches mich oftmals zur Verzweiflung gebracht hat.

Ein besonderer Dank gilt natürlich meiner Arbeitsgruppe. Ich könnte mir keine witzigere, sportlichere, musikalischere oder kreativere Gruppe vorstellen!

Vielen Dank auch meinen wechselnden Zimmerkollegen Thierry, Matthias und Lena (der einzigen Nichtfranzösin) mit denen stets abwechslungsreiche Gespräche außerhalb des fachlichen möglich waren.

Dankeschön auch an die diversen IUP-Sportgruppen, die einem die ein oder andere Auszeit vor dem Rechner gegönnt haben - speziell danke an die Beachvolleyballer, Fußballer, Ultimate Frisbeeler, Basketballer, Squashler und natürlich insbesondere der Truppe aus dem 'Tischtennislabor'.

Am Schluß möchte ich mich natürlich noch bei meiner Familie für die moralische und finanzielle Unterstützung bedanken. Vielen lieben Dank an meine Mutter Gabi, an Manuel, Matthias und Anni.

Der letzte Dank gilt meinem Vater, Reiner Polag, der immer an mich geglaubt hat und der leider die Fertigstellung dieser Arbeit nicht mehr miterleben konnte.